Analysis of Stratospheric Bromine Monoxide from SCIAMACHY using Comparison with Model Results

Vom Fachbereich für Physik und Elektrotechnik
der Universität Bremen

Zur Erlangung des akademischen Grades eines

Doktor der Naturwissenschaften (Dr. rer. nat.)

genehmigte Dissertation

von

Ninad V. Sheode

Eingereicht am:	6 June 2006
Tag des Kolloquiums:	11 July 2006
Gutachter:	Prof. Dr. J. P. Burrows
	Prof. Dr. J. Notholt
Weitere Prüfer	Prof. Dr. M. Rhein
	Prof. Dr. P. Richter

Dedication

This thesis is dedicated to the Memory of my grandmother
Prabhavati Sheode

Contents

Abstract

This thesis presents an analysis of the stratospheric bromine monoxide (BrO) profiles retrieved globally from two years of limb measurements from the Scanning Imaging Absorption Spectrometer for Atmospheric Chartography (SCIAMACHY) instrument on board ENVISAT.

In order to have a confidence in the quality of the retrieved SCIAMACHY BrO profiles, they need to be validated with BrO measurements, performed using different methods. Hence, as a first step towards a validation of SCIAMACHY BrO retrievals, BrO profiles are compared with the set of balloon-borne BrO measurements. The comparison with a set of four balloon-borne BrO profiles shows mean relative differences in the altitude range from 18 to 30 km between $+17\%$ and -42%. In order to validate our current understanding of bromine chemistry, the SCIAMACHY BrO retrievals are compared with modeled BrO profiles, based on estimated inorganic bromine (Br_y) from CFC-11 retrievals by the Michelson Interferometer for Passive Atmospheric Sounding (MIPAS), also on ENVISAT, and the calculated BrO/Br_y ratio from a photochemical model constrained by SCIAMACHY nitrogen di-oxide (NO_2) retrievals. The BrO observations are found to be broadly consistent with our current understanding of stratospheric bromine chemistry and a total stratospheric bromine loading of approximately 18.5 pptv.

Further a global climatology of stratospheric BrO is constructed using the two years' retrievals of BrO. The analysis of SCIAMACHY BrO observations provide for the first time a picture of the seasonal variation of stratospheric BrO on a global scale. At the midlatitudes of both hemispheres BrO shows a strong seasonal cycle with a maximum in winter and a minimum in summer. The seasonal variation of BrO is closely correlated with changes in NO_2 in accordance with our present understanding of bromine chemistry. The two years' BrO climatology constructed using the nadir measurements of SCIAMACHY and the climatology constructed in this work is used to calculate the amount of BrO below 15 km in the atmosphere. This calculation shows that a global background BrO of 1.4 pptv, averaged over all latitudes and months, exists throughout the year below 15 km in the atmosphere.

The knowledge of the total amount of bromine present in the atmosphere is an important issue as it has direct implications on our prediction of the ozone trends. Using the SCIAMACHY BrO observations together with the calculated bromine partitioning from a photochemical model constrained by the SCIAMACHY NO_2 observations, the total stratospheric bromine loading is estimated to be 18.5 ± 4 pptv. This indicates a contribution of about 3.5 ± 4 pptv from short lived bromine species in addition to methyl bromide and the halons.

Publications

Parts of the work described in this thesis have been published in various journals:

Publications in peer reviewed journals

1. Amekudzi L. K., Sinnhuber B.-M., **Sheode N. V.**, Meyer J., Rozanov A., Lamsal L. N., Bovensmann H., Burrows J. P.
   Retrieval of stratospheric NO_3 vertical profiles from SCIAMACHY lunar occultation measurement over the Antarctic, *J. Geophys. Res.*, 110, D20304, doi:10.1029/2004JD005748.
   Sections of this article are included in Chapter 3.

2. Sinnhuber B.-M., Rozanov A., **Sheode N.**, Ofe O. T., Richter A, Sinnhuber M.,Wittrock F., Burrows J. P., Stiller G. P., von Clarman T., and Linden A.
   Global observations of stratospheric bromine monoxide from SCIAMACHY, *Geophys. Res. Lett.*, 32(20), L20810, doi:10.1029/2005GL023839.
   Sections of this article are included in Chapters 7 and 10.

Submitted or under revision

1. **Sheode N.**, Sinnhuber B.-M., Rozanov A., Burrows J. P.
   Towards a climatology of stratospheric BrO from SCIAMACHY limb observations
   Submitted to Atmos. Chem. Phys. Discuss., 2006,
   Sections of this article are included in Chapters 5, 6, 7, and 10.

2. Sinnhuber B.-M., **Sheode N.**, Sinnhuber M., Chipperfield. M., Feng W.
   The contribution of anthropogenic bromine emissions to past stratospheric ozone trends: A modeling study *Submitted to Atmos. Chem. Phys. Discuss., 2006*

In preparation

1. Fietkau, S., Medeke T., Richter A., **Sheode N.**, Sinnhuber B.-M., Wittrock F., and Burrows J.P.
   Comparison of ground based measurements and model calculations of Bromine Monoxide above Nairobi (1°S, 36°E)
   To be submitted to Atmos. Chem. Phys. Discuss., 2006,
   Sections of this article are included in Chapters 8.

Conference contributions

1. Oetjen H., Medeke T., Richter A., **Sheode N. V.**, Sinnhuber B.-M., Wittrock F., and Burrows J. P.
   Comparison of Modelled and Measured Chlorine Dioxide Slant Columns for the Arctic Winter 2004/2005
   Deutsche Physikalishe Gesellschaft e. V. (DPG) Conference, Heidelberg, Germany, March, 2006

2. **Sheode N. V.**, Sinnhuber B.-M., Rozanov A., Burrows J.P.
   Towards a Climatology of Stratospheric Bromine Monoxide from SCIAMACHY Limb Measurements
   Aura Science Team Meeting, The Hague, Holland, 8-10 November, 2005

3. Sinnhuber B.-M., **Sheode N. V.**, Burrows J. P.
   Stratospheric Bromine Chemistry
   CCMVal 2005, NCAR, Boulder, Colorado, USA, October 17 - 19, 2005

4. **Sheode N. V.**, Sinnhuber B.-M., Rozanov A., Burrows J.P.
   SCIAMACHY Measurements of Stratospheric Bromine Monoxide and Comparison with Model Results
   European Geosciences Union, General Assembly, Vienna, Austria, 24 - 29 April, 2005

5. Sinnhuber B.-M., **Sheode N.**, Sinnhuber M.
   The Role of Bromine in Stratospheric Ozone Depletion and its Relation to Changes in Stratospheric Water Vapour European Geosciences Union, General Assembly, Vienna, Austria, 24 - 29 April, 2005

6. Fietkau S., Medeke T., Richter A., **Sheode N.**, Sinnhuber B.-M., Wittrock F., Burrows J. P.
   Comparison of Ground-based Observations and Model Calculations of Stratospheric Bromine Monoxide above Nairobi (1°S, 36°E)
   European Geosciences Union, General Assembly, Vienna, Austria, 24 - 29 April, 2005

7. Amekudzi L. K., Sinnhuber B.-M., **Sheode N. V.**, Meyer J., Rozanov A., Lamsal L. N., Bovensmann H., Burrows J. P.
   Comparison of Retrieved NO_3 Vertical Profiles from SCIAMACHY with 1-D Model Outputs
   European Geosciences Union, General Assembly, Vienna, Austria, 24 - 29 April, 2005

8. **Sheode N. V.**, Sinnhuber B.-M., Rozanov A., Burrows J.P.
   Global Measurements of Stratospheric Bromine Monoxide and Comparison with Model Results

Deutsche Physikalishe Gesellschaft e. V. (DPG) Conference, Berlin, Germany, March, 2005

9. Fietkau S., Medeke T., Richter A., **Sheode N.**, Sinnhuber B.-M., Wittrock F., Burrows J. P.
Comparison of Ground-based Measurements and Model Calculations of Bromine Monoxide in Nairobi (1°S, 36°E)
Deutsche Physikalishe Gesellschaft e. V. (DPG) Conference, Berlin, Germany, March, 2005

10. Burkert J., Sinnhuber B-M., **Sheode N.**, Wang P., Bremer H., Kleinbohl A., Rozanov A., Strohl F., Burrows J.P.
Process Studies of the Day-Night and Twilight Chemistry of Halogen Oxides in the Lower and Middle Stratosphere
SPARC 3rd General Assembly, Victoria, British Columbia, Canada, August, 2004

11. Rozanov A., Bracher A., Bovensmann H., Goutail F., Hrechany S., Rozanov V., Sinnhuber B.-M., Sinnhuber M., **Sheode N.**, Stroh F., and Burrows J.P.
NO_2 and BrO Vertical Profile Retrieval from SCIAMACHY Limb Measurements: Sensitivity Studies
35th COmmittee on SPAce Research (COSPAR) Scientific Assembly Meet,Paris, France, July, 2004

12. Amekudzi L., Bracher A., Meyer J., Sinnhuber B.-M., **Sheode N.**,Rozanov A., Sinnhuber M., Burrows J. P.
Lunar Occultation with SCIAMACHY: First Retrieval Results 35th COmmittee on SPAce Research (COSPAR) Scientific Assembly Meet, Paris, France, July, 2004

13. Fietkau S., Ladstatter-Weissenmayer A., Medeke T., Oetjen H., Richter A., **Sheode N.**, Sinnhuber B.-M., Wittrock F., Burrows J. P.
BrO Measurements in Nairobi (1°S, 36°E) with the Multi-axis DOAS Method
European Geosciences Union, General Assembly, Nice, France, 25 - 30 April, 2004

14. **Sheode N. V.**, Sinnhuber B.-M., Rozanov A., Burrows J.P.
First Near Global Measurements of Stratospheric Bromine Monoxide and Comparison with Model Results Deutsche Physikalishe Gesellschaft e. V. (DPG) Conference, Munich, Germany, March, 2004

1 Introduction

1.1 Motivation and objective

The industrial revolution in the 19th century started a new era of development in human society. It opened new opportunities to better the quality of human life in general. The progress and prosperity also brought with it- not so positive- effects of industrialisation and anthropogenic activities on the health of the planet Earth which directly or indirectly has been affecting the human life, for example,

- Air pollution resulting from industrial emissions, vehicular emissions, anthropogenic activities, and biomass burning,
- Global warming due to the emissions of green house gases,
- Ozone depletion in the stratosphere due to halocarbons.

The stratospheric ozone depletion is probably the worst effect, industrialisation has had on the atmosphere of the Earth, threatning the existence of life itself. The discovery of the ozone hole [*Farman et al.*, 1985] lead to an extensive scientific activity in order to understand the reasons and mechanisms causing the ozone hole. Halogen compounds containing chlorine and bromine were identified as the likely causes for the depletion of stratospheric ozone [*Molina and Rowland*, 1974; *Stolarski and Cicerone*, 1974; *Wofsy et al.*, 1975; *Yung et al.*, 1980]. Their role as ozone depleting substances was further confirmed by various laboratory investigations, analysis of measurements done in the stratosphere, and modeling studies. As a result of extensive scientific activity which followed the discovery of the ozone hole, the main physical and chemical mechanisms which cause the ozone depletion have been well understood but still there continue to be some discrepancies between the model predictions and observed ozone trends [*WMO*, 2002].

The "Montreal Protocol on Substances that Deplete the Ozone Layer" was signed in 1987 which called for planned phasing out of ozone depleting substances viz. chlorofluorocarbons (CFC) and brominated fluorocarbons (halons). It was further strengthened by various amendments (London, 1990; Copenhagen 1992; Vienna 1995; Montreal 1997). As a result of this protocol, contribution to chlorine from major CFCs is no longer increasing and stratospheric chlorine has plateaued in recent years [*WMO*, 2002]. However there remains an uncertainty in the total bromine in the atmosphere. There are indications that bromine in the atmosphere has more than doubled between 1980 and the late 1990s due to anthropogenic emissions of bromine containing species [*Montzka et al.*, 2003b]. The information on total bromine in the atmosphere is very important as bromine compounds have been found to have a potential to cause far greater ozone losses at per molecule level than their chlorine counterparts, owing to the short life time of the bromine reservoir species. A few parts per trillion difference can lead to

significant changes in ozone (e.g. see *Salawitch et al.* [2005]) and consequently wrong prediction in ozone trends. Bromine was predicted to be 45 times more effective than chlorine for global ozone destruction [*Daniel et al.*, 1999]. However our recent study has found that it could be 68 times more effective than chorine counterparts in global ozone destruction [*Sinnhuber et al.*, 2006].

The main contributors to bromine in the atmosphere are halons and methyl bromide (CH_3Br). The contribution from halons has continued to increase and there remains an imbalance in estimate of source and sink magnitudes for CH_3Br with sinks outweighing the sources [*WMO*, 2002]. There is also a non-negligible contribution to the total bromine from very short lived bromine species [*Dvortsov et al.*, 1999; *Nielsen and Douglass*, 2001; *Sinnhuber and Folkins*, 2005]. The work done in this thesis estimates that very short lived bromine species could contribute to about 0-7 ppt to total bromine in the stratosphere (See Chapter 10 for details).

Despite its important role in the ozone chemistry, there have been only few measurements of inorganic bromine compounds primarily due to their very low cocentration in the atmosphere. The compounds like bromine nitrate ($BrONO_2$) and bromine chloride (BrCl) have never been measured and there exist only few measurements of hydrogen bromide (HBr) and only upper limit measurements of hypobromouos acid (HOBr) in the stratosphere [*Johnson et al.*, 1995; *Nolt*, 1997]. The only major inorganic bromine compound that has been measured previously in the stratosphere is bromine monoxide (BrO) though at isolated latitudes and longitudes. Global BrO column density measurements have also been done from space by GOME instrument [*Wagner and Platt*, 1998; *Chance*, 1998; *Burrows et al.*, 1999; *Richter et al.*, 2002]. However, there existed no global profile measurements of BrO in the stratosphere previously and hence the chemical mechanisms are also not thoroughly validated. Though models reproduce the *in-situ* measurements, there are inconsistencies and differences between model results and observations.

Modeling studies suggest that almost all inorganic bromine (Br_y) in the stratosphere is in the form of BrO, $BrONO_2$, HBr, and HOBr (and BrCl if chlorine is activated) and that BrO, the ozone depleting compound could represent 40-70 % of total Br_y during the day time [*Lary et al.*, 1996a; *Sinnhuber et al.*, 2002]. The next large fraction of Br_y is formed by $BrONO_2$. The remaining inorganic bromine compounds form a very small fraction of Br_y. Thus most of the experimental information on stratospheric bromine comes from BrO and thus it is an important source of information to understand bromine chemistry in the stratosphere. Further *Richter et al.* [1999] have shown that bromine chemistry is, to a large extent, controlled by nitrogen di-oxide (NO_2) during the day time.

The Scanning Imaging Absorption Spectrometer for Atmospheric Chartography (SCIAMACHY) was launched in March 2002 [*Bovensmann et al.*, 1999]. The aim of the SCIAMACHY mission is to better our understanding of chemistry and physics of the atmosphere. Global stratospheric profiles of BrO and NO_2 can be retrieved from measurements of radiances done by SCIAMACHY. With global coverage of BrO and NO_2 profiles in the stratosphere available, it gives us a good opportunity to analyse the BrO in the stratosphere and study stratospheric bromine chemistry included in the chemical

models and validate our understanding of the chemical mechanisms. This is the main objective of this thesis.

The knowledge of the amount of BrO in the troposphere is still a topic of debate. The measurements of SCIAMACHY offer the possibility to detect the amount of BrO in the troposphere. This can be done by calculating the difference between the nadir and the limb measurements. The ability to separate tropospheric and stratospheric trace gas concentration is becoming increasingly important with our growing awareness of the very different processes in these two regions [*Schofield et al.*, 2004]. This thesis has calculated the amount of BrO below 15 km in the atmosphere using the nadir-limb measurements of SCIAMACHY.

Another major issue in atmospheric bromine chemistry, which has direct effect on the prediction of trends in ozone, is the total amount of bromine in the atmosphere. As mentioned previously, there is still an uncertainty in the total bromine present in the atmosphere. With global measurements of BrO and with known bromine partitioning from the models, it is possible to have an estimate of total bromine in the atmosphere. This thesis has estimated the total bromine in the atmosphere using the global BrO measurements. The major contributors to the total bromine in atmosphere are halons and CH_3Br and the remaining is believed to be from very short lived bromine substances (VSLS). This knowledge of contribution of VSLS to the total bromine is also still uncertain, primarily due to the lack of their measurements. This thesis has estimated this contribution using an indirect method.

In order to achieve the above mentioned, the major tasks of this study have been:

1. First comparison of SCIAMACHY data with model.
2. A validation of the retrieved BrO profiles with profiles retrieved using different methods e.g. balloon-borne measurements.
3. Preparing a climatology of BrO.
4. Calculation of BrO diurnal variation.
5. The effect of NO_x on bromine chemistry.
6. Calculation of the amount of BrO below 15 km in the atmosphere using the nadir and the limb measurements of SCIAMACHY.
7. Estimating total bromine in the atmosphere.
8. Estimating the contribution of very short lived species to total bromine in the atmosphere.

1.2 Thesis content

Chapter 2 reviews the structure and composition of the Earth's atmosphere. The ozone chemistry is also discussed in brief in this chapter.

One of the best ways to validate the understanding of chemistry of the atmosphere (stratosphere, in case of this work) is using models. Chapter 3 describes the photochemical model used in this work. As an illustration of how a photochemical model can be used to validate our understanding of chemistry, an example of a comparison of profiles of nitrate radical (NO_3), with simulations from the photochemical model used in this work is also presented.

Bromine plays an important role in the chemistry of the atmosphere, particularly in the chemistry related to depletion of the ozone in the stratosphere. Bromine chemistry is, to a large extent, controlled by nitrogen oxides. Chapter 4 discusses the stratospheric bromine and nitrogen chemistry.

The measurements of SCIAMACHY instrument on board the ENVISAT makes it possible for the first time to retrieve BrO profiles globally. Chapter 5 describes the SCIAMACHY instrument in brief. The retrieval of BrO from the SCIAMACHY measurements along with a sensitivity study done on a retrieved profile has also been discussed in this chapter.

In order to exploit the retrievals of BrO intended for scientific applications with full confidence, they need to be validated with the BrO profiles retrieved using different measurement techniques. Chapter 6 discusses the validation of the retrieved profiles with BrO profiles retrieved using the balloon-borne measurements.

The first global observations of SCIAMACHY stratospheric BrO are presented in Chapter 7. This chapter also presents the first comparison of SCIAMACHY stratospheric BrO data with simulations from the 1-D photochemical model. The construction of climatology using the data of 2003 and 2004 along with, annual variation of stratospheric BrO and impact of NO_2 on BrO is also discussed in this chapter.

The measurements of BrO in the tropical region have been sparse. Hence, in order to have a long term data set of BrO, a permanent DOAS measurement station has been set up in Nairobi (1°, 36°E) as a part of BRemian DOAS network of atmospheric measurements (BREDOM). A comparison of one year data of BrO retrieved using the Differential Optical Absorption Spectroscopy (DOAS) technique from this station with 1-D photochemical model is presented in Chapter 8.

One of the important and novel features of the SCIAMACHY instrument is the ability to observe the same air mass first in limb and thereafter in nadir-viewing geometry within about 8 minutes. This special feature of SCIAMACHY can be used to detect the amount of BrO present in the troposphere. The calculation of BrO below 15 km in the atmosphere is presented in Chapter 9.

In Chapter 10 the estimate of inorganic bromine is given along with an estimate of total bromine in the atmosphere and the contribution of very short lived species to total bromine.

Finally the summary of the thesis, conclusions reached from this study along with an outlook is given in Chapter 11.

2 The Earth's atmosphere

Our terrestrial environment can be broadly divided into five components:

1. The Lithosphere : the upper crust of the Earth
2. The Hydrosphere : the realm of water (oceans, seas, lakes, rivers, etc.)
3. The Cryosphere : the realm of ice (polar ice caps and mountain glaciers)
4. The Biosphere : all forms of animals and vegetable life
5. The Atmosphere : the gaseous envelope of the Earth

All the five components form an inter-related system in a state of dynamic equilibrium evolved through the ages.

Meteorological phenomena depend on conditions within the atmosphere and its interactions with the other four components. The earth-ocean-atmosphere system can be pictured as a vast laboratory in which variety of experiments are incessantly in progress under the influence of the energy received from the Sun. Unlike the scientific laboratory, where we can perform controlled experiments to investigate the role of different parameters associated with a particular phenomenon, the experiments which the "Nature" performs in the atmospheric laboratory are beyond human control and often several processes are simultaneously at work. This introduces a great deal of complexity in the understanding and interpretation of atmospheric phenomena.

2.1 Vertical thermal structure of the atmosphere[1]

The atmosphere is kept bound to the Earth by gravitational attraction and in a large measure rotates with it. Vertical probings of the atmosphere by temperature sensors carried aloft by balloons, rockets, and more recently remote sensing techniques have shown a broad variation of temperature up to 100 km as shown in Figure 2.1. From the surface of the Earth up to a height of about 16 km in the tropics, 10 - 12 km in the midlatitudes and 8 - 10 km in polar latitudes, temperature decreases with height at the rate of about 6.5° C km^{-1}. This decrease in temperature is called the lapse rate. This region of the atmosphere is known as troposphere. It contains almost 90% of the total mass of the Earth's atmosphere and virtually all the water vapour, clouds, aerosols[2] in the Earth's atmosphere. The troposphere is characterised by strong convective processes which result

[1] The material for this section is collected from the notes distributed during the summer school in 1987 at Indian Institute of Tropical Meteorology, Pune, India. The notes were prepared by Prof. Dr. Ananthkrishnan.

[2] Aerosols are fine suspended particulate matter (solid or liquid) in the atmosphere. They play an important role in cloud formation and condensation processes in the atmosphere.

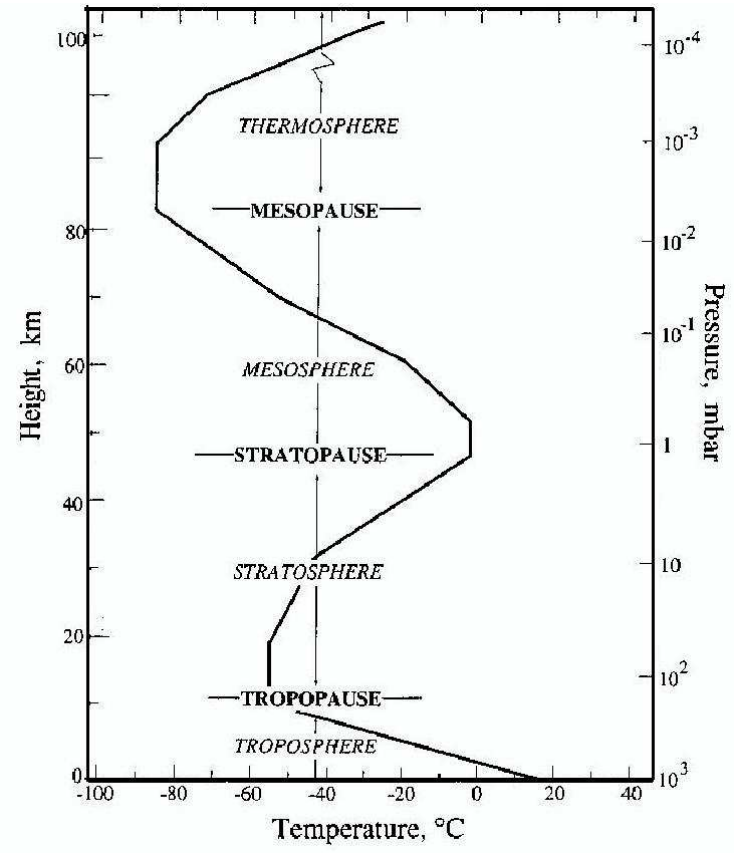

Figure 2.1: Vertical thermal structure of the atmosphere. Figure: Adapted from *Brasseur et al.* [1999]

in occurence of many weather phenomena. Above the troposphere up to the altitude of about 50 km, the temperature increases with altitude and the atmosphere becomes stable. This region is called stratosphere and contains almost all the atmospheric ozone. The rise in temperature in the stratosphere is due to the absorption of the UV radiation by ozone. Above 50 km the temperature again decreases with height reaching minimum value around 80 km. This region is known as mesosphere. Beyond the mesosphere temperature progressively increases with height up to the outer fringes of the atmosphere several hundered kilometers aloft. This region is called thermosphere.

The transitional level between the troposphere and the stratosphere is known as tropopause, that between the stratosphere and the mesosphere is called stratopause, while that between the mesosphere and the thermosphere is called mesopause.

Table 2.1: Composition of dry air

Gas	Molecular wt.	Proportion by volume in %
Dry air	28.96	100
Principal Gases		
Nitrogen	28.01	78.09
Oxygen	32.00	20.95
Argon	39.94	0.93
Carbon dioxide	44.01	0.03
Minor constituents		
Helium	4.00	4 parts per million
Neon	20.18	18 parts per million
Krypton	83.80	01 parts per million
Hydrogen	2.016	0.5 parts per million
Ozone	48.00	0-12 parts per million
Chlorine	70.9	3.5 parts per billion
Bromine	159.8	18-20 parts per trillion

2.2 Composition of the atmosphere[3]

The atmosphere is a mixture of various gases. Dry air consists of four principal gases and a number of minor constituents. The principal gases, their molecular weights and relative proportions in 100 parts of air are given in Table 2.1. Nitrogen and oxygen are the most important constituents of the atmosphere. The abundance of the inert gas Argon is about 30 times more than that of carbon dioxide (CO_2). Despite its relatively low concentration among the principal gases, CO_2 has an important role in radiative processes associated with the heat balance of the Earth-atmosphere system. Bromine and chlorine, despite their low concentration, play a very important role in the chemistry of the ozone in the atmosphere. An important constituent of the atmosphere which has not been mentioned in Table 2.1 is water vapour. The proportion of water vapour is highly variable in the atmosphere and the concentration can be as high as 4% by volume in the lowest layers of the atmosphere and plays an important role in the processes that govern the heat balance of the Earth-atmosphere system. Water has a unique feature that it exists in the atmosphere in all the three forms- gas, liquid, and solid. Excluding water vapour and gases of small concentration such as CO_2 and ozone, the composition of the atmosphere is practically constant upto the level of mesopause. This part of the atmosphere is referred to as the ”homosphere” in contrast to the overlying atmosphere which is called as the ”heterosphere” on account of changing its compostion with height.

Among the six minor constituents that are listed in Table 2.1, ozone plays an important role in the atmospheric processes and is the topic of the next section.

[3]The material for this section is collected from the notes distributed during the summer school in 1987 at Indian Institute of Tropical Meteorology, Pune, India. The notes were prepared by Prof. Dr. Ananthkrishnan.

2.3 Ozone in the stratosphere

Ozone comes from a greek word *ozein* which means "to smell". Discovered in 1840 by a german chemist Christian Friedrich Schönbein, ozone (O_3) received a widespread attention since the discovery of ozone hole in the 1980s [*Farman et al.*, 1985]. O_3 plays an important role not only in the chemistry but also in the radiation budget of the Earth's atmosphere. The concentration of O_3 varies sharply with altitude. While the concentration is very low in the lowest troposphere it increases with altitude and is highest in the stratosphere. The primary reason of O_3's importance in the Earth's atmosphere is the relationship of its absorption spectrum to the living system on the Earth. O_3 absorbs almost all the ultraviolet radiation between 240 - 290 nm. These radiations can damage macromolecules such as proteins and nucleic acid which are the characteristic of a living cell. They can also be harmful to the surface cells of plants and animals. In summary the existance of O_3 in the stratosphere makes life possible on the Earth. The absorption of the UV radiations in the stratosphere by O_3 molecules is the reason of positive lapse rate of temperature in the stratosphere and its stratified nature.

A model of production and loss of O_3 in the stratosphere was first proposed by an english scientist Sydney Chapman in 1930. It is called static pure oxygen photochemical steady state model. He suggested that O_3 is formed in two steps. In the first step oxygen (O_2) is photolysed to form oxygen atoms which then react with O_2 molecules to form O_3. He further suggested that O_3 molecule is destroyed by photolysis or reaction with an oxygen atom. The reaction mechanism proposed by Chapman is shown below.

$$O_2 + h\nu \rightarrow O + O \tag{2.1}$$

$$O + O_2 + M \rightarrow O_3 + M \tag{2.2}$$

$$O_3 + h\nu \rightarrow O + O_2 \tag{2.3}$$

$$O + O_3 \rightarrow 2\ O_2 \tag{2.4}$$

Oxygen atoms can also react with each other to form O_2 molecule

$$O + O + M \rightarrow O_2 + M \tag{2.5}$$

However it is known now that Reaction (2.5) is too slow to play an important role in stratospheric chemistry. The photodissociation of O_2 is an important step in the formation of O_3 in the Chapman mechanism. It depends on the intensity of the radiation. Also the altitude of maximum absorption of radiation depends on the absorption cross section of the molecules and the solar zenith angle (SZA). At high altitude the concentration of O_2 is too low and though the solar intensity is high it would not give too high a concentration of oxygen atoms. At lower altitudes though the O_2 molecules are in abundance, the solar intensity is too low for it to dissociate O_2 molecules to oxygen atoms. At some altitude maximum efficiency of the above mentioned mechanism is reached and consequently the maximum concentration of O_3. A mathematical function that describes the variation of the concentration of species with altitude, absorption cross section, and SZA

is called Chapman function. For absorption by molecular O_2 in the Earth's atmosphere at $\lambda \sim 220$ nm, this altitude is around 35 km. Thus according to Chapman's theory, the highest amount of O_3 concentration should be around 35 km for 0 degree SZA. But in the real atmosphere it is found that the altitude of highest photolysis rates does not necessarily correspond to the highest concentration of O_3. For example, at the equator the highest concentration is found at around 25 km but the photolysis rates are highest around 40 km. Improvements in the above simple model were suggested by taking into consideration the variation of solar intensity and SZA with latitudes, curvature of the Earth, real atmospheric temperatures, and so on. But the O_2 only chemistry model of O_3 proposed by Chapman always tended to overestimate the observed O_3 absolute concentration in the atmosphere. Hence new mechanisms, especially those causing destruction of O_3, were proposed in order to explain the discrepancy between theoretical predictions and actual observations.

The idea that loss of O_3 in the stratosphere is possible through catalytic cycle originated from the suggestion by [*Bates and Nicolet*, 1950]. They proposed a catalytic destruction cycle of O_3 which was equivalent to Reaction (2.4) but far more efficient. This chain mechanism can be represented in the following form

$$X + O_3 \rightarrow XO + O_2 \tag{2.6}$$

$$XO + O \rightarrow X + O_2 \tag{2.7}$$

– – – – – – – – – – – – – –

$$\text{Net}: \; O + O_3 \rightarrow O_2 + O_2 \tag{2.8}$$

where, X = Catalyst

Bates and Nicolet [1950] discussed the role of H and OH in regulating the abundance of the stratospheric O_3. This is called HO_x catalytic cycle. Later several species were suggested for the catalyst 'X' in the atmosphere and the corresponding catalytic cycles were named after the species. The most important of them were NO (NO_x cycle) [*Crutzen*, 1970; *Johnston*, 1971], Cl (ClO_x cycle) [*Molina and Rowland*, 1974; *Stolarski and Cicerone*, 1974] and Br (BrO_x cycle) [*Wofsy et al.*, 1975]. The catalytic cycles were indeed the missing link in solving the discrepancy between theoretical prediction and actual observation. The catalytic cycles are interlinked and the effectiveness of the cycles depend on the presence of reactive species such as OH, NO, Cl, or Br. In addition to these, there are also the so called null cycles which interconvert the X and XO species and thus not removing the odd oxygen.

Species of the catalytic families have natural sources in the unpolluted atmosphere in the troposphere. For example, for HO_x the source is water vapour or methane oxidation; NO_x originates from N_2O which is released by bactereal activities at the Earth's surface and biomass burning; the natural source of ClO_x and BrO_x is methylhalogenide produced by biological activities in the oceans and biomass burning.

In the contemporary atmosphere, anthropogenic activities have contributed significantly to the loading of ClO_x and BrO_x species through chlorofluorocarbons (CFCs) and

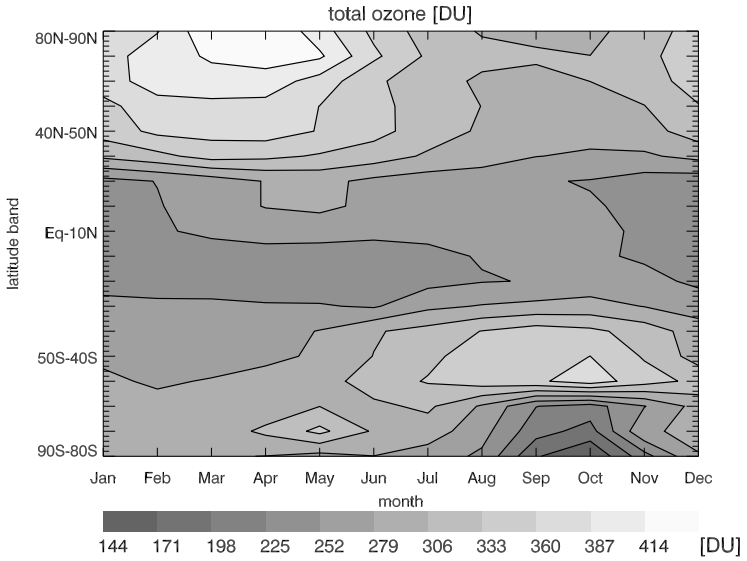

Figure 2.2: Monthly zonal mean ozone (in DU) profile climatology for the period 1990-2000. Note the hemispheric asymmetry between northern and southern mid-latitudes. The tropics show little variability. Figure courtesy: Lok Nath Lamsal

brominated fluorocarbons (halons). The halocarbons were invented in 1928 and were considered a great invention for they were non-toxic, non-inflammable, non-explosive, easy to store, and cheap to manufacture. They were primarily used as coolants, propellants in spray cans, blowers for making soft foams. The halocarbons have long life due to their insolubility in water and low reactivity and cannot be photolysed by radiations with wavelength $\lambda > 300$ nm. Thus they can easily well mix in the troposphere and transported to the stratosphere where the UV ($\lambda < 300$ nm) radiations photolyse them thus releasing the halogens which trigger the catalytic cycles discussed above. Concerns were raised about their increased usability, especially in the developed countries of the world and immense potential to cause ozone destruction through catalytic cycles [*Molina and Rowland*, 1974; *Stolarski and Cicerone*, 1974]. The fears were confirmed with the observation of large ozone depletion in the Antarctic in the 1980s.

In recognition of their huge capacity to destroy ozone, the halocarbons have been banned by an agreement reached by the international community in what is known as the "Montreal Protocol on Substances that Deplete the Ozone Layer" in 1987. The subsequent amendments (London, 1990; Copenhagen 1992; Vienna 1995; Montreal 1997) have called for systmatic phasing out of the halocarbons with large ozone depleting potentials in developed as well as developing countries.

2.3.1 Distribution of ozone

Figure 2.2 shows the distribution of monthly zonal mean ozone in Dobson Unit[4] (DU) over the period 1990-2000 for all seasons and latitudes [*Lamsal et al.*, 2006]. It is interesting to note that the rates of highest production are not in line with the areas of highest concentration. For example the rate of production of O_3 is highest at the equator but the concentration is found to be highest in the northern midlatitudes. The tropical region does not show any significant seasonal variation in ozone concentration while there is recognizable asymmetry in the northern and southern hemisphere midlatitude O_3 values. The northern hemisphere midlatitude is found to have more ozone concentration as compared to the southern counterparts. The reason for this observation is that apart from chemistry, the vertical and horizontal transport of air masses also plays an important role in distributing the ozone in the stratosphere. Air enters the stratosphere most efficiently in the tropical region. Once in the stratosphere it is dispersed further vertically and horizontally towards the poles. The exchange of air masses between the tropics and midlatitudes and that between polar region and midlatitudes in both the hemispheres are important components of the stratospheric transport. Another important component of the stratospheric transport is the exchange of air between the stratosphere and the troposphere- the so called Stratospheric and Tropospheric Exchange (STE) [*Holton et al.*, 1995].

2.4 The ozone hole in the Antarctic

The scientists of the British Antarctic Survey (BAS) had been detecting a decline in spring time O_3 at Halley Bay (76°S) in the Antarctic since 1977 and by 1984 they were certain that something dramatic was happening to the behavior of O_3 over the Antarctic. They had detected a decrease in O_3 up to 30% with depletion increasing in 1982, 1983, 1984 [*Farman et al.*, 1985]. This decrease in the ozone was called "The Ozone Hole". The present day understanding of the ozone hole can be classified into 3 parts.

2.4.1 The pre-hole condition

During the polar night, air cools and descends during winter, setting a westerly circulation of high wind speed. This sets a pronounced circumpolar wind field which is called as *vortex*. The absence of heating results in a very cold temperature within the vortex. The sinking temperature results in the formation of the so called Polar Stratospheric Clouds (PSCs). PSCs are liquid and solid condensates of nitric acid (HNO_3), sulfuric acid (H_2SO_4) and water (H_2O) which is a major component. The PSCs have been classified into two types. Type-1 PSCs primarily consist of hydrates. They have a diameter of less than 1 μm and mass mixing ratio of 10 parts per billion[5] (ppb). They are formed

[4] 1 Dobson Unit = 2.69 x 10^{16} molecules cm^{-2} at standard temperature and pressure. The unit is named in honor of G. M. B. Dobson- a British scientist, who developed a spectrophotometer for measuring ozone column. The instrument is in widespread use even today.

[5] 1 part per billion = 10^{-9}

at temperature of around 195 K. With decreasing temperature they may grow and have sedimentation. The hydrates are mainly NAD[6], NAT[7] or SAT[8]. The PSCs of type-2 have size greater than 1 mm and a mass mixing ratio of around 1000 ppb. These PSCs are primarily composed of H_2O - ice along with HNO_3 - hydrates. The PSCs act just as the surfaces for heterogeneous reactions. These heterogeneous reactions change the partitioning of chemical species by converting the relatively stable reservoir species into species which can be easily photolysed. For example

$$ClONO_2 + H_2O \rightarrow HOCl + HNO_3 \tag{2.9}$$

$$ClONO_2 + HCl \rightarrow Cl_2 + HNO_3 \tag{2.10}$$

$$HOCl + HCl \rightarrow H_2O + Cl_2 \tag{2.11}$$

$$N_2O_5 + HCl \rightarrow ClNO_2 + HNO_3 \tag{2.12}$$

$$N_2O_5 + H_2O \rightarrow 2\ HNO_3 \tag{2.13}$$

It should be noted that the presence of PSCs is not compulsory for the above reactions. The important pre-requisites are the low temperatures and the presence of surfaces for heterogeneous reactions which can equally be offered by (say) aerosols. It is a mere co-incidence that the PSCs forming at low temperatures offer a good surface for heterogeneous reactions. The above mentioned reactions then proceed with efficiency according to the nature of surface.

Reactions (2.9), (2.10), and (2.11) convert reservoir species into gaseous form (in this case to Cl_2 and HOCl). At the end of polar night and begining of the spring Cl_2 gets converted to reactive form and balance between active and reservoir species is tilted in favour of active species which starts ozone destruction through Reactions (2.6) and (2.7). This situation is called as the perturbed chemistry.

2.4.2 The begining of O_3 hole

When the sunlight returns to the poles, conversion of reservoir compounds to catalytically active species (or their precursors) begins on the surface of the PSCs leading to catalytic destruction of ozone. Figure 2.3 gives the summary of chlorine related chemistry which takes part in the O_3 destruction process. It should be noted that the two reservoir species $ClONO_2$ and HCl can react with each other on PSCs to produce Cl_2 in gaseous form

$$ClONO_2 + HCl \rightarrow Cl_2 + HNO_3 \tag{2.14}$$

[6] Nitric Acid Dihydrate
[7] Nitric Acid Trihydrate
[8] Sulfuric Acid Trihydrate

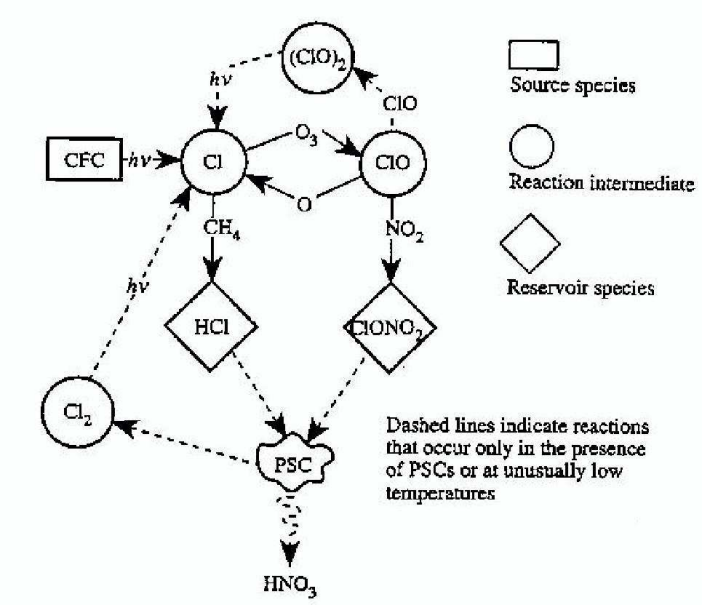

Figure 2.3: Chlorine chemistry. Chlorofluorocarbons (CFCs) are the source gases for chlroine in the atmosphere. Figure: Adapted from *Wayne* [2002]

HNO_3 formed in Reaction (2.14) remains in ice (as hydrates -NAT). The ice particles subsequently transport water and HNO_3 out of the vortex. Thus the PSCs, apart from providing a surface for chemical reactions also help in removing the nitrogen species e.g. HNO_3 out of the stratosphere and hence reducing $ClONO_2$ reservoir. Ignorance of reactions such as Reaction (2.14) on the ice particles is the prime reason that O_3 hole went undetected by chemical models. The release of molecular chlorine from the chlorine reservoir species species through the surface reactions such as Reaction (2.14) continues during the polar winter. The return of the Sun in spring results in photodissociation of Cl_2 species, trigerring the catalytic destruction of O_3 through Reactions (2.6) and (2.7). This reaction cycle is effective in the middle stratosphere however the effect decreases in the lower stratosphere due to the decrease in oxygen atoms. Of the various catalytic cycles proposed to explain the large O_3 depletion in the polar regions, the two most important reaction cycles are those involving ClO-ClO dimer cycle [*Molina and Molina*, 1987]

$$\mathrm{ClO} + \mathrm{ClO} + \mathrm{M} \rightarrow (\mathrm{ClO})_2 + \mathrm{M} \tag{2.15}$$

$$(\mathrm{ClO})_2 + \mathrm{h}\nu \rightarrow \mathrm{Cl} + \mathrm{ClOO} \tag{2.16}$$

$$\mathrm{ClOO} + \mathrm{M} \rightarrow \mathrm{Cl} + \mathrm{O}_2 + \mathrm{M} \tag{2.17}$$

$$2\,(\mathrm{ClO} + \mathrm{O}_3 \rightarrow \mathrm{ClO} + \mathrm{O}_2) \tag{2.18}$$

– – – – – – – – – – – – – – – – – – –

$$\text{Net}: \ 2\,O_3 + h\nu \rightarrow 3\,O_2 \tag{2.19}$$

and BrO with ClO cycle [*McElroy et al.*, 1986]

$$BrO + ClO + M \rightarrow Br + OClO \tag{2.20}$$

$$\rightarrow Br + ClOO \xrightarrow{M} Br + Cl + O_2 \tag{2.21}$$

$$\rightarrow BrCl + O_2 \xrightarrow{h\nu} Br + Cl + O_2 \tag{2.22}$$

$$Br + O_3 + M \rightarrow BrO + O_2 \tag{2.23}$$

$$Cl + O_3 + M \rightarrow ClO + O_2 \tag{2.24}$$

– – – – – – – – – – – – – – – – – – –

$$\text{Net}: \ 2\,O_3 + h\nu \rightarrow 3\,O_2 \tag{2.25}$$

Reaction (2.20) is the only stratospheric source of OClO. Because the concentration of OClO is directly proportional to the concentration of BrO and ClO, the presence of OClO is a good indicator of chlorine activation. These two cycles are the most efficient cycles causing large scale depletion of ozone in the Antarctic lower stratosphere.

2.4.3 The end of O_3 depletion

The breaking of the polar vortex due to rise in temperatures, the dissappearence of the PSCs and the subsequent build up of the inactive reservoir species such as $ClONO_2$ stops the ozone depletion. The conversion of the species such as ClO to reservoir species depends upon the extent of denitrification of the stratosphere and the speed with which the NO_2 rich air from the midlatitudes mixes with the polar air.

As an example Figure 2.4 summarizes the photochemical and dynamical features of polar ozone depletion. The conversion of reservoir chlorine species to active chlorine species during winter and vise versa in spring is shown in the upper panel. The lower panel shows the evolution of the polar vortex. The conversion of the reservoir species such as $ClONO_2$ and HCl to active species occurs quickly in winter. The reverse procedure begins in late spring. In general it is found that the concentration of $ClONO_2$ is more than that of HCl. The reason for this observation is that the formation of $ClONO_2$ is more rapid than the reaction which yields HCl.

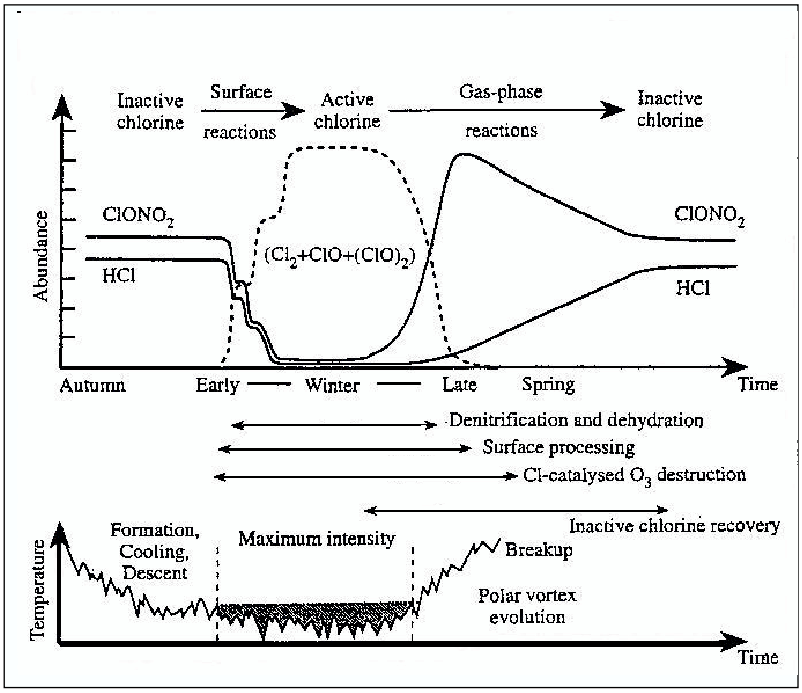

Figure 2.4: Chlorine chemistry. Figure: Adapted from *Wayne* [2002]

2.5 The ozone hole in the Arctic

In comparison to the Antarctic, the Arctic has had a less O_3 loss. The main driver which triggers the O_3 depletion is the cold temperature. The temperatures in the Arctic reach the threshhold values needed for the formation of the PSCs which offer a good surface for the heterogeneous reactions. For example Figure 2.5 shows comparison of Arctic and Antarctic temperatures. The low temperature leads to the formation of the vortex and subsequently to the formation of the PSCs. However in contrast to the Antarctic, the Arctic is less symmetric geographically. This results in the instability of the vortex region due to large scale weather systems such as the planatary waves, which increases the variability of the temperatures. This variability of temperatures results in less number of PSCs. Though the chemical mechanism for the depletion of the O_3 is exactly the same as that in the Arctic, the cold conditions which are a pre-requisite for the beginning of the O_3 hole rarely persist into March when sunlight is available to trigger a catalytic O_3 depletion cycle.

However in recent years, the Arctic has also seen unusually cold winters as compared to last 30 years. The significant among them are those of the years 1995/96, 1996/97, 1999/2000 [*Sinnhuber et al.*, 2000]. The reasons for this unusually cold winters are still not understood. However the prevailing conditions have lead to an increased ozone depletion in the Arctic as well.

Figure 2.6 shows average spring time total O_3 in DU in the polar region. From the

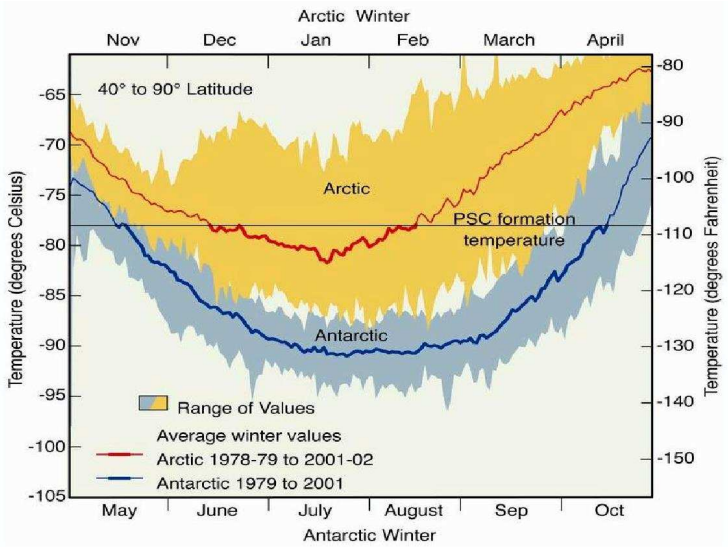

Figure 2.5: Arctic and Antarctic temperatures. The Arctic has always been warmer as compared to the Antarctic due to the geographical asymmetry between the two poles thus causing variability in the Arctic temperatures leading to less PSCs in the Arctic as compared to the Antarctic. Figure: Adapted from WMO, 2002

comparison between average ozone in the 1970s and later years it is seen that there has been increase in the ozone depletion since the 1980s. The depletion has been attributed to the halogen chemistry. The depletion has been more in the Antarctic as compared to the Arctic, the reasons for which have already been discussed. A recent past has seen an increased depletion in the Arctic as well.

2.6 Ozone at midlatitudes

Observed changes in O_3 occur primarily in polar regions and midlatitudes while no significant trends in Total Column Ozone[9] (TCO) have been observed in the tropics [*WMO*, 2002]. As already discussed in Sections 2.4 and 2.5, the polar O_3 losses are well understood. The changes in O_3 at midlatitudes have been smaller as compared to that at poles and are less well understood. The behavior of O_3 is different at midlatitudes in both hemisphere. For example, *WMO* [2002] reported that

- The Northern Hemisphere (NH) midlatitudes winter/spring decrease is approximately double ($\sim$ 4%) the summer/autumn decrease. In contrast the Southeren Hemisphere (SH) midlatitudes O_3 shows a decrease of same magnitude ($\sim$ 6%) for all seasons.

[9] TCO is the vertically integrated ozone amount

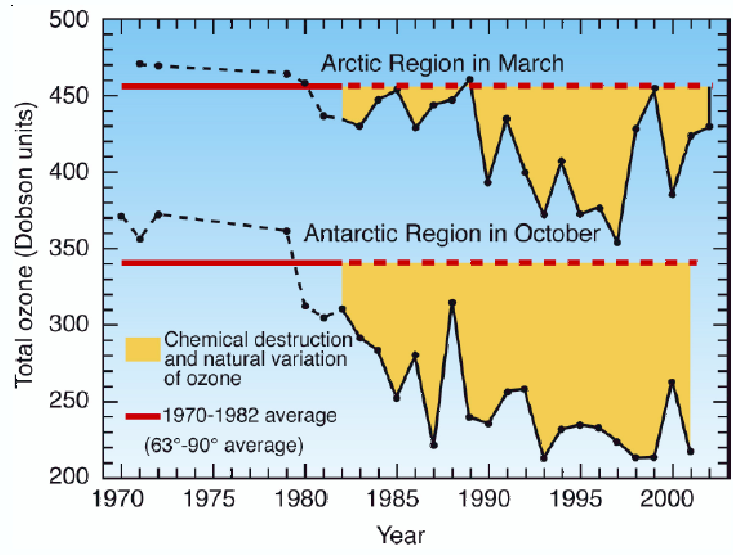

Figure 2.6: Average total ozone during spring in polar regions. The Antarctic has the largest ozone depletion as compared to the Arctic. Figure: Adapted from *WMO* [2002]

• The NH midlatitudes had a pronounced negative anomolies in TCO during 1992-95 winter/spring but are not observed in the SH midlatitudes.

• A sharp drop in the SH midlatitudes in TCO during 1985-86 is observed but not in the NH midlatitudes.

• While the TCO averaged over a period 1997-2001 was 3% below the their pre 1980 values in the NH midlatitudes, it was 6% in the SH midlatitudes.

The understanding of mechanisms responsible for the midlatitude ozone loss is important as majority of the human population resides here.

Gas phase as well as heterogeneous reactions [*Evans et al.*, 1985; *Solomon et al.*, 1998] similar to those at poles are involved in midlatitude O_3 depletion. The key reaction is the heterogeneous hydrolysis of N_2O_5 on sulfate aerosols (Reaction (2.13)). This reaction forms a stable species HNO_3 by removing active species NO_2. This decreases the effect of NO_x catalytic cycle. However this also slows the production of reservoir species such as $ClONO_2$ and $BrONO_2$ thus increasing the effect of ClO_x abd BrO_x cycles in destroying O_3. Cirrus clouds could also be a source of halogen activation [*Borrmann et al.*, 1997]. In comparison to chlorine, bromine compounds are found to play a more active role the TCO loss. Our study has found that anthropogenic bromine emissions are responsible for 45% of the column loss at northern midlatitudes between the years 1980 and 2005 [*Sinnhuber et al.*, 2006].

Dynamical variability due to enhanced aerosols [*Hadjinicolaou et al.*, 1997], north atlantic oscillations [*Appenzeller and amd J. Staehelin*, 2000], solar proton events [*Sinnhuber et al.*, 2003], solar cycle, Quasi-Biennial Osciallations (QBO), El-Nino

[*Zerefos et al.*, 1997; *Dhomse et al.*, 2006], mixing of polar air with the midlatitude air [*Millard et al.*, 2003] have also been shown to affect changes in midlatitude O_3.

Though the exact mechanisms and quantitative understanding of midlatitude O_3 changes are still not clear, results show that the combination of dynamical effects, gas phase/heterogeneous chemistry and mixing of polar air with midlatitude air tends to explain the O_3 trends at midlatitude. However the uncertainties in this trend analysis makes this an active area of research.

2.7 Ozone in the troposphere

While ozone in the stratosphere is thinning, ozone in the troposphere is rising [*WMO*, 2002]. The rise in O_3 is indeed of concern because apart from its harmful effects on human health and plants due to its poisonous nature, O_3 is an important greenhouse gas and plays a vital role in the Earth's radiation budget. Though only 10% of the total O_3 in the atmosphere resides in the troposphere, the formation and its removal is central to the chemistry of the troposphere. The sources of O_3 in the troposphere are natural as well as anthropogenic. The main natural source is the Stratosphere - Troposphere Exchange (STE) which accounts for about 475 Tg O_3/year based on observed correlation with other gases [*Murphy and Fahey*, 1994; *McLinden et al.*, 2000], while the anthropogenic sources include the photochemistry involving the nitrogen oxides and other trace gases.

The chemistry of the troposphere is different than that of the stratosphere. The negative temperature lapse rate in the troposphere leads to rapid vertical mixing through diffusion and convection. The troposphere contains 90% of the total atmospheric mass and myriad of minor trace gases are found there. Though only the solar radiation of wavelength $\lambda > 290$ nm reaches the troposphere (because of the absorption of the $\lambda <$ 290 nm by the stratospheric O_3) the important chain reactions in the troposphere are photochemically driven. O_3, NO_2, HCHO are the important chemical species which are photochemically labile at $\lambda > 290$ nm, e. g., Reaction (2.3) results in the formation of $O(^1D)$ atom. The $O(^1D)$ atom then reacts with water to form OH radical.

$$O(^1D) + H_2O \rightarrow OH + OH \tag{2.26}$$

The day time chemistry of the troposphere is dominated by OH radicals. It oxidises and chemically converts most trace constituents. This oxidative capacity of OH radicals provides an efficient scavenging mechanism for both natural and anthropogenic gases. Approximately 70% of the OH reacts with CO and 30% with methane in unpolluted atmosphere [*Wayne*, 2002].

Since H_2O itself is minor component of the atmosphere Reaction (2.26) is minor fate of $O(^1D)$ atoms as compared with quenching

$$O(^1D) + M \rightarrow O + M \tag{2.27}$$

where, M= O_2, N_2

The ground state oxygen atom formed in the Reaction (2.27) reacts with O_2 to form O_3(Reaction (2.2)). The ground state oxygen atom can also be formed through photolysis of NO_2. In fact photolysis of NO_2 is the only known way of producing O_3 in the troposphere.

$$NO_2 + h\nu \rightarrow NO + O \tag{2.28}$$

$$O + O_2 + M \rightarrow O_3 + M \tag{2.29}$$

$$OH + CO \rightarrow H + CO_2 \tag{2.30}$$

$$H + O_2 + M \rightarrow HO_2 + M \tag{2.31}$$

$$HO_2 + NO \rightarrow OH + NO_2 \tag{2.32}$$

$$---------- \tag{}$$

$$CO + 2\,O_2 + h\nu \rightarrow CO_2 + O_3 \tag{2.33}$$

Similar chain reactions can be written which involve Non-Methane Hydro-Carbons (NMHCs) and methane but in all cases NO_x must be present in order to form O_3.

2.7.1 The role of halogens in the ozone chemistry of the troposphere

The depletion of ozone very similar to that in the stratosphere has also been observed in the tropospheric boundary layer during spring time at many sites in the Arctic and northern high midlatitudes [*Barrie et al.*, 1988; *Oltmans et al.*, 1989; *Solberg et al.*, 1996; *Bottenheim et al.*, 1990; *Wagner and Platt*, 1998; *Richter et al.*, 1998] as well as in the Antarctic [*Kreher et al.*, 1997]. Data from various field campaigns and the subsequent analysis have revealed that the halogen chemistry similar to that in the stratosphere but dominated by bromine rather than chlorine is responsible for this low ozone episodes [*Barrie et al.*, 1988; *Bottenheim et al.*, 1990]. Bromine destroys O_3 in two interlinked catalytic cycles in gas phase,

$$Br + O_3 \rightarrow BrO + O_2 \tag{2.34}$$

and the reaction

$$BrO + HO_2 \rightarrow HOBr + O_2 \tag{2.35}$$

The catalytic destruction of ozone due to bromine takes place through Reaction (2.34) followed by Reaction (2.35) [*Foster et al.*, 2001]. HOBr can further photolyse to release Br atom, thus continuing Reaction (2.34). Alternatively, HOBr can react with Br ions in presence of slightely acidic sea salt solutions and releases Br_2 and BrCl into gas phase. The Br_2 molecules are easily pohotodissociated to give two bromine atoms. This sequence of reaction causes an exponential rise of Br radicals and is called bromine explosion.

3 Chemical modeling

Past, present, and future trends in atmospheric composition are the results of numerous complex physical, chemical, and biological processes which occur simultaneously in the atmosphere. Field observations and measurements give only a snapshot of atmospheric conditions at a particular time and location. To understand the underlying complex phenomenon behind such processes, a more conceptual understanding of the working of these processes is needed. Atmospheric chemistry models have the primary objective of explaining the basic science behind these complex phenomenon as well as quantifying it. Such conceptual models are a mathematical representation of the fundamental laws that govern the working of the atmosphere and other components of the geosphere. These models try to replicate the complex processes occuring in the natural system. As diagnostic tools they help us in diagnosing the key processes involved in the atmospheric phenomena. The development of these models is an iterative process which requires validation against the field measurements and the sensitivity studies of the various components of the model. Deviation of the model results from the observations is an indication of conceptual lack of our understanding of the system, which leads to further refinement of the model. Once sufficient confidence level in the model is obtained then it can be also used as a prognostic tool to provide information on the future trends of the system.

One of the aims of this work is to understand and validate our current understanding of bromine chemistry in the stratosphere using a chemical model. This chapter discusses the photochemical model used in this work. A brief overview of the different types of atmospheric chemistry models is also given in this chapter. As an illustration of how a photochemical model can be used to validate the data, an example of a comparison of profiles of nitrate radical, NO_3[1], with simulations from the photochemical model used in this work is also presented.

3.1 Components of chemical models

The central element of chemical models is the continuity equation. The concentration of each species is calculated at each pre defined individual point (called grid point). Solving the mass conservation equation taking into account advective, diffusive, convective transport as well as surface and in-situ emissions, chemical and photochemical conversions, wet and dry depositions provides the link between sources and sink of compounds

[1]The NO_3 profiles presented in this chapter have been retrieved using the lunar occultation measurements of the satellite instrument SCIAMACHY. The details of the retievals can be obtained in our publication in *Amekudzi et al.* [2005b] and can also be found in *Amekudzi* [2005]. The satellite instrument SCIAMACHY, its modes of operation, and the basics of retrieval method are discussed in Chapter 5.

and their mixing ratios. The total change in concentration (C) with respect to time (t) can be written as

$$\frac{\partial C}{\partial t} = (\frac{\partial C}{\partial t})_{advec} + (\frac{\partial C}{\partial t})_{diff} + (\frac{\partial C}{\partial t})_{convec} + (\frac{\partial C}{\partial t})_{cloud} + (\frac{\partial C}{\partial t})_{dep} + (\frac{\partial C}{\partial t})_{aero} + P - L + E \quad (3.1)$$

where, $\frac{\partial C}{\partial t}$= Change in concentrations due to advection (advec), diffusion (diff), convection (convec), cloud processes (cloud), dry and wet deposition (dep), production (P) and loss (L) due to reactions in gas phase, and E is the sources of emission.

Above equation is usually solved with the so called ”operation spliting” formulation. In this formulation different processes are isolated and each process is solved at each time step individually. Various numerical methods are used to solve the isolated processes and it should be noted that no single method is uniformly best for all models. The relative contribution of a specific process to the overall solution as well as other considerations such as boundary conditions, wind fields can lead to the use of different numerical method.

3.2 Model types

Atmospheric models have been classified into different types according to their dimensionality.

3.2.1 Zero dimensional models

A zero dimensional model (or a box model) is the simplest type of chemical model. An air parcel is considered to consist of a single independent box. The constituents of the atmosphere are assumed to be uniformly mixed and all the chemical transformation occurs in this box. A schematic of various sources, sinks, and processes affecting the chemical species considered in a box are shown in Figure 3.1. The chemical species enter or leave the box horizontally (along the wind direction). The species may enter vertically as well. The change in concentration is considered to occur through chemical interaction. The N chemical species considered in the model are represented by N differential equations which are generally non-linear. The chemical reaction rates included in the equation may have different time scales ranging from milli-seconds to years, which can present numerical difficulties in solving these equations. The equations are then said to be numerically stiff. The equations are solved using different numerical techniques. The different numerical parameters such as pressure, temperature, photolysis rates are also included in the model through their effect on chemical reaction rates.

A box model can be used in two different ways. When the box is considered to be fixed at a particular location as shown in Figure 3.1, it is called Eulerian formulation.

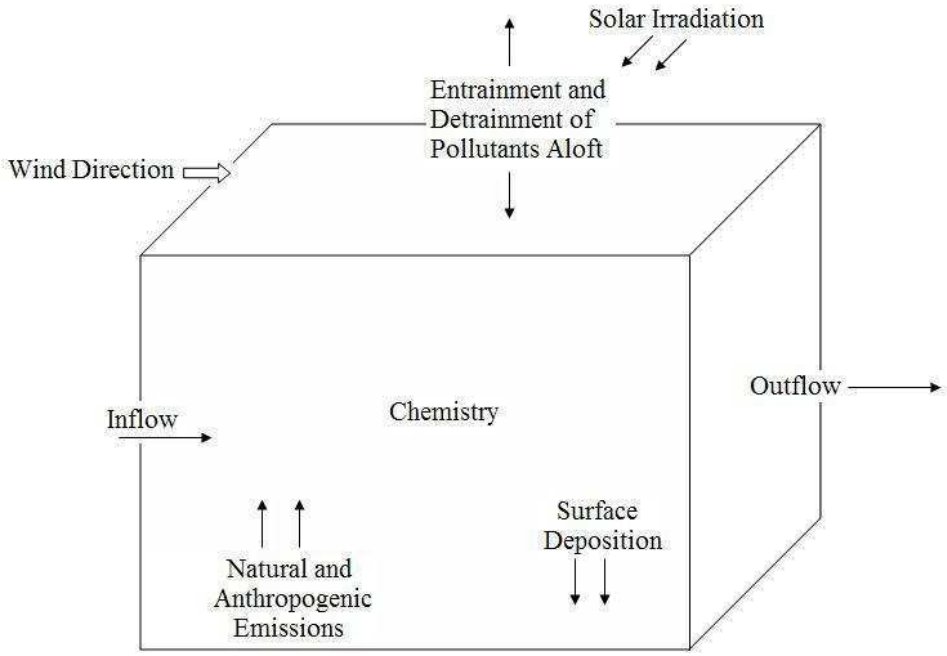

Figure 3.1: Schematic of a zero dimensional model.

In another approach, which is called the Lagrangian formulation, the box follows the atmospheric motions. In this case, the different metereological parameters affecting the chemistry in box are those which correspond to that particular location. Thus these parameters vary as the box moves along the atmospheric motions. The information about the meteorology is taken from observations or forecasts.

Though the processes considered in a box model are simplified, we do get a first impression about the atmospheric problems using box models. Box models are ideal for studying complex chemical systems which include large number of reactions and for studying the chemical relationship between species rather than individual budget. In addition the low computing demand makes them a very attractive tool to get the feel of an atmospheric issue.

3.2.2 One dimensional models

Figure 3.2 shows the schematic of one dimensional model. Most of the pioneering work in atmospheric chemistry and aeronomy has been performed using one dimensional (1-D) model [*Brasseur et al.*, 1999]. These are also called column models and consist of several box models stacked on each other. The concentration of the species is assumed to be a function of height and time. Thus, they simulate only the vertical distribution of the atmospheric species. The horizonal variation of the species is included in the model as the averaged variation only. The 1-D models consider only the latitudinal and

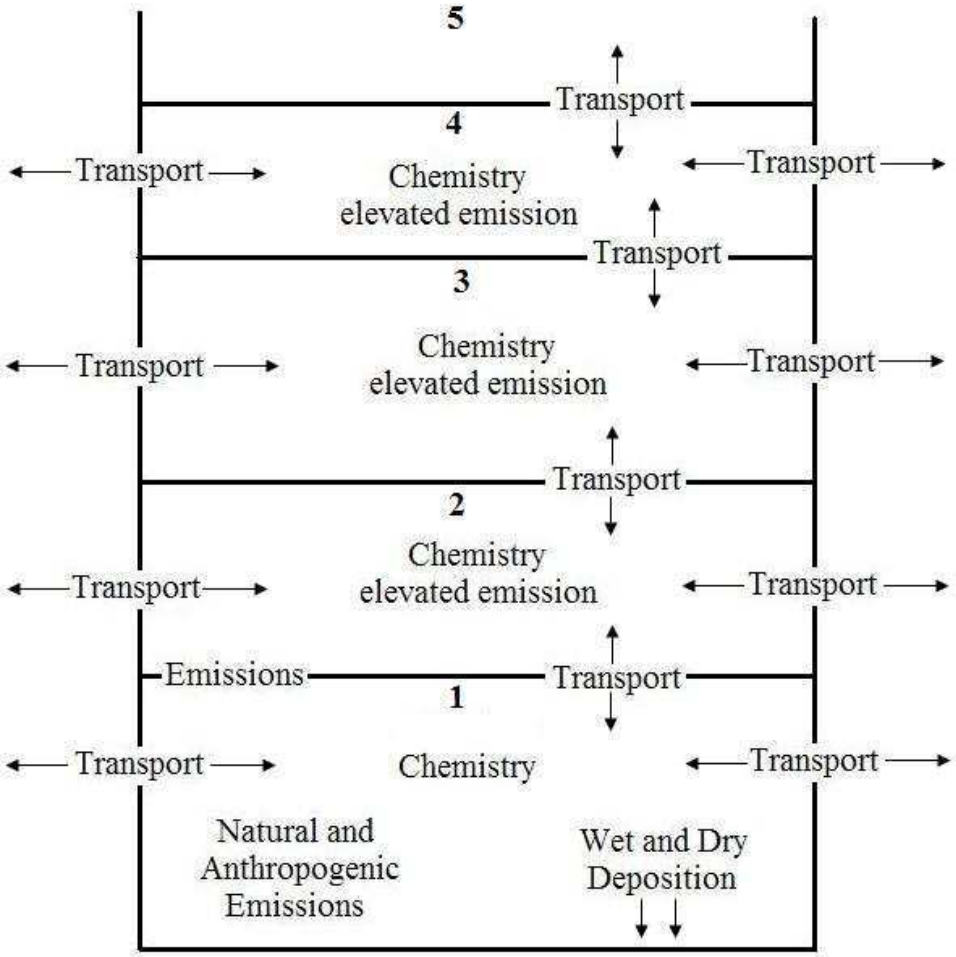

Figure 3.2: Schematic of a one dimensional model. The numbers in each block imply the layer of the model.

longitudinal average of transport. Thus they include atmospheric transport, scattering, reflection, attenuation of solar radiation and detailed chemistry. The 1-D models provide a very crude representation of dynamical exchanges. But since they are computationally inexpensive sensitivity studies are usually done using these models. In this work 1-D model has been used and is described in detail in Section 3.3.

3.2.3 Two dimensional models

The main assumption in two dimensional (2-D) model is that the atmospheric conditions are a function of latitude and altitude. The basic assumption mentioned above is true in the region above the tropopause and the variation of meteorological parameters is indeed weak longitudinally as compared to those in the troposphere and the small zonal variations are included in the model as averaged variation. Hence the 2-D mod-

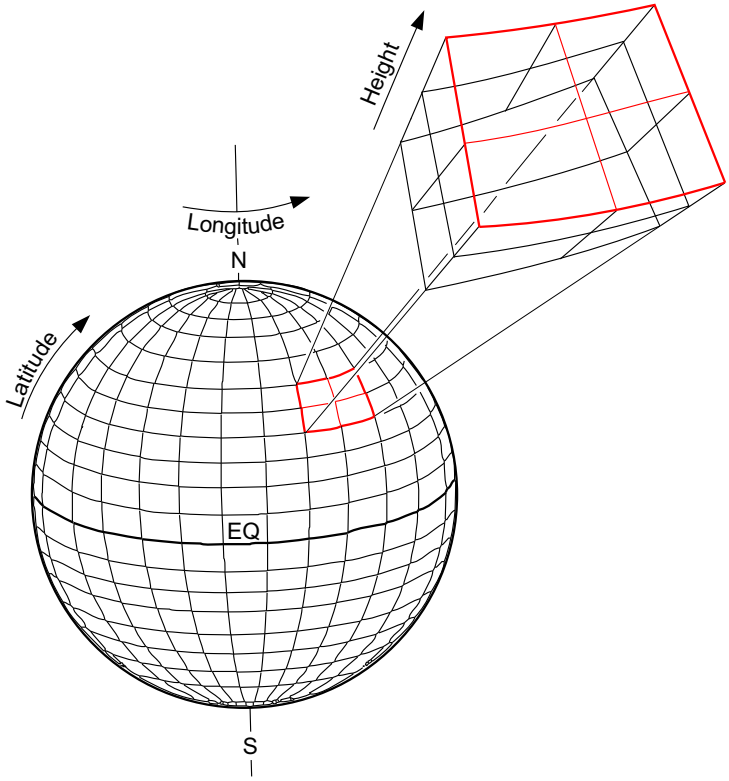

Figure 3.3: A schematic of 3-D model. Figure: Adapted from *Brasseur et al.* [1999]

els are most suited to study the stratosphere and mesosphere and are used to simulate the chemical compound behavior as a function of latitude and altitude only. However this can make the model unrealistic as some processes can be highly localised e.g. processes invoving heterogeneous chemistry [*Wayne*, 2002]. But these processes can be improved by using paramaterization that permit the incorporation of some effects of zonal assymetries [*Wayne*, 2002]. The processes of chemistry, trasport and radiation are coupled in the 2-D models and also includes feedback mechanisms. The evolution and budget of atmospheric species is studied using the 2-D models.

3.2.4 Three dimensional models

In reality, the atmosphere and the processes occuring in it are three dimensional and hence in order to simulate its radiative-chemical-dynamical behaviour the most efficient model would be a three dimensional (3-D) model. Different types of 3-D models, depending on the extent of area covered e.g. regional, mesoscale, and global, have been developed. In case of regional model the horizontal resolution is 10-100 km and the

integration time can vary from 1-5 days. On the other hand global models have a horizonal resolution between 100-500 km and the time integration is over several days to months. Figure 3.3 shows a schematic of a 3-D model. 3-D models include the advective scheme, convection, mixing, emission, depostion as well as chemical conversions in the atmosphere which need to be solved at each grid point for each species considered. This makes 3-D models computationally very expensive and demanding.

The 3-D models are often run ”off line” where the dynamical variables needed for atmospheric transport are precalculated and are stored periodically. They can also be run ”on line” but become computationally more expensive and demanding. However the ”on line” run has an advantage of having variable at each time step. Also the dynamics and chemistry are coupled unlike the ”off line” run, where it is decoupled. Coupling of dynamics and chemistry brings the 3-D models close to the reality.

3.3 One dimensional photochemical box model

The one dimensional photochemical stacked box model (henceforth 1-D model) used in this work consists of multiple boxes stacked on each other and hence the name. Each box is treated as an independent chemical system with no exchange of chemicals or mixing from the adjacent box. Thus the transport process is not included in the model. Thus there is no coupling between two boxes except for the radiation which is coupled. With slight modifications in the computer code of this 1-D model, it can be coupled with 3-D chemical transport model as well.

3.3.1 Chemical scheme

The 1-D model used in this study is meant to study stratospheric chemistry and thus contains a detailed description of the same. The appendix gives all the chemical reactions included in the model. The simplest approach to include the stratospheric chemistry in a model is to assume no photochemical equilibrium and then integrate each chemical species separately. This approach has been used in this model as well.

3.3.2 Chemical integration

Several methods are available to solve numerically, the non linear equation of the type 3.1. The acceptance of any method depends upon the ability to conserve the number of atoms and produce positive concentration values. Besides their ability to give accurate and stable solution and computational efficiency are also important criteria.
The simplest and computationally cheapest method is the Euler forward method. The direct solution of equation 3.1 is given by

$$C_{n+1} = C_n + \triangle t\, Q(t_n, C_n) \tag{3.2}$$

where,
$\triangle$ t = Time step = t_{n+1} - t_n, n=0, 1, 2...

Table 3.1: List of species included in the model

Coupled short lived species	O_x, H_2O_2, NO_x, NO_3, N_2O_5, HNO_3, HO_2NO_2, ClO_x, $ClONO_2$, HCl, HOCl, OClO, BrO_x, $BrONO_2$, BrCl, HBr, HOBr
Steady state	H, OH, HO_2, CH_3, CH_3O_2, CH_3O, CH_2O, HCO, CH_3OOH
Source gases and long-lived species	CH_4, N_2O, CO, H_2O, $CFCl_3$ (F-11), CHF_2Cl (F-22), $C_2F_3Cl_3$ (F-113), CH_3Cl, CH_3CCl_3, CCl_4, CH_3Br, $CBrClF_2$, $CBrF_3$, COF_2, COFCl, HF
Fixed species	O_2, N_2, H_2

C = Concentration of species
Q = Chemical source and sink term

Since the unknown concentration C_{n+1} at time step t_{n+1} is expressed strictly in terms of the known quantities at time step t_n, the method is called fully explicit scheme. However, this method is conditionally stable with severe restrictions on time steps.

This drawback of the restriction on time step to ensure numerical stability is overcome by the Euler backward method (fully implicit scheme), where the concentration at time step t_{n+1} is obtained by

$$C_{n+1} = C_n + \triangle t\ Q(t_{n+1}, C_{n+1}) \tag{3.3}$$

Here unfortunately we need to know C_{n+1} – the thing we are trying to calculate - to feed into the function Q. *Prima facie*, the formula seems to be of very little use. However there is a perfectly good way of solving it using the iteration technique, where a first guess for C_{n+1} is made and the process is iterated till the successive guesses for C_{n+1} converge to a single value. The accuracy however is achieved, if sufficiently small time step is used, which introduces the computational contraint similar to that of the explicit scheme. Many schemes e.g. the semi-implicit scheme, Runge-Kutta scheme exist which can be used to solve 3.1, provide accurate solutions for the stiff systems only for very small time steps making them computationally very expensive.

The default scheme used in this model to solve 3.1 is the Semi-Implicit Symmetric (SIS) proposed by *Ramaroson* [1989] for integrating the stiff set of continuity equation. Since the model is 1-D stacked box model, the change in concentration due to advection, diffusion, convection, cloud processes, dry and wet deposition, emission is not considered and equation 3.1 is expressed as

$$\frac{dc_i}{dt} = P_i - L_i c_i = Q_i \tag{3.4}$$

For N species this,3.4 can be written in vectorial form as

$$\frac{d\vec{c}}{dt} = \vec{Q}(t,\vec{c}(t)) \tag{3.5}$$

Using the trapezoidal formula, this equation reduces to

$$\vec{c}_{t+\triangle t} - \vec{c}_t = \frac{\triangle t}{2}\left[\vec{Q}(t,\vec{c}(t)) + \vec{Q}(t+\triangle t,\vec{c}(t+\triangle t))\right] \tag{3.6}$$

Using the Taylor series expansion of $\vec{Q}(t+\triangle t,\vec{c}(t+\triangle t))$ and rearranging, we get,

$$\vec{c}_{t+\triangle t} = \vec{c}_t + \frac{\triangle t}{2}\vec{J}_t\,\vec{c}_{t+\triangle t} \tag{3.7}$$

where $\vec{J}_t$ is the Jacobian matrix. Again rearranging we get,

$$\vec{c}_{t+\triangle t} - \frac{\triangle t}{2}\vec{J}_t\,\vec{c}_{t+\triangle t} = \vec{c}_t \tag{3.8}$$

$$\vec{c}_{t+\triangle t}\left[I - \frac{\triangle t}{2}\vec{J}_t\right] = \vec{c}_t \tag{3.9}$$

$$\vec{c}_{t+\triangle t}\,\vec{M} = \vec{c}_t \tag{3.10}$$

where,

$$\vec{M} = \vec{I} - \frac{\triangle t}{2}\vec{J}_t \tag{3.11}$$

The concentration at time t+$\triangle$t is thus obtained be inverting the matrix $\vec{M}$. The SIS system is unconditionally stable, accurate and relatively fast as compared to other methods solving stiff differential equations.

3.3.3 Photolysis rates calculation

Upon absorption of electromagnetic radiations, the absorbing species go to higher excited energy state. Once in excited state, they can return to a lower energy state by re-emmiting the photons (fluorescence or phosphorescence); or tranfer energy to another molecule through collision (quenching) or undergo a chemical reaction with the chemical partner. They can also undergo a unimolecular chemical change via photodissociation. The probability of occurence of any of these processes on absorption of radiation is called quantum yield (ϕ). Of these processes, photodissociation is the most

common relevant process to atmospheric chemistry. To asses the effect of photodissociationm it is important to know the rate of reaction (photolysis rate). It is calculated using the formula

$$\int_{\lambda_1}^{\lambda_2} \sigma_{\mathrm{a}}(\lambda)\ \phi_{\mathrm{a}}(\lambda)\ \mathrm{I}(\lambda)\ \mathrm{d}\lambda \tag{3.12}$$

where,
σ_a = absorption cross section[2] of species 'a' ($cm^2 molecule^{-1}$)
ϕ_a = quantum yield
I = Spectral actinic flux[3] (photons cm^{-1} sec^{-1} nm^{-1})
e.g. the reaction

$$NO_2 + h\nu \rightarrow NO + O(^3P)$$

is paramaterised in the model as

$$\frac{dNO_2}{dt} = j\ [NO_2] \tag{3.13}$$

where $[NO_2]$ is the concentration of NO_2. The photolysis rates in the 1-D model are calculated using the schemes based on *Meier et al.* [1982]; *Nicolet et al.* [1982]; *Lary and Pyle* [1991]; *Lary* [1991]. In this scheme a four dimensional look table having cordinates of pressure altitude, temperature, ozone column and solar zenith angle (SZA) is used to interpolate pre calculated values of "J" to a particular location and time in the atmosphere. Taking into consideration multiple scattering and spherical geometry, "J" values for SZA upto 96° (which is important for polar lower stratosphere) can be calculated. The photochemical data (i. e. absorption cross-section, σ, and quantum yield, ϕ) needed to calculate "J" are taken from the Jet Propulsion Laboratory (JPL) catalogue [*Sander et al.*, 2003].

3.3.4 Chemical reaction rates calculation

Apart from photodissociation there are many bi-molecular and tri-molecular reactions occuring in the atmosphere, which need to be included in the model in order to understand the chemistry of the atmosphere realistically. To include the

[2] defined as the absorption coefficient of the absorbing molecules divided by the number density of the molecules. Recall that the absorption coefficient has its origin in the Beer lamberts law.

[3] defined as the radiative flux from all directions on a volume of air. Actinic means capable of causing photochemical reactions.

effects of these reactions it is important to know the rate of the reactions. As an example consider a typical bimolecular reaction which may be occuring in the atmosphere

$$AB + C \rightarrow A + BC \tag{3.14}$$

The rate of decay of the reactants (which is equal to the rate of formation of products) is given by

$$-\frac{d[AB]}{dt} = -\frac{d[C]}{dt} = \frac{d[A]}{dt} = \frac{d[BC]}{dt} = k\ [AB]\ [C] \tag{3.15}$$

where, the square brackets denote the concentration of species and k is the reaction rate coefficient (concentration^{-1}time^{-1}). This rate coefficient is given by the Arhenius equation and is paranaterised in the model using the same

$$k = A\ \exp(-\frac{E}{RT}) \tag{3.16}$$

where,
A = A numerical constant characteristic of the reaction
E = Activation energy of the reaction
R = Gas constant in energy units, 8.314 J mol^{-1} K^{-1}
T = Temperature in Kelvin

These reaction rates are experimentally calculated, updated, and documented in the JPL catalogue. The reaction rates in the 1-D model are taken from the JPL catalogue [*Sander et al.*, 2003].

3.3.5 Negative species concentration

A chemical model may produce negative concentration of species due to the chemical integration scheme or the model transport scheme. Here we are concerned with the former as the 1-D model does not take into consideration the transport scheme. Negative concentrations are unrealistic and must be corrected. The SIS scheme used in the model conserves the total number of atoms by producing an 'overshoot' in one or more of the species belonging to a family if a family member becomes negative in concentration. This is done as follows. Consider a family of species A having n members. Then

$$P_A = \sum_{i=1}^{n} A_i \qquad (\text{for } A_i \geq 0) \tag{3.17}$$

$$N_A = \sum_{i=1}^{n} A_i \qquad (\text{for } A_i \leq 0) \tag{3.18}$$

The negative values are corrected by setting them to zero say A´= 0 for A_i less than 0 and partitioning the negative mass around the other family members of the family in proportion to their concentration as follows.

$$A'_i = A_i \left(1 + \frac{N_A}{P_A}\right) \qquad (\text{for } A_i \geq 0) \tag{3.19}$$

Thus the total concentration of the family A remains constant. It should be noted that this correction is done for each box independent of the other boxes.

3.4 Heterogeneous chemistry

Heterogeneous chemistry plays an important role in the partitioning of chemical species by converting the active halogen species to the reservoir species at high midlatitudes and polar region which subsequently affects the ozone depletion processes. The absence of heterogeneous chemistry in the model would lead to wrong analysis of halogen chemistry. In the context of this work it is important, as an active halogen species bromine monoxide (BrO) is being analysed. Hence detailed treatment is given to the heterogeneous chemical reactions considered to be important in the stratosphere including those occuring on the surface of PSCs and liquid aerosols in the model. The appendix gives the list of reactions. The analytical scheme of *Carslaw et al.* [1995a, b] is used to calculate the composition of liquid H_2O, H_2SO_4, HNO_3, and HCl aerosols along with solubilities of HBr, HOBr, and HOCl.

The prediction of the presence of NAT PSCs is done by using the model mixing ratios of HNO_3, H_2O, and temperature are used along with expression from *Hanson and Mauersberger* [1988]. The available surface area for reaction is calculated from the amount of HNO_3 condensed assuming that there are 10 NAT particles per cm^{-3}.

The presence of ice particles is found out using the Teten's equation [*Murray*, 1967].

$$P_s = 610.78 \exp\left(21.875 \frac{T - 273.16}{T - 7.66}\right) \tag{3.20}$$

where, P_s = Saturation vapour pressure (Pa)
T = Temperature (K)

By assuming that the radius of the ice particles formed is 10 μm and calculating the amount of water condensed, the surface area available for the reaction is calculated. HCl and HBr are assumed not to dissovle on the ice particles. The equilibrium NAT expression [*Hanson and Mauersberger*, 1988] is used to remove HNO_3 from the gas phase in the presence of ice particles assuming a coating of NAT on ice particles as opposed to a liquid coating.

3.5 Application of the model

As mentioned in the begining of this chapter, the primary objective of chemical models is to explain the basic science behind the complex phenomenon as well as quantifying it. The model used in this work is aimed at studying the chemistry of the stratosphere. As an illustration of how 1-D models can be used to understand and validate our understanding of the chemical processes in the stratosphere, a comparison of nitrate radical (NO_3) profiles with photochemical model used in this work is presented in this section. The NO_3 profiles were retrieved from the lunar occultation measurements of the satellite instrument SCIAMACHY on board ENVISAT from February to June 2003. But before presenting the comparison, the importance of NO_3 in the stratosphere is discussed in brief in the next sub-section[4].

3.5.1 Nitrate radical in the stratosphere[5]

Nitrate radical, NO_3, affects the chemistry of the stratosphere significantly. The concentration of odd nitrogen NO and NO_2 is controlled by NO_3 at night. It plays an active role in the conversion of NO_x to NO_y (N_2O_5 and HNO_3) which affect the diurnal variability of NO_2- a molecule which contributes significantly to stratospheric O_3. The nighttime NO_3 chemistry is governed by the following reactions,

$$NO_2 + O_3 \rightarrow NO_3 + O_2 \tag{3.21}$$

$$NO_3 + NO_2 + M \rightarrow N_2O_5 + M \tag{3.22}$$

$$N_2O_5 + M \rightarrow NO_2 + NO_3 + M \tag{3.23}$$

Reactions (3.21) and (3.22) are the main source and sink of NO_3 respectively. The reaction rate constants of Reaction (3.22) are temperature independent [*Norton and Noxon*, 1986; *Sanders et al.*, 1987; *Wangberg et al.*, 1997]. If one assumes steady state based on Reactions (3.21) and (3.23), the concentration of NO_3 can be calculated as

$$NO_3 = \frac{k_1[O_3]}{k_2[M]} + \frac{k_3[N_2O_5]}{k_2[NO_2]}, \tag{3.24}$$

where, k_1, k_2, and k_3 are the reaction rate constants of Reactions (3.21), (3.22), and (3.23) respectively and M is the number density of air. Reaction (3.23) is slow if the stratospheric temperatures are low, and one can neglect the second term on the right hand side of Equation (3.24). *Norton and Noxon* [1986]; *Sanders et al.* [1987] have show that for such conditions NO_3 concentration can be approximated as

[4] More details can be found in [*Amekudzi*, 2005]

[5] The text of this section is mainly collected from our publication in *Amekudzi et al.* [2005b]

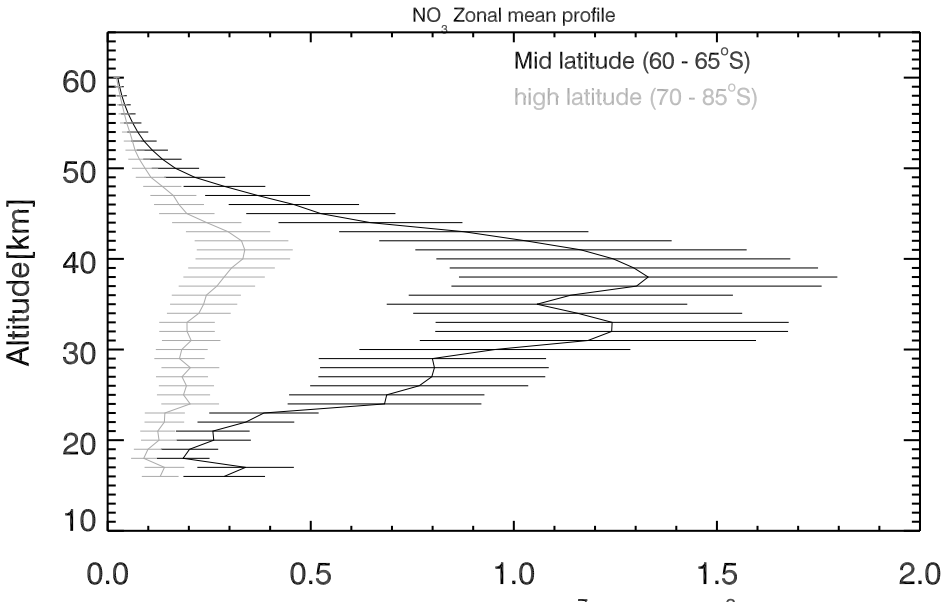

Figure 3.4: Zonal mean profiles of NO_3 retrieved from lunar occultation measurements of SCIAMACHY from March to June 2003 with possible error of 35% shown by the error bars. The black line represents the zonal mean based on the analysis of 35 profiles for the latitude band 60°S – 65 °S while the grey line represents the zonal mean based on the analysis of 95 profiles for the latitude band 70°S – 85 °S.

$$[NO_3] = \frac{k_1[O_3]}{k_2[M]}, \tag{3.25}$$

and that life time, τ, of NO_3 is given by

$$\tau = \frac{1}{k_2[NO_2][M]}. \tag{3.26}$$

During the polar winter and spring, reaction,

$$N_2O_5 + H_2O \rightarrow 2\ HNO_3, \tag{3.27}$$

is an efficient mechanism of formation of HNO_3 and PSCs.

As an example a zonal mean profile of NO_3 concentration retrieved from the lunar occultation measurements of SCIAMACHY is shown in Figure 3.4. The occultation measurements were done between March and June 2003. The latitude band of 60°S –

65°S shows highest concentration in the altitude range 36 – 40 km, while the low concentration values are observed in the latitude band 70°S – 85°S. The reason for high concentration in latitude band 60°S – 65°S is due to the contribution from the measurement data of March where the stratosphere was relatively warm. The low values of NO_3 were retrieved in the latitude band 70°S–85°S due to the contribution from the measured data in April, May, and June when the temperature in the stratosphere was relatively low.

3.5.2 Comparison of NO_3 profiles with model calculations[6]

A comparison of the retrieved profiles with appropriate chemical model is a good way to test how well the retrieved profiles agree with our current understanding of the chemistry and also to check the internal consistency of the observations. The comparison of retrieved NO_3 profiles with calculated NO_3 profiles from the photochemical model (used in this work) for 14 March 2003 (a) and for 12 April 2003 (b) is shown in Figure 3.5. The 1-D model described in Section 3.3 is initialized with the output of a global 2-D chemistry and transport model [*Sinnhuber et al.* [2003] and references therein] for the geolocation and day of the SCIAMACHY measurements. The reaction rate constants and photolysis cross sections are taken from JPL catalogue [*Sander et al.*, 2003]. The 1-D model is constrained by temperature and pressure profiles from ECMWF analyses and ozone and NO_2 profiles from SCIAMACHY observations. NO_2 is constrained by scaling the modeled NO_y (in particular NO, NO_2, N_2O_5, and HNO_3) until the modeled NO_2 agrees with measured NO_2 at the time of the SCIAMACHY measurements.

A good agreement between observed and modeled NO_3 is observed within the expected error of 35% between the altitude range of 24 - 45 km. There is a relatively large uncertainty in the modeled NO_3 concentration as a result of uncertainties in the temperature profile. We find that a 1 K increase in temperature increases NO_3 concentration by about 6%. A 5 K uncertainty in the temperature profile – which seems realistic for the Antarctic winter stratosphere – will then result in a 30% uncertainty in the modeled NO_3 profile.

The nighttime concentration of NO_3 in a steady state is given by Equation (3.24). The second term on the right hand side of Equation (3.24) accounts for the production of NO_3 due to the thermal decomposition of N_2O_5. Neglecting this term, the night time steady state concentration of NO_3 is simple and depends only on ozone and temperature as give by equation 3.25.

In order to identify the altitude regions where the second term in Equation (3.24) can be neglected, we assume that the concentration of N_2O_5 during night is in the same order of magnitude as the concentration of NO_2 or smaller. Then Equation (3.25) is a reasonable approximation, if the ratio k_3/k_2, which is the inverse of the equilibrium constant for Reactions (3.21) and (3.22), is much smaller than the NO_3 concentrations. We find that for the conditions investigated here, the simple steady state formulation is expected to be valid below an altitude of about 35 to 40 km. This is because, below

[6]The text of this section is mainly collected from our publication in *Amekudzi et al.* [2005b]

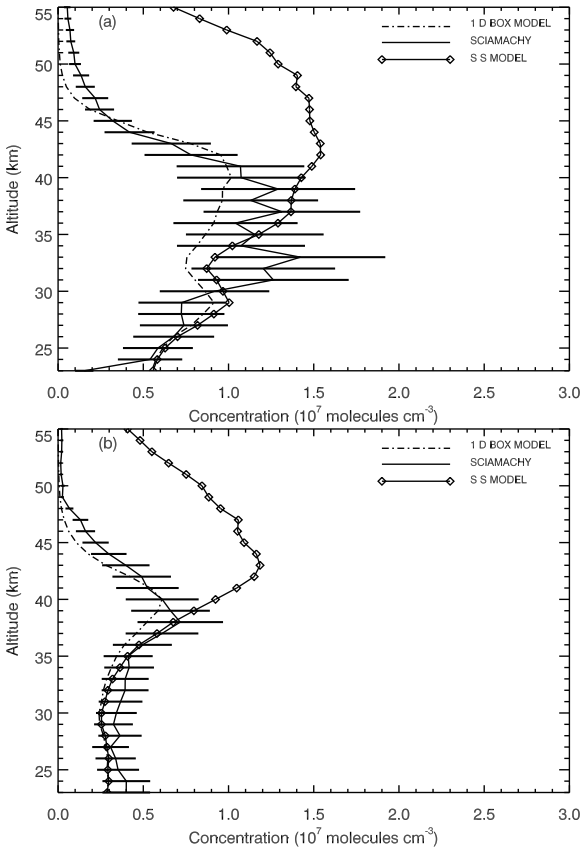

Figure 3.5: Comparison of NO_3 profiles (solid line) retrieved from lunar occultation measurements of SCIAMACHY with calculations of NO_3 from a 1-D photochemical box model (dash-dotted line) and SS model (solid line with diamonds). (a) NO_3 profile for 14 March 2003 at SZA 110 $^\circ$ (b) NO_3 profile for 12 April 2003 at SZA 115 $^\circ$.

35 km the time scales of Reactions (3.21) and (3.22) to reach steady state are in the order of an hour or less.

Also included in Figure 3.5 is the steady state (SS) model calculation according to Equation (3.22). As expected, we find a good agreement between the full time dependent model calculations and the SS model below 35 km, where the agreement is better for the April profile where temperatures are lower. Above 40 km the SS model overestimates the NO_3 concentrations.

A comparison between retrieved NO_3 profiles and those calculated using the SS model has also been carried out. The results of the monthly mean of these comparisons are shown in Figure 3.6. The dash lines are the retrieved NO_3 profiles and the solid lines with diamonds points are the SS model outputs. In general the SS model outputs are in good agreement with retrived profiles between 24 and 35 km, however some

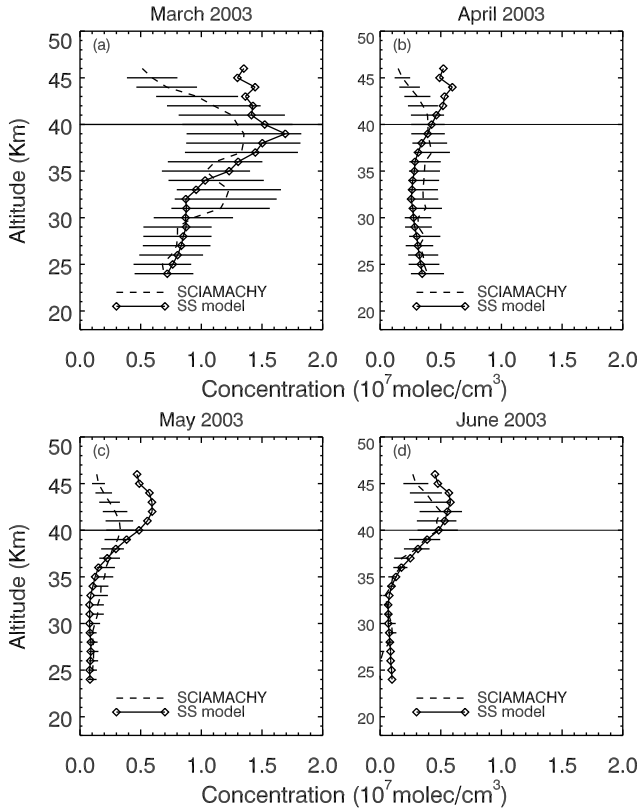

Figure 3.6: Comparison of NO_3 profiles (dashed lines) retrieved from lunar occultation measurements of SCIAMACHY with calculations of NO_3 from a SS model (solid lines with diamonds) with maximum possible error of 35 % as in Figure (3.4). (a) March, (b) April, (c) May, (d) June.

discrepancies could be observed between 30 and 35 km for March, April, and May. The SS model outputs underestimate or overestimate the NO_3 concentration retrieved from SCIAMACHY data between 30 and 35 km. The discrepancies are due to a large temperature gradient observed at such altitudes [*Solomon et al.*, 1991; *Renard et al.*, 2001]. Another possible source of error in the steady state profiles is the systematic error of less that 13% in the SCIAMACHY O_3 profiles [*Amekudzi et al.*, 2005a].

3.6 Conclusion

This chapter discusses the different types of chemical models and introduces the one dimensional photochemical stacked box model used in this work. As a real illustration of how a model can be used to validate and understand the chemistry of the stratosphere, a zonal mean retrieved NO_3 profile from SCIAMACHY lunar occultation measurements over the Antarctica has been presented. The NO_3 profiles calculated from the full 1-D

photochemical model are in good agreement with retrieved NO_3 profiles between 24 and 45 km with estimated accuracy of 20 – 35%. SS model NO_3 agree with retrieved NO_3 in the altitude range 24–40 km. The agreement supports the use of steady state approximation model to calculate global NO_3 concentrations in the middle stratosphere (24 – 40 km) and use of full photochemical model to calculate NO_3 concentrations above 40 km. The NO_3 chemistry in the stratosphere depends strongly on temperature and inaccuracy in the stratospheric temperature of less than 5 K will contribute approximately 30% error in the observed NO_3 concentrations. The lunar occultation measurements of SCIAMACHY demonstrate that we have a reasonable understanding of the behaviour of NO_3 in the stratosphere. The ratio of NO_3 and N_2O_5 is very sensitive to temperature.

4 Stratospheric bromine and nitrogen chemistry

As already discussed in Chapter 2, halogen compounds containing chlorine and bromine play a dominant role in the depletion of stratospheric ozone. The availability of active halogens, to destroy ozone, is controlled by nitrogen compounds. Here, we discuss the present understanding of stratospheric bromine and nitrogen chemistry. The diurnal variation of inorganic bromine and nitrogen compounds is also calculated using the 1-D model described in Chapter 3.

4.1 Stratospheric bromine chemistry

That bromine might have an important role in atmospheric chemistry was suggested by *Wofsy et al.* [1975]. The general importance of the atmospheric bromine chemistry and its role in the catalytic destruction of ozone by ClO/BrO cycle was proposed for the first time by *Yung et al.* [1980]. Since then a lot of progress has been made in our understanding of bromine chemistry.

Bromine compounds have a potential to cause far greater ozone losses at per molecule level than their chlorine counterparts. This is because unlike their chlorine counterparts, bromine reservoir species have very small concentration and short life time in the atmosphere and hence most of the bromine exists in active form thus participating in the catalytic ozone destruction cycles far more effectively than chlorine. Bromine was assumed to be 45 times more chemically effective than chlorine in destroying total ozone [*Daniel et al.*, 1999]. However our recent model studies have shown that bromine is roughly 68 times more effective than chlorine for global total ozone destruction [*Sinnhuber et al.*, 2006].

4.1.1 Sources of bromine

The primary sources of bromine in the atmosphere are natural and anthropogenic methyl bromide (CH_3Br) and anthropogenically produced halons released at the Earth's surface. CH_3Br accounts for more than 50% and halons account for around 40% of the total organic bromine sources (see Figure 4.1). Remaining sources are in the short lived organic bromine compounds [*WMO*, 2002], for example bromoform. The natural sources of CH_3Br include biological activities in the oceans [*Singh et al.*, 1983], biomass burning, salt marshes, wet lands, rapseed, rice fields, shrublands, fungus, and peat lands [*WMO*, 2002]. Anthropogenically, it is used primarily as fumigant, particularly for the treatment of soils, durables, perishables, and structures. It is also used

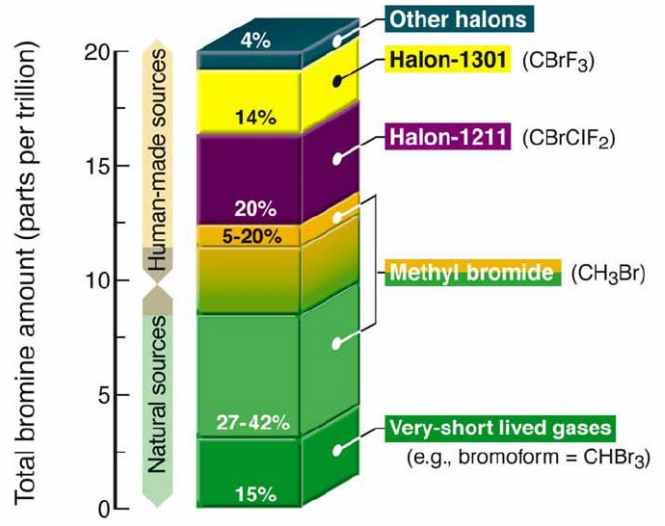

Figure 4.1: Bromine source gases. Methyl bromide and halons make largest contribution to the bromine in the atmosphere. Very short lived organic bromine gases also make non-negligible contribution to the bromine in the atmosphere. Figure: Adapted from *WMO* [2002]

in quarantine treatments and in insect and rodent control. The sinks are the oceans, photodissociation or reaction with hydroxyl radical (OH), soils and plants. Still many sources of CH_3Br are unknown and the sinks outweigh the sources [*WMO*, 2002]. The life time of CH_3Br is about 0.7 years [*WMO*, 2002]. The global mixing ratio of CH_3Br in the atmosphere is believed to range between 9 to 10 parts per trillion[1] (ppt) before the reduction in industrial usage began in the late 1990s due to the implementation of the Montreal Protocol.

Halons such as $CHBrClF_2$ (H-1211), $CBrF_3$ (H-1301) and $C_2Br_2F_4$ (H-2402) are the anthropogenic sources of bromine in the atmosphere. Halons were used mainly in fire extinguishers and as coolants. They have since been banned under the agreement reached in Montreal Protocol. However due to their long life time they would continue to contribute to the bromine in the atmosphere for many years.

Short lived species such as $CHBr_3$ [*Dvortsov et al.*, 1999; *Sturges et al.*, 2000; *Nielsen and Douglass*, 2001], dibromochloromethane ($CHBr_2Cl$), bromodichloromethane ($CHBrCl_2$) also contribute to the bromine in the stratosphere. Volcanic plumes can

[1] 1 part per trillion = 10^{-12}

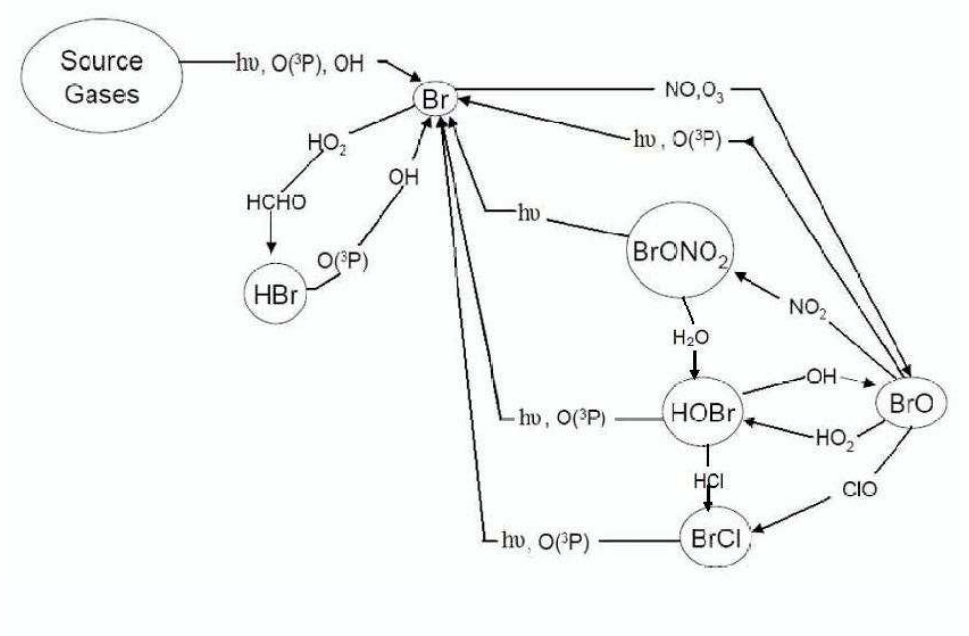

Figure 4.2: Summary of gas phase bromine chemistry. Figure: Adapted from *Lary* [1996b]

also contribute to the stratospheric bromine [*Bobrowski et al.*, 2003]. However the contribution of volcanic eruptions to the stratospheric bromine is debatable and presently uncertain. *Afe et al.* [2004] using retrievals from Global Ozone Mapping Experiment (GOME) and SCIAMACHY, found no indication of enhanced BrO during large volcanic eruptions.

The organic sources of bromine are converted to inorganic forms (Br_y = Br, BrO, $BrONO_2$, HOBr, HBr, BrCl) by photolysis or reactions with OH radicals at higher altitudes in the troposphere and stratosphere. It is these inorganic bromine species that participate in the catalytic destruction of ozone not only in the presence but also in the absence of reactive nitrogen, hydrogen and chlorine species. Of the inorganic bromine species, Br and BrO are called as reactive species while $BrONO_2$, HOBr, HBr and BrCl are called as reservoir species.

Figure 4.2 shows the schematic summary of atmospheric bromine chemistry. During the day time, the most abundant reactive species in the stratosphere is BrO. Photochemical models have shown that it forms around 40-70% of Br_y [*Lary et al.*, 1996a; *Sinnhuber et al.*, 2002]. The primary source of BrO in the stratosphere is the reaction

$$Br + O_3 \rightarrow BrO + O_2 \tag{4.1}$$

Other sources are photolysis of reservoir species like $BrONO_2$ or its reaction with $O(^3P)$ [*Soller et al.*, 2001; *Sinnhuber et al.*, 2002, 2005] and the reaction of HOBr with $O(^3P)$. The primary sink of BrO is by photolysis and reaction with NO in the lower

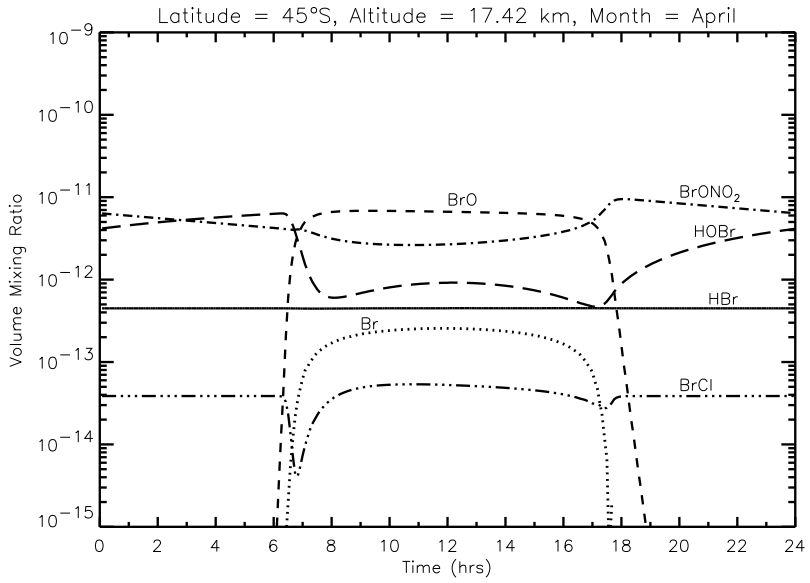

Figure 4.3: Diurnal variation of bromine species calculated by our 1-D photochemical model at 45° S for a typical condition is April.

stratosphere and reaction with $O(^3P)$ in the upper stratosphere. The reaction of BrO with ClO is also an important sink of BrO as well as an important reaction for catalytic ozone destruction (Reaction (2.20)).

Among the reservoir bromine species, the most abundant species in the stratosphere during the day time is $BrONO_2$. $BrONO_2$ is formed by a three-body reaction

$$BrO + NO_2 + M \rightarrow BrONO_2 + M \tag{4.2}$$

The concentrations of $BrONO_2$ respond very quickly to any changes in NO_2 as can occur during denoxification processes. This is not surprising as Reaction (4.2) is the primary source of $BrONO_2$ in the stratosphere. Due to its short life time it photolyses rapidly to produce BrO and NO_2 again. Thus, $BrONO_2$ is very close to a photochemical steady state during the day time. Another sink of $BrONO_2$ is the hydrolysis on sulfate aerosols to form HOBr [*Hanson and Ravishankara*, 1995; *Hanson et al.*, 1996].

$$BrONO_2 + H_2O(aq.) \rightarrow HOBr + HNO_3 \tag{4.3}$$

Reaction (4.3) is not able to compete with the rapid photolysis of $BrONO_2$ during the day time. However as the Sun sets, the photolysis of $BrONO_2$ ceases and Reaction (4.3) becomes dominant. Hence during the night time HOBr is expected to be the largest bromine reservoir species. *Erle et al.* [1998] have shown that Reaction (4.3) on cold stratospheric aerosols can be an important source of halogen activation. At night HOBr reacts with HCl forming BrCl. In the presence of large amount of aerosols (as

can happen during volcanic eruptions) and cold temperatures the rate of reaction of HOBr with HCl is faster [*Lary*, 1996b; *Danilin and McConell*, 1995].

As the Sun rises HOBr is photolysed which results in rapid increase in HO_x species.

$$HOBr + h\nu \rightarrow Br + OH \tag{4.4}$$

HOBr is also destroyed through its reaction with $O(^3P)$.

$$HOBr + O(^3P) \rightarrow BrO + OH \tag{4.5}$$

Thus Reaction (4.3) influences HO_x and NO_x concentrations which has siginificant effect on ozone depletion [*Hanson et al.*, 1996; *Lary*, 1996b].

Of the reservoir species, HBr is relatively the longest lived species. According to our present understanding of bromine chemistry, HBr forms only a small fraction of Br_y in the stratosphere. The primary source of HBr are the following reactions

$$Br + HO_2 \rightarrow HBr + O_2 \tag{4.6}$$

$$Br + HCHO \rightarrow HBr + HCO \tag{4.7}$$

Reaction (4.6) is an important source of HBr in upper stratosphere while Reaction (4.7) in an important source of HBr in the lower stratosphere [*Lary et al.*, 1996a]. A possible minor channel of source of HBr also exists through the reaction

$$BrO + HO_2 \rightarrow HBr + O_3 \tag{4.8}$$

Photochemical models which included 0-2% production of HBr through this reaction have been found to be in good agreement with field measurements [*Johnson et al.*, 1995]. The important sinks of HBr are reactions with OH and $O(^3P)$.

As already mentioned the night time source of BrCl is the reaction of HOBr with HCl. During the period of chlorine activation reservoir species BrCl is also produced by the following reaction

$$BrO + ClO \rightarrow BrCl + O_2 \tag{4.9}$$

Infact this is the smallest of the three channels which exist in the reaction of BrO and ClO. The other two channels of the reaction of BrO and ClO result in the formation of (a) OClO + Br (yield is 59%) (b) ClOO + Br (yield is 34%). The channel mentioned above in Reaction (4.9) produces 7% yield of BrCl and O_2. The yields mentioned are observed at 195 K using JPL 2002 kinetics [*Sander et al.*, 2003; *Canty et al.*, 2005]. During the day time BrCl photolyses quickly to produce Br or reacts with $O(^3P)$ to produce BrO.

Figure 4.3 shows a typical diurnal variation of bromine species at 45° S in April calculated by our 1-D photochemical model using the latest chemical reaction rates [*Sander et al.*, 2003]. Despite their important role in ozone depletion there have been only few measurements of bromine compunds in the stratosphere primarily because of their low concentration in the atmosphere. BrO can now be retrieved from the measurements of the SCIAMACHY instrument on board the ENVISAT on a global basis since March 2002. The SCIAMACHY instrument and the retrieval technique of BrO is discussed in the topic of the next chapter.

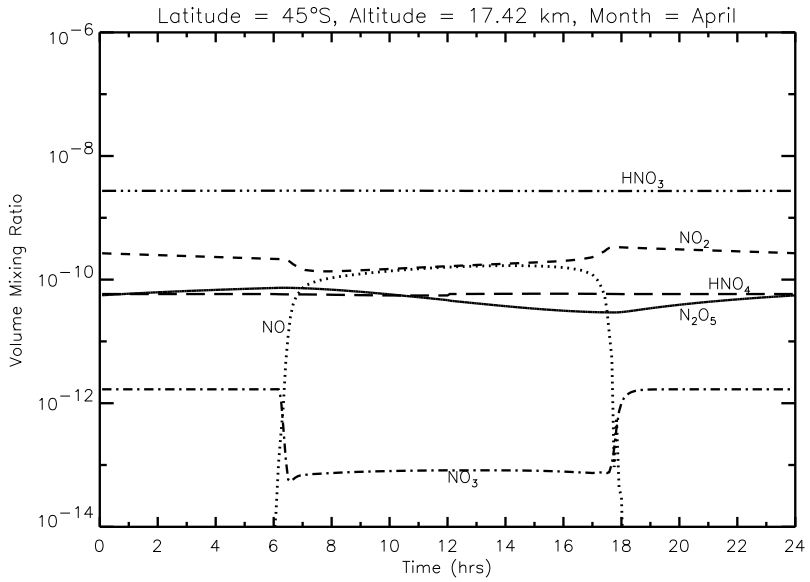

Figure 4.4: Diurnal variation of nitrogen species calculated by our 1-D photochemical model at 45° S for a typical condition is April.

4.2 Stratospheric nitrogen chemistry

Among the various catalytic cycles which cause the destruction of O_3 in the stratosphere, the cycles involving nitrogen oxides are equally important in controlling stratospheric O_3 abundance. The abundance of NO_x (NO, NO_2, NO_3) controls the concentration of ClO, BrO as well as the ratio of OH to HO_2 in the lower stratosphere and consequently the O_3. NO_x is also involved in the processes which buffer chlorine activation and oxides of nitrogen through formation of reservoir species such as HNO_3, HNO_4, $ClONO_2$,and $BrONO_2$. The following section will review the NO_x chemistry in the stratosphere.

4.2.1 Sources of nitrogen

The main source of NO_x in the stratosphere is from nitrous oxide (N_2O). N_2O is released from soils at the Earth's surface as a results of incomplete microbiological nitrification and to small extent by anthropogenic activities. It enters the stratosphere mainly through the tropical convection. Most of the N_2O in the stratosphere is destroyed by photolysis

$$N_2O + h\nu \rightarrow N_2 + O(^1D) \tag{4.10}$$

The rest reacts with $O(^1D)$ to form NO

$$N_2O + O(^1D) \rightarrow 2\,NO \qquad (58\%) \tag{4.11}$$

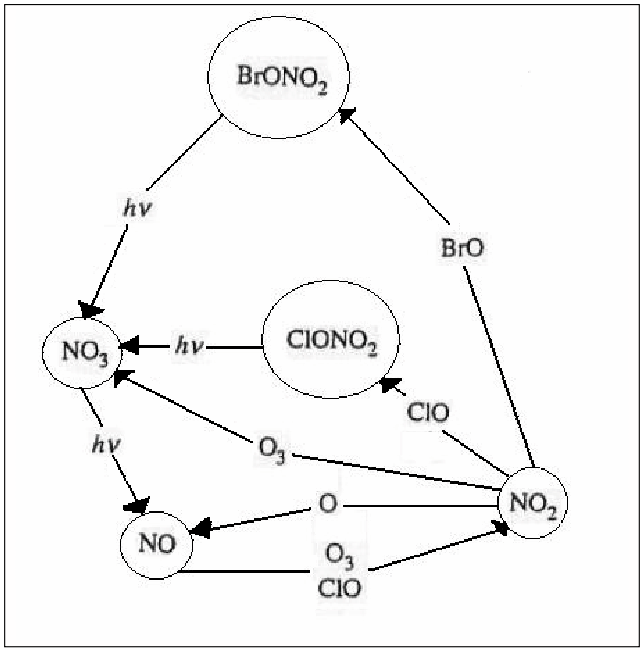

Figure 4.5: Summary of nitrogen chemistry. Adapted from *Wayne* [2002]

$$\rightarrow N_2 + O_2 \qquad (42\%) \tag{4.12}$$

Reaction (4.11) is the main source of NO in the stratosphere. The resulting NO is oxidized to NO_2 through the following reactions

$$NO + O_3 \rightarrow NO_2 + O_2 \tag{4.13}$$

$$NO_2 + h\nu \rightarrow NO + O \tag{4.14}$$

NO_2 can react with oxygen atom to form NO

$$NO_2 + O \rightarrow NO + O_2 \tag{4.15}$$

Reactions (4.13) and (2.28) form a null cycle with respect to changing odd oxygen and Reactions (4.13) and (4.15) is a classic O_3 destruction cycle. During the daytime the interconversion between NO and NO_2 is very rapid in the stratosphere and they are in the state of photochemical equilibrium.

Another NO_x cycle can also lead to the conversion of odd oxygen to even oxygen. This can take mainly in the lower stratosphere where O_3 is more abundant.

$$NO + O_3 \rightarrow NO_2 + O_2 \tag{4.16}$$

$$NO_2 + O_3 \rightarrow NO_3 + O_2 \tag{4.17}$$

$$NO_3 + h\nu \rightarrow NO + O_2 \tag{4.18}$$

– – – – – – – – – – – – – –

$$\text{Net : } 2\ O_3 \rightarrow 3\ O_2 \tag{4.19}$$

However this is a minor cycle as most of the NO_3 photolysis to give NO_2 + O_2. NO_3 plays an important role in the nighttime stratospheric chemistry and controls the concentration of NO_x. As the Sun sets the production of NO stops which results in the slow rise in the concentration of NO_2. In the absence of light, NO_3 plays a role of an intermediate molecule in the conversion of NO_x to NO_y (N_2O_5 and HNO_3) (also see Chapter 3, Section 3.5). Reaction (4.17) is the main source of NO_3 formation. NO_3 further reacts with NO_3 to form N_2O_5

$$NO_3 + NO_2 + M \rightarrow N_2O_5 + M \tag{4.20}$$

This Reaction (4.20) in the reverse direction is also an additional source of NO_3. During the night time N_2O_5 builds up at the expense of NO_x. As the Sun rises N_2O_5 is photolysed back to NO_2 and NO_3.

$$N_2O_5 + h\nu \rightarrow NO_2 + NO_3 \tag{4.21}$$

$$N_2O_5 + M \rightarrow NO_2 + NO_3 + M \tag{4.22}$$

However soon a steady state is reached between NO and NO_2 as NO_3 further photolyses to NO and O_2.

N_2O_5 is an example of a long lived reservoir species, which is formed during the night time. Other important reservoir species of NO_x are $ClONO_2$, $BrONO_2$, HNO_4, and HNO_3. Most of the reservoir species is in the form of HNO_3 below 30 km [*Jucks et al.*, 1999]. HNO_3 is formed by the following reaction

$$NO_2 + OH + M \rightarrow HNO_3 \tag{4.23}$$

Another source of HNO_3 is heterogeneous hydrolysis of N_2O_5 on PSCs and sulphate aerosols

$$N_2O_5 + H_2O \rightarrow 2\ HNO_3 \tag{4.24}$$

The formation of $ClONO_2$, $BrONO_2$, and HNO_4 takes place through the following reactions

$$NO_2 + ClO + M \rightarrow ClONO_2 + M \tag{4.25}$$

$$NO_2 + BrO + M \rightarrow BrONO_2 + M \tag{4.26}$$

$$NO_2 + HO_2 + M \rightarrow HNO_4 + M \tag{4.27}$$

The formation of these reservoir species results is decrease of active NO_x, ClO_x, BrO_x, and HO_x thus decreasing the rate of O_3 destruction. These reservoir species however can return to the active species either by their reaction with atomic species or photolysis. The bromine and nitrogen chemistry are coupled through Reaction 4.26. The Reaction 4.26 controls the amount of BrO in the stratosphere and thus the presence or absence of bromine can significantly affect the bromine chemistry. Thus BrO and NO_2 are expected to be anti-correlated. Figure 4.4 shows a typical diurnal variation of nitrogen species at 45° S in April predicted by our 1-D photochemical model using the latest chemical reaction rates [*Sander et al.*, 2003] and Figure 4.5 shows the schematic summary of atmospheric nitrogen chemistry in brief.

4.3 Conclusion

This chapter discusses the stratospheric bromine and nitrogen chemistry and their role in ozone depletion along with the known sources of bromine and nitrogen in the atmosphere. The bromine and nitrogen chemistry is coupled through reaction of BrO with NO_2. The amount of nitrogen in the stratosophere controls the amount of BrO and they are anticorrelated. The calculation of the diurnal cycle of bromine and nitrogen compounds using 1-D photochemical model has also been presented in this chapter.

5 The SCIAMACHY instrument and retrieval of BrO profiles

As mentioned in Chapter 2, significant changes have been occuring in the composition and behaviour of the Earth's atmosphere, for example, the depletion in the Antarctic and Arctic ozone during a specific period of the year, increase in the tropospheric pollution, increase in the green house gases and the consequent rise in atmospheric temperatures. This has stressed the need for measurements of the Earth's atmospheric composition. The need is further enhanced by the fact that these changes directly or indirectly affect the biological beings on the Earth. Measurement of constituents in the atmosphere can be done *in-situ* or using remote sensing techniques. Measurements of trace gas species using the *in-situ* and remote sensing techniques are performed using balloon, aircraft and ground based stations. The advantages of these platforms are high temporal and spatial coverage but the disadvantage is that they do not give global coverage of the data.

However, over the past two decades significant efforts have been made by the scientific community to increase the global coverage of such measurements by establishing more ground based measurement networks and organising multiple field campaigns. The measurement of atmospheric constituents from space has brought new dimensions to the understanding and distribution of trace gas species like O_3, NO_2, ClO, etc. The near global coverage of satellite data also helps the study of

- Transport of species (both regional and intercontinental) and dispersion of pollutants
- Regional emission strength of trace species
- Identify biomass burning areas, volcanic eruptions, etc.

The global data in association with models can be used to understand and validate our understanding of atmospheric chemistry and dynamics. This chapter gives an overview of a satellite instrument called SCIAMACHY on board ENVISAT of the European Space Agency. The basic technique to retrieve trace species from measurements of a satellite instrument is also discussed in brief. Bromine monoxide (BrO) is being retrieved globally using the limb measurements of SCIAMACHY. The retrieval process of BrO is also presented in this chapter along with sensitivity studies done on a retrieved profile of BrO. The analysis of this stratospheric BrO using the comparison with model (decribed in Chapter 3) results is the main aim of this thesis.

5.1 SCIAMACHY on ENVISAT

The Environmental Satellite (ENVISAT) was launched by the European Space Agency (ESA) in March, 2002. It flies in a sun-synchronous low polar orbit at an altitude of approximately 800 km with the equator crossing time of 10:00 local time. Scanning Imaging Absorption Spectrometer for Atmospheric Chartography (SCIAMACHY) [*Bovensmann et al.*, 1999] is one of the 10 instruments[1] on board ENVISAT. The main aim of SCIAMACHY is to help improving our knowledge of atmospheric changes and the related issues of physics and chemistry of the atmosphere such as the stratospheric ozone chemistry at high and midlatitudes, stratospheric-tropospheric exchange (STE), tropospheric pollution and its global impact, mesospheric chemistry and dynamics, etc.

The SCIAMACHY is a passive remote sensing instrument and measures extra terrestrial irradiance and upwelling radiance (i. e. sunlight which is transmitted through the Earth's atmosphere and also that reflected and scattered by the Earth's atmosphere and surface) continuosly from 240 nm to 1750 nm and in two smaller spectral windows 1940 nm – 2040 nm and 2265 nm – 2380 nm in the infra-red. The entire wavelength range is divided into eight channels to focus on a particular wavelength range. One of the most prominent features of the SCIAMACHY instrument is its ability to measure the radiations in various observational modes (nadir, limb, and solar/lunar). The inversion of these upwelling, scattered, and transmitted radiances yields information about concentration and distribution of atmospheric constituents. The concentration of trace gases is determined by their spectral features. For example, SCIAMACHY provides information about the amount and distribution of trace gases such as O_3 [*von Savigny et al.*, 2005c], CH_4, CO, CO_2, H_2O [*Buchwitz et al.*, 2000; *Buchwitz and Burrows*, 2004], NO_2, BrO [*Rozanov et al.*, 2005b], NO_3 [*Amekudzi et al.*, 2005b], H_2O [*Noël et al.*, 2004], and other parameters such as clouds, aerosols, and albedo of the Earth's surface. Another unique feature of the SCIAMACHY instrument is the combination of near simultaneous limb and nadir observations which can give information about the tropospheric contribution by subtracting the stratospheric contribution from the total column measurements in the nadir mode of observation.

5.2 Viewing geometries

SCIAMACHY measures sunlight transmitted through the Earth's atmosphere and also that reflected and scattered by the Earth's atmosphere and surface in different observa-

[1] The other instrument which is relevant to this work and is also on board ENVISAT is the Michelson Interferometer for Passive Atmospheric Sounding (MIPAS).MIPAS is a Fourier transform spectrometer. The main objectives of MIPAS are simultaneous and global measurements of atmospheric trace species in the middle atmosphere to improve our understanding of stratospheric chemistry, global climatology, atmospheric dynamics, and radiation budget of the middle atmosphere. It measures high-resolution atmospheric limb emission spectra in the near to mid infrared where many atmospheric trace species playing an important role in the chemistry of the Earth's atmosphere have emission features. The operating wavelength ranges from 14.15 microns to 14.6 microns. The atmospheric species measured in the stratosphere include for example O_3, H_2O, HNO_3, N_2O, CFCs. This work has used the CFC-11 retrievals to calculate bromine loading in the stratosphere and is discussed in Chapter 10.

Table 5.1: Spectral range and resolutions of various channels and PMDs of SCIAMACHY instrument

Channel	Spectral range	Spectral resolution	PMD	Spectral range
1	240 - 314	0.24	1	310 - 377
2	309 - 405	0.26	2	450 - 525
3	394 - 620	0.44	3	617 - 705
4	604 - 805	0.48	4	805 - 900
5	785 - 1050	0.54	5	1508 - 1645
6	1000 - 1750	1.48	6	2290 - 2405
7	1940 - 2040	0.22	45 $^{\circ}$	802 - 905
8	2265 - 2380	0.26		

tion geometry modes viz. nadir, limb, and solar/lunar occultation. The scattered and reflected spectral radiance is measured in nadir and limb geometry, while spectral radiance transmitted through the atmosphere is measured in the solar/lunar occultation mode.

5.2.1 The nadir mode

In the nadir mode of measurement, the instrument probes the volume of the Earth's atmosphere directly under it with an instantaneous field of view (FOV) of approximately 25 km along the track and 0.6 km across the track. Figure 5.1 shows a typical scan in this mode. The instrument scans the atmosphere perpendicular to the flight direction. A typical scan across the track (i. e. scanning East-West) covers a ground swath size of 960 km in duration of approximately 4 seconds followed by a fast backscan of 1 second. A possibility to use a smaller swathsize of 120 km also exists. In the nadir mode of observation a spatial resolution of 30 km (along track) and 60 km (across track) is obtained

5.2.2 The limb mode

In the limb geometry mode of observation, SCIAMACHY measures scattered and reflected radiances. The instrument observes the edge of the atmosphere in the flight direction as shown in Figure 5.1. The instantaneous FOV is approximately 103 km along the track and 2.6 km across the track at the tangent point 3000 km ahead of the satellite. A scan of 1,960 km is performed in the horizontal direction (across the track i. e. scanning East-West). During the scan, tangent altitude is kept fixed by correcting for the Earth's curvature. At the end of the scan, the line of sight is stepped by 3 km (which is the vertical resolution of the instrument in limb mode of observation) and then a reverse scan is performed. This goes up to an altitude of 100 km. The limb observations are performed in such a way that the atmospheric volume, which is observed in the limb scan, is again observed after 8 minutes in the nadir mode. A proper synchronisation

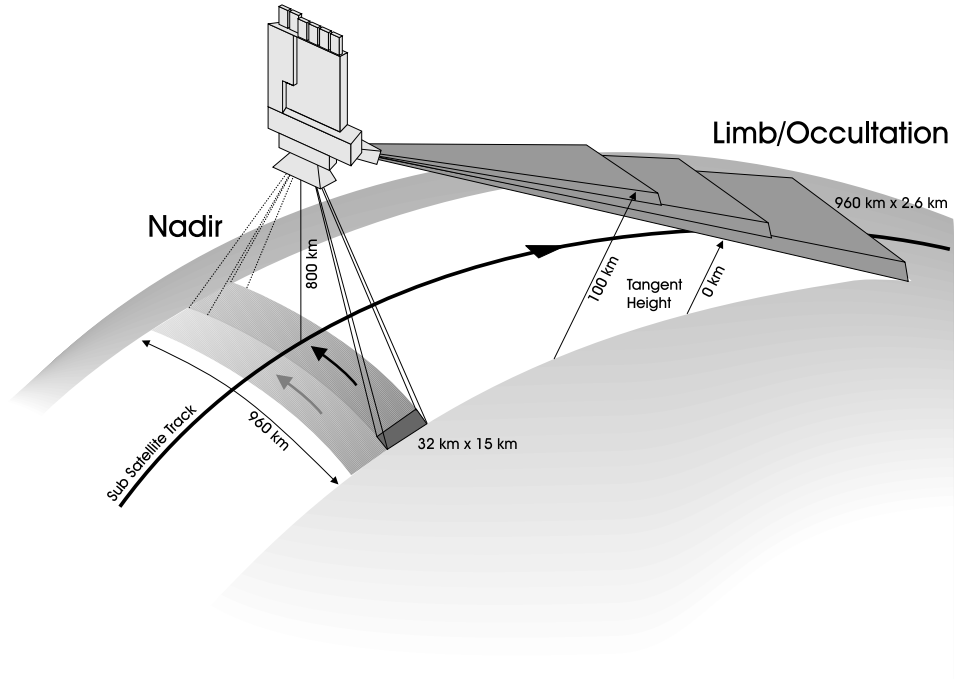

Figure 5.1: SCIAMACHY nadir and limb modes of observation. Figure courtesy: Dr. S. Noël

of this special ability (to observe same atmospheric volume in two viewing geometry modes) of SCIAMACHY enables retrieval of tropospheric column by subtracting the limb column from the nadir column as shown in Figure 5.2.

5.2.3 Occultation mode of observation

The observation geometry in the occultation mode is similar to the limb viewing geometry discussed in Section 5.2.2. SCIAMACHY observes only the rising Sun because of the forward viewing direction of the instrument and sun-fixed orbit of the ENVISAT (see Figure 5.3). The sun-tracker of the instrument has small FOV of 0.72° x 2.2°. The solar azimuth angle can be easily calculated from the orbital position of the instrument but exact time of the sunrise (i. e. the solar elevation), which depends on the variable atmospheric refraction has to be known in advance to start the measurements. The sunrise time is estimated using models. In the model the sunrise is defined as the time when the centre of the geometrical Sun reaches 17.2 km tangent height[2] [*Noël et al.*, 2000]. This is because the geometrical Sun and the refracted image of the Sun overlap at this altitude and they rise with almost identical elevation rates. This time is subsequently used

[2]In limb/occultation mode of measurements, the point where the line of sight of the satellite instrument intercepts a line that is perpendicular to the Earth geoid is called as tangent point. Then the length of line (which is perpendicular to the Earth geoid at the time of interception) from the surface of the Earth to this tangent point is called as tangent height.

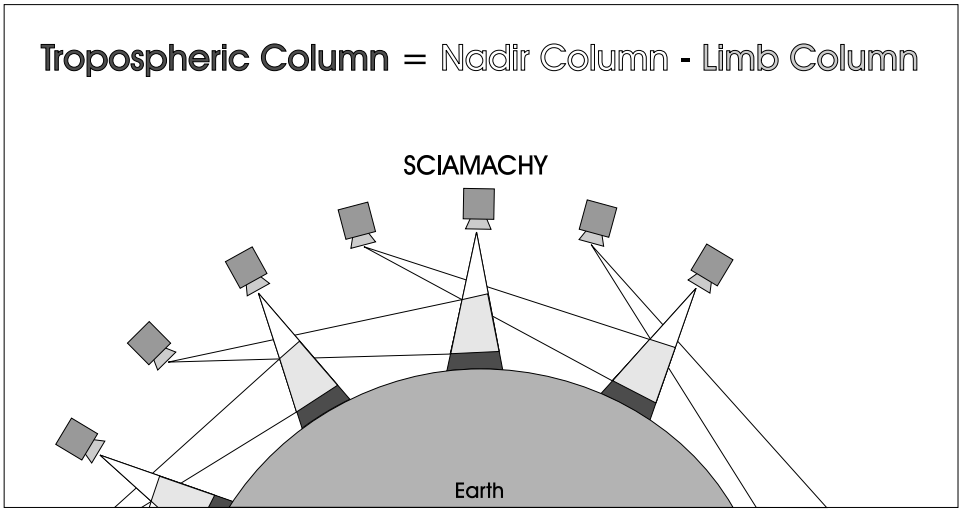

Figure 5.2: Syncronisation of SCIAMACHY nadir and limb modes of observation. Figure courtesy: Dr. S. Noël

as the reference time for the rest of the occultation measurements. The measurements in the occultation mode are performed by complete vertical scan of the Sun. The vertical tangent height resolution is approximately 2.6 km. The solar occulation measurements are limited to a small latitude band of 50°N – 70°N.

5.2.4 Lunar occultation mode

The lunar occultation mode uses the same strategy as that used for the solar occultation mode (see Figure 5.3). The measurements are performed in the Earth's atmosphere between 30°S – 90°S during local nighttime. The measurements are also possible in the northern hemisphere as well but the moonrise events usually coincide with the sunrise. While the sunrise is defined by the relatively stable position of the Sun with respect to ENVISAT's orbital plane, the properties of moonrise in SCIAMACHY's limb field of view are determined by the orientation of the lunar orbital plane and the ecliptic. In this plane a synodic period of 29.53 days is required for the Moon to complete one orbit. The rate of motion of the Moon in the limb field of view from left to right is 1° per orbit, starting lunar occultation measurements at a lunar phase of 0.6 – 0.7 and ending shortly after full Moon.

The instantaneous FOV of the SCIAMACHY instrument in the lunar occultation mode is 0.045° in the vertical direction and 1.8° in the horizontal direction. The measurements begin when the Moon reaches at an elevation of approximately 17 km similar to solar measurements. The Moon is tracked effectively up to an altitude of approximately 100 km by adjusting the moon-follower to the brightest point of the apparent Moon [*Noël et al.*, 2000]. The measurements are also performed above 100 km for instrument calibration purposes. The vertical tangent height resolution is approximately 3 km. The

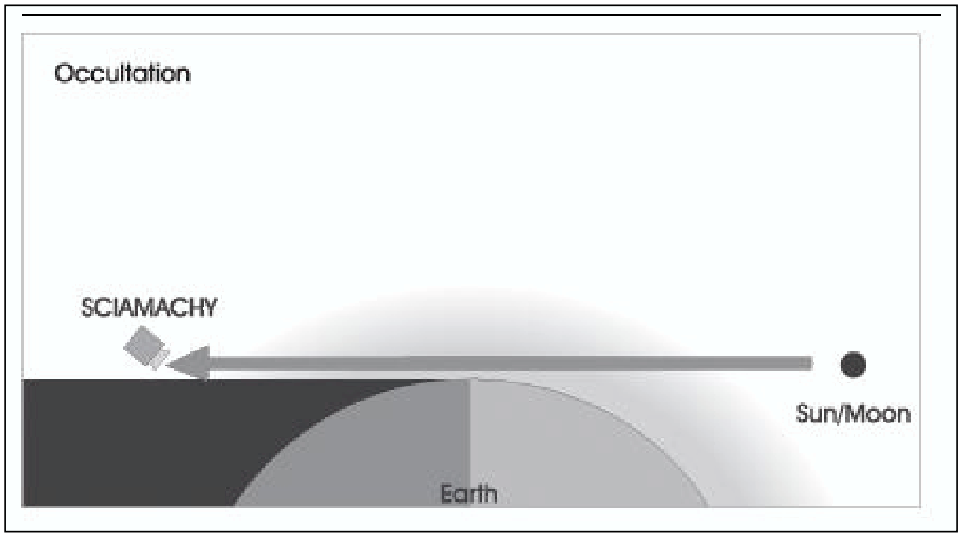

Figure 5.3: SCIAMACHY occulatation mode of observation. Figure courtesy: Dr. S. Noël

profiles presented in Chapter 3(Section 3.5) have been retrieved using the SCIAMACHY measurements in this mode.

5.3 Instrument layout

The SCIAMACHY instrument consists of three major assemblies: The optical assembly (a mirror system, a telescope, and a spectrometer), a radiant cooler and electronic subsytem. Two scan mechanisms namely the Azimuth Scan Mechanism (ASM) and the Elevation Scan Mechanism (ESM) are used to steer the viewing directions of SCIAMACHY and direct light into the instrument. The viewing angles are delivered by the optical encoders in the scan mechanisms. Figure 5.4 shows a schematic view of optical configuration of the instrument. The light enters the instrument via one of the three ports:

1. In nadir observation mode, the nadir mirror (ESM) directs the light into the telescope which collimates the beam and directs it into the entrance slit of the spectrometer.

2. For limb and solar/lunar observation mode, limb and nadir mirrors (ESM/ASM) are used to direct the beam to the telescope which subsequently focuses it on to the entrance slit of the spectrometer.

3. The light from the spectral and white lamps is directed by the nadir mirror into the telescope and then to the entrance slit. These lamps are used for calibration purposes.

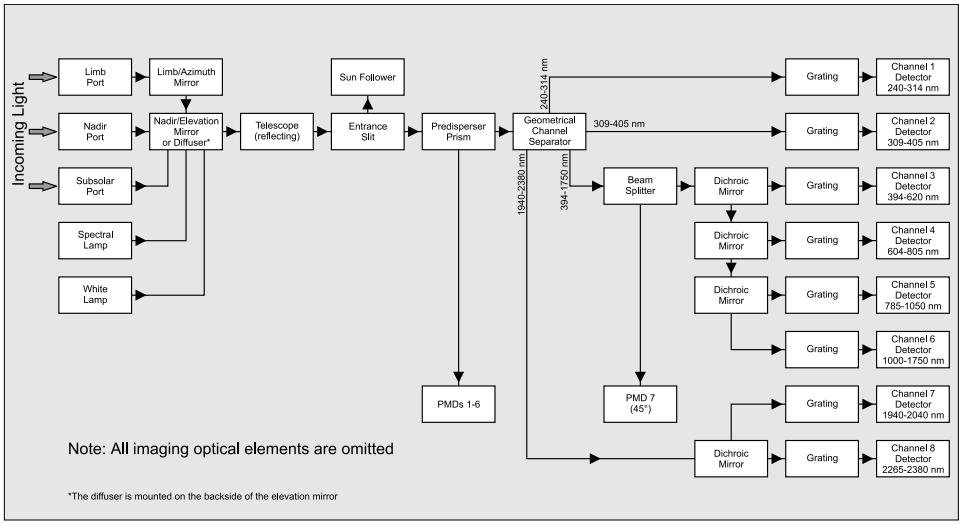

Figure 5.4: Schematic layout of optics of SCIAMACHY. Adapted from *Bovensmann et al.* [1999]

The collimated beam of light enters the predispersing prism. The light is separated into four parts using reflective optics. The radiations of shorter wavelengths are directed to channels 1 and 2. The majority of the beam is directed to channels 3 to 6. The high wavelength radiations of the beam in the infrared are directed to channels 7 and 8. Dichroic mirrors select the wavelength range for channels 3 to 6 and separate light for channel 7 from channel 8. Each channel is an assembly of grating, transmission optics and diode array detector. The grating is used to disperse and focus the light on detectors consisting of 1024 pixels. Table 5.1 gives the wavelength range of all the channels along with spectral resolution of all the channels. The raw measurements (detector counts) of the instrument need radiometric correction which depends on the state of polarization of the incoming light as well as on the properties of polarization of the instrument. This correction can be done using on-ground and in-flight radiometric correction measurements. The in-flight radiometric measurements are performed using the 7 Polarization Measurement Devices (PMDs) (see Table 5.1) fitted in the instrument. The combination of array detector data, PMD measurements and on ground polarization measurement calibration data enables the polarization of the incoming light for nadir measurements [*Kruizinga et al.*, 1994; *Frerick et al.*, 1997]. The light is off the optical plane of the spectrometer in limb measurement mode. This demands an additional polarization information and thus also the measurement which is performed by PMD 7 by measuring 45° component of the light extracted from the channels 3 – 6 light path.

A radiant cooler is used to cool the diode array detectors in order to minimise noise and dark currents. The UV channels are cooled at 200 K, the visible channels at 235 K and the infrared channels are cooled at constant temperature of 150 K. The electronic assembly of the SCIAMACHY instrument consists of the main electronic units with power,

command and control and telemetry interfaces. A more detailed description of the instrument and its capabilities can be found in *Bovensmann et al.* [1999].

5.4 Data products

The organization of the SCIAMACHY data products is shown in Figure 5.5. The raw data i. e. the detector counts, are called the Level-0 data. Applying calibration parameters using the instrument characteristics data base obtained from on-ground and in-flight data base, orbit and altitude information gives geo-located and calibrated radiance spectra which is called the Level-1 data. Retrieval algorithms are used subsequently to get Level-2 data which contains information about the various atmospheric components such as vertical profiles and columns of trace gases, cloud top height, cloud coverage and aerosol optical depth. The retrieval procedure needs a radiative transfer model and various parameters mentioned in Figure 5.5. The Level-2 data is based on measurements performed during each orbit of approximately 100 minutes duration. The global coverage is obtained in approximately 3 days by assembling a total of 42 orbits. The Level-2 products are further processed to yield global maps of say trace gas distribution.

The data products are futher divided in to Near Real Time (NRT) and off-line products. NRT products are a fast delivery products available within few hours after obtaining the measurements. NRT processing employs look up tables for radiative transfer instead of using the operational running models. Off-line products are produced using ancillary data that becomes available after spectrum aquisition e. g. analysed temperature and pressure fields.

5.5 Performance of the SCIAMACHY instrument

Since its launch, the performance of SCIAMACHY, is in general excellent. No hardware problems have been encountered and the performance is on expected lines of tests performed on ground. The degradation with time is very small. However there are some problems associated with near infrared channels 7 and 8. There is an unexpected formation of water ice on channels 7 and 8 [*Lichtenberg et al.*, 2005]. The source, which has been speculated to be the reason of contamination, is the carbon fibres, which support the structure of ENVISAT and which are known to accumulate water. The observed phenomenon is due to the gasing out of water. Two other instruments on ENVISAT have also reported a similar problem [*Smith*, 2002; *Perron*, 2004]. The formation of ice on the channels attenuates the signal which results in low signal-to-noise ratio in the reflectances. This could consequently affect the retrieval of the trace gases. The correction of the transmission has not been applied in the operational processing, however the operation of the instrument now includes running of the decontaminators regularly [*Lichtenberg et al.*, 2005] in order to remove the accumulated ice. Another problem which has been reported is the light leak in channel 7 [*Lichtenberg et al.*, 2005] for which no correction algorithm has been developed so far and which could affect the retrievals in this channel [*Lichtenberg et al.*, 2005].

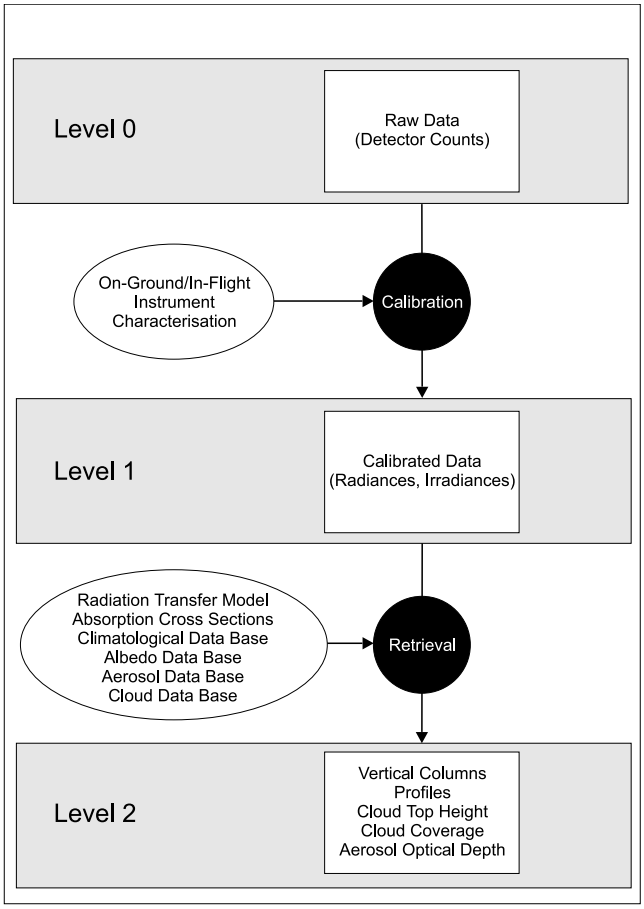

Figure 5.5: Organisation of SCIAMACHY data products. Figure courtesy: Dr. S. Noël

An important issue which is the main source of errors (and relevant to this work as well) for retrievals of trace gases using limb measurements is the limb pointing of the SCIAMACHY which has shown seasonal behaviour [*von Savigny et al.*, 2005a]. This incorrect pointing information results in wrong tangent height (TH) information of the retrieved trace gas. A wrong TH information results in errors in the retrieved gas as well. For example, 500 m TH error leads to errors in the retrieved ozone concentrations up to 10 % in the stratosphere [*von Savigny et al.*, 2005b]. Hence the pointing error needs to be taken into consideration in the retrieval procedure which then improves the accuracy of the retrieved profiles.

5.6 Retrieval of trace gases

5.6.1 Radiative transfer equation

The Earth and the rest of the universe exchange energy by way of radiative transfer. The solar radiations are continuously absorbed by the Earth and the atmosphere. They also emit radiations. These emitted radiations by the Earth and the atmosphere are intercepted by the sensors of the satellite instruments, and form the basis of technique which is used to retrieve temperatures, pressures and concentrations of various trace gases.

At the base of any retrieval technique is the Radiative Transfer Equation (RTE). The RTE deals with the change of radiance[3] as the radiation passes through the atmospheric volume. Consider a radiation beam passing through atmosphere, then the various processes that could affect the radiation are as follows:
A- Radiation can be absorbed by the atmosphere
B- Radiation can be emitted by the atmosphere
C- Radiation can be scattered out of the beam into other directions
D- Radiation from other directions can be scattered into the beam

The rate of changes in radiance, L_λ, with distance, s, is given by

$$\frac{dL_\lambda}{ds} = A + B + C + D \tag{5.1}$$

The terms A and C remove the radiation from the beam and hence they are called depletion terms while the terms B and D add radiation to the beam and hence are called addition terms. Equation (5.1) is known as the RTE. It should be noted that we have ignored the polarization of light which should also be considered in the above equation. The basic laws of physics which are used to replace the more general terms given on the right hand side of the Equation (5.1) are Beer-Lambert's law and Planck's function.

5.6.2 Retrieval technique

A set of computer codes, which solves the RTE is called as the radiative tranfer model or more popularly as forward model in the realm of satellite data analysis. The main aim of a forward model is to simulate the measurements of remote sensing instruments which measure the radiations emitted by the Earth and its atmosphere. The calculation of observed radiances on the basis of known temperature and trace gas profiles is called as the forward problem. The measurement of the radiations by the satellite instrument poses a question: What temperature and trace gas concentration profiles could produce a set of observed radiances ? This is known as the inverse problem or retrieval problem.

Representing the atmospheric measurements by measurement vector y and the corresponding state of the atmosphere by state vector x and noting that for each state vector there is a corresponding measurement vector, then y and x are related non-linearly as:

[3] Defined as the rate of change of energy per unit area per unit solid angle.

$$\mathrm{y} = \mathbf{F}\mathrm{x} + \varepsilon, \tag{5.2}$$

where, **F** is a non-linear forward model operator and ε is the vectors of errors which includes contributions from measurement errors and short comings of the forward model. If the forward model is linear then the above relation can be modified by expanding Fx using Taylor series as follows:

$$\mathbf{F}\mathrm{x} \approx \mathbf{F}\mathrm{x}_0 + \frac{\delta \mathbf{F}}{\delta \mathrm{x}}\|_{\mathrm{x}_0} \times (\mathrm{x} - \mathrm{x}_0), \tag{5.3}$$

The Equation (5.2) gets modified using Equation (5.3) to:

$$\mathrm{y} = \mathrm{y}_0 + \mathbf{K}(\mathrm{x} - \mathrm{x}_0) + \varepsilon. \tag{5.4}$$

Here, **K**= $\frac{\delta F}{\delta x}\|_{x_0}$ is the linearised forward model operator, x_0 is an *a priori* state vector, and y_0 is a measurement vector corresponding to the *a priori* state vector x_0 i. e.

$$\mathrm{y}_0 = \mathbf{F}\mathrm{x}_0,$$

The above calculation is done by the forward model. With known *a priori* information, the forward problem is easy to solve. In comparison the inverse problem (i. e. Equation (5.4)) is difficult to solve as infinite solutions are possible. The retrieval problem then becomes of finding profiles that will minimise the difference between the observed radiance and simulated profile. One of the most popular methods to minimise these differences is the so called optimal estimation method. A more detailed information on the RTE and can be found in *Rodgers* [2000]; *Rozanov* [2001]. But the general approach to the retrieval technique is as follows:

1. A first guess of the profiles is chosen (also called as *a priori* profile).
2. The weighting functions[4] are calculated.
3. The forward model is used to simulate the observed radiances.
4. If the simulated radiances match the observed radiances within the specified errors of the noise levels, the current profile is accepted as the solution.
5. If the convergence has not been achieved, the current profile is adjusted.
6. Steps 3 to 5 (or 2 to 5) are repeated until a solution is found.

[4]Weighting function at a particular wavelength is defined as a variation of the outgoing radiances due to a variation distribution of the atmospheric parameter (say) temperature or the concentration of a trace gas. The weighting function is also called as Jacobian.

5.7 Retrieval of BrO profiles from limb measurements[5]

Bromine chemistry plays an important role in ozone depletion process and is discussed in detail in Chapter 4. Among the inorganic bromine species, the only major inorganic bromine compound that has been measured previously in the stratosphere is bromine monoxide (BrO). BrO has been measured in-situ by resonance fluorescence spectroscopy from both aircraft [*Brune et al.*, 1989; *Toohey et al.*, 1990; *Avallone et al.*, 1995] and balloon *McKinney et al.* [1997]. BrO profiles have also been measured from balloon borne UV-visible spectroscopy [*Pundt et al.*, 2002; *Harder et al.*, 1998]. Ground based UV-visible spectroscopy [*Carroll et al.*, 1989; *Solomon et al.*, 1989; *Fish et al.*, 1997; *Richter et al.*, 1999; *Otten et al.*, 1998; *Frieß et al.*, 1999; *Sinnhuber et al.*, 2002] has been used to measure BrO slant column densities. BrO column density measurements have also been done from space by the GOME instrument [*Wagner and Platt*, 1998; *Chance*, 1998; *Burrows et al.*, 1999; *Richter et al.*, 2002]. BrO can now be retrieved from the measurements of the SCIAMACHY instrument on board the ENVISAT on a global basis since March 2002 [*Rozanov et al.*, 2005a; *Afe*, 2005]. Also, SCIAMACHY now allows for the first time a global view of stratospheric BrO profiles. The limb scattering retrieval is a powerful technique in the sense that it combines global coverage with high vertical resolution of the order of 3 km. Thus the retrieval of BrO offers a wealth of information and an opportunity to understand and validate our knowledge of bromine chemistry in association with chemical models. This section discusses the retrieval of BrO from SCIAMACHY measurements. A sensitivity study done on a retrieved BrO profile is also presented.

The basics of the retrieval procedure of have already been explained in Section 5.6. The forward simulations of the SCIAMACHY limb measurements are done employing the SCIATRAN radiative transfer model (RTM) [*Rozanov*, 2004; *Rozanov et al.*, 2005c]. In the spherical mode the SCIATRAN model calculates the limb radiance properly considering the single scattered radiance and using an approximation to account for the multiple scattering. The RTM also calculates the weighting functions of atmospheric trace gases which are needed in the retrieval procedure to evaluate the vertical distributions.

For the measurements presented in this work, vertical distributions of BrO were retrieved from the SCIAMACHY limb measurements using the spectral information in the 337 – 357 nm wavelength interval. To improve the retrieval quality, vertical profiles of O_3 and NO_2 were estimated in combination with BrO retrievals using the same spectral information. Limb measurements performed at tangent heights from 12 to 30 km were considered. To reduce the impact of the Fraunhofer structure and incorrect instrument calibration all selected limb scans were divided by the reference limb measurement obtained at a tangent height of about 33 km. To account for broadband features resulting from unknown scattering properties of the atmosphere as well as instrument calibration issues, a cubic polynomial was subtracted from all spectral ratios and weighting functions.

[5]The text of this section is mainly collected from our publication in [*Sheode et al.*, 2006]

The forward model was initialized using a climatological data base, a background aerosol loading according to the LOWTRAN aerosol parameterization [*Kneizys et al.*, 1996], a surface albedo of 0.3, temperature dependent absorption cross sections of O_3, NO_2 and BrO, and the O_4 cross section from *Greenblatt et al.* [1990]. The cross sections of O_3 and NO_2 were measured by the SCIAMACHY Proto Flight Model (PFM) Satellite Spectrometer [*Bogumil et al.*, 1999] and the BrO cross sections were obtained by the time-resolved rapid scan Fourier Transform Spectroscopy (FTS) method [*Fleischmann et al.*, 2004] and then convolved to the SCIAMACHY resolution assuming the Gaussian form of the instrument slit function. The absorption cross sections, which are used in the SCIAMACHY BrO limb retrievals have an accuracy of 10 - 20 % [*Fleischmann et al.*, 2004].

The retrieval of BrO profiles was performed as described by *Rozanov et al.* [2005a] using a two-step retrieval procedure. At the preprocessing step, which is done for each tangent height independently, a possible misalignment of the wavelength grids of the limb spectra, of the reference spectrum, and of the forward model is accounted for. Additionally, known corrections, namely, the ring and tilt spectra, as well as instrument calibration functions, are applied. The main retrieval step is based on the solution of the linearized forward equation given by

$$\mathbf{y} = \mathbf{K}\mathbf{x} + \varepsilon\,. \tag{5.5}$$

As already mentioned in Section 5.6.2, the measurement vector, **y**, contains the differences between ratios of simulated and measured differential limb spectra at all tangent heights selected for the retrieval with all corrections from the preprocessing step applied, the state vector, **x**, contains relative differences of trace gas number densities (with respect to the initial values) at all altitude layers for all gases to be retrieved, and ε denotes errors of any kind (e.g., measurement noise, linearization error, etc.). The linearized forward model operator, **K** comprises of appropriate weighting functions. The final solution is found iteratively employing the optimal estimation technique [*Rodgers*, 2000]. Since no reliable statistical information on the vertical distribution of BrO is available, the Levenberg-Marquard iteration type [*Dennis and Schnabel*, 1983; *Hanke*, 1997] is employed replacing the a priori information at each iteration step by the results obtained at the previous iteration.

5.7.1 Sensitivity studies

In this section the dependence of the retrieved vertical profiles of BrO on the assumed atmospheric composition, surface reflection, and measurement geometry parameters is investigated. This is done for a selected limb measurement performed on July 3rd, 2004 in the tropical region. The vertical profile of BrO obtained using the standard input for the forward model and the retrieval algorithm is treated as the reference. The vertical distributions retrieved using perturbed input parameters provide an estimate of the sensitivity of the retrieval to the corresponding parameter.

The influence of atmospheric composition parameters such as pressure, temperature, and aerosol loading as well as of the surface reflection on the retrieved BrO mixing

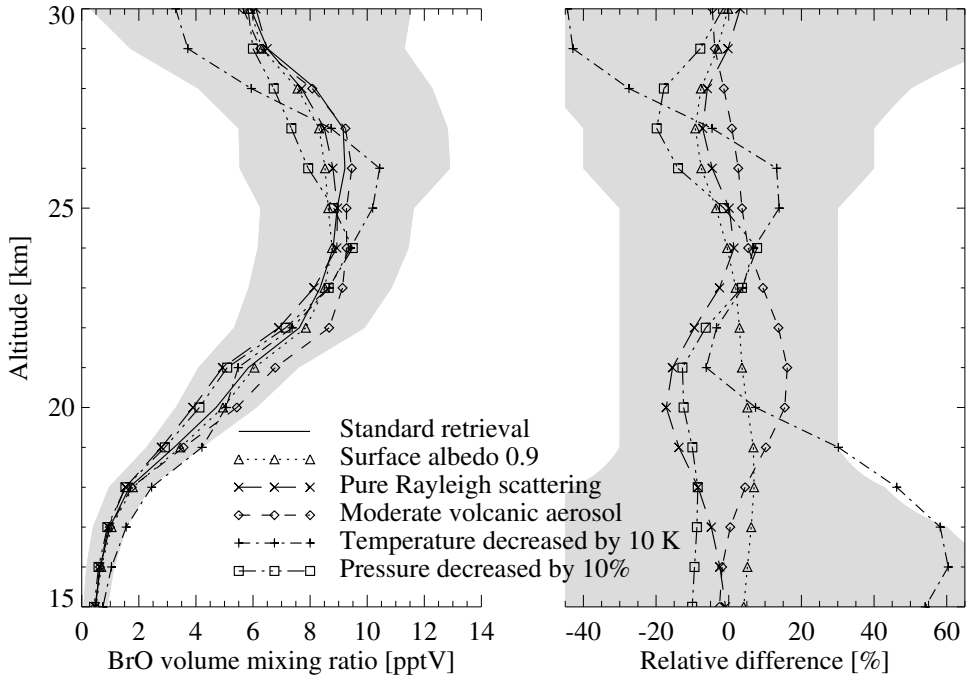

Figure 5.6: Dependence of the retrieved vertical distribution of BrO on the atmospheric composition and surface properties. Left panel: BrO volume mixing ratio retrieved assuming different input parameters. Right panel: Relative differences of BrO profiles obtained using perturbed input parameters with respect to the standard retrieval.

ratios is presented in Figure 5.6. The reference vertical distribution of BrO obtained using the standard settings in the forward model and in the retrieval algorithm is shown by the solid line. Other curves in the left panel in Figure 5.6 depict the BrO volume mixing ratio profiles obtained for the perturbed input parameters. The shaded area represents the total estimated uncertainty of the retrieved profile. The right panel shows the relative differences of the corresponding profiles with respect to the reference (i.e., "unperturbed") profile. As seen from the plot, the largest influence on the retrieved BrO profile is due to the change in the temperature profile. For example, a decrease in the temperature by 10 K results in a relative deviation in BrO mixing ratio of up to 60% in the lower stratosphere and up to 42% at higher altitude (shown by the dot-dashed line with pluses in the plot). However, it is worth mentioning that despite relatively high relative values, the absolute deviation in the retrieved BrO volume mixing ratio due to the change in the temperature profile by 10 K is always less than 0.5 pptv below 23 km. The dependence of the retrieved profiles on the temperature is most probably due to the temperature dependent cross sections, mostly of ozone, used in the forward model. The second largest influence on retrieved BrO profiles demonstrates the changes in the scattering properties of the atmosphere which may be caused by the changes in

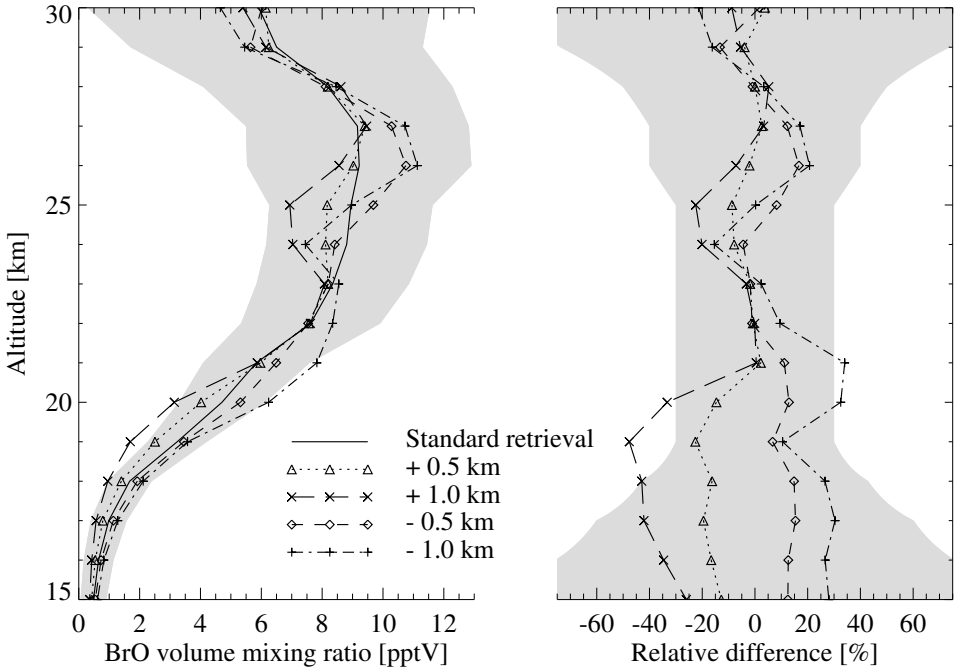

Figure 5.7: Influence of the instrument mispointing on the retrieved vertical distribution of BrO. Left panel: BrO volume mixing ratio retrieved assuming different pointing corrections. Right panel: Relative differences of BrO profiles obtained using pointing corrections with respect to the standard retrieval.

the pressure or aerosol loading. Thus, a decrease in pressure by 10 % (dot-dot-dashed line with squares) and a reduction of scattering events in a pure Rayleigh atmosphere (dot-dot-dot-dashed line with crosses) result in nearly the same relative deviations in the retrieved BrO profile of up to 20% whereas an increased stratospheric aerosol loading simulated using the moderate volcanic aerosol instead of background according to the LOWTRAN aerosol parameterization (dashed line with diamonds) causes a relative deviation of nearly the same amount with an opposite sign. Illustrating a weak sensitivity of the employed method to the optical properties of the surface, the relative deviation in the retrieved BrO caused by the increase of the surface albedo to 0.9 remains always below 10% (dotted line with triangles).

One of the main issues for all limb scattering instruments is the accuracy with which the tangent heights can be determined [*von Savigny et al.*, 2004]. Already in the early stage of SCIAMACHY mission, a substantial error in the SCIAMACHY pointing as provided by ESA was identified. We studied the effect of wrong tangent height alignment on the retrieval of the SCIAMACHY BrO. Figure 5.7 illustrates the influence of the instrument mispointing on the retrieved BrO profiles. The presentation form here is similar to Figure 5.6. The perturbed profiles were obtained associating the limb measurements to “wrong” values of the tangent height and then running the forward model and the

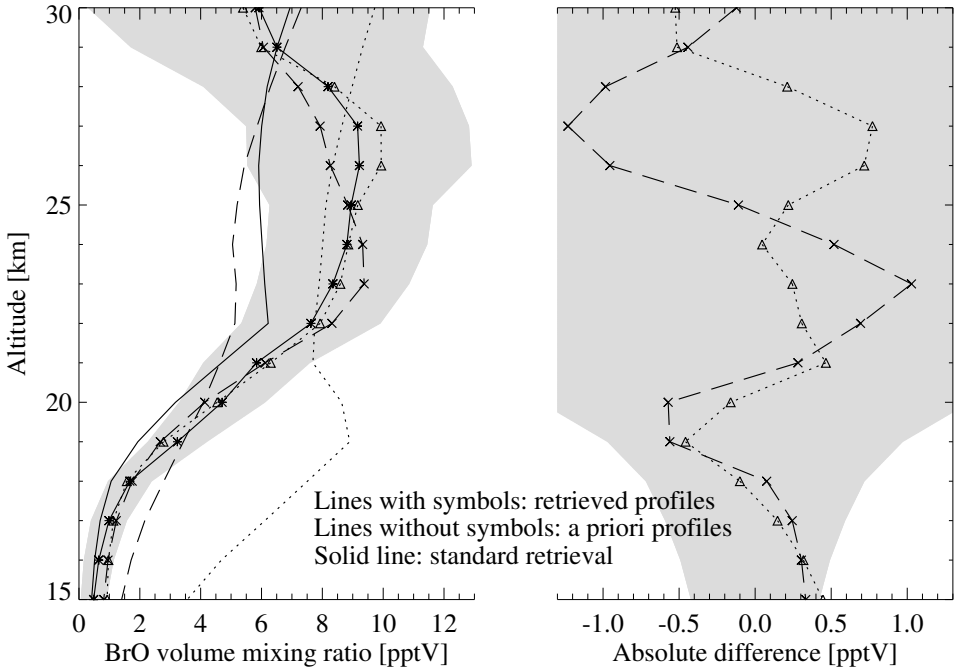

Figure 5.8: Influence of a priori information on the retrieved vertical distribution of BrO. Left panel: Curves with symbols show BrO volume mixing ratio retrieved assuming different a priori profiles shown by the lines of the same type without symbols. Solid line depicts the standard retrieval. Right panel: Absolute differences of BrO profiles obtained using different a priori profiles with respect to the standard retrieval.

retrieval. All tangent height values were changed by the same amount simulating a constant shift in the tangent height alignment. Negative values for the tangent height shift denote that the assumed tangent height grid was shifted downwards with respect to the original one. Afterwards the retrieved BrO number density profiles were shifted back by the mispointing amount and converted into the volume mixing ratios. This is done to simulate the post-processing pointing correction as it was applied to BrO profiles. As seen from the plot, the resulting error in BrO volume mixing ratio profiles due to 1 km mispointing is 10-20% above 21 km increasing to about 40% in the lower layers.

Figure 5.8 illustrates the influence of a priori information used in the forward model and in the retrieval algorithm on the retrieved BrO volume mixing ratio profiles. In the left panel BrO volume mixing ratio retrieved assuming different a priori profiles shown by curves with symbols. Corresponding a priori profiles are shown by the lines of the same type without symbols. Solid line depicts the standard retrieval. Due to decreasing information content of the limb measurements the largest impact of a priori information is expected in the lower stratosphere. Since the absolute values of BrO mixing ratio in this altitude region are low it is more convenient to show absolute differences in the BrO

profile as presented in the right panel of Figure 5.8. As seen from the plot, differences in BrO volume mixing ratio caused by the usage of different a priori profiles are typically within 0.6 pptv.

5.8 Conclusion

This chapter gives an overview of the SCIAMACHY instrument on board the ENVISAT. The basic concepts involved in the retrieval of atmospheric constituents from satellite instrument have also been discussed.

Also, the technique used to retrieve BrO from SCIAMACHY limb measurements along with sensitivity studies has been presented. The retrieval error is approximately 40% between 15 - 20 km and 25 - 30 km and it is approximately 30% between 20 - 25 km. The largest influence on the retrieved BrO profile is of temperature. While the influence is insignificant between 20 - 28 km it cannot be ignored in the lower stratosphere and at higher altitudes. The influence of pressure and scattering events on the retrieved BrO is moderate. The effect of the mispointing on the retrieval of BrO has also been tested. A mispointing of 1 km can result in error of about 10 - 20% above 21 km and increasing to about 40% in the lower layer.

6 Validation of SCIAMACHY BrO limb profiles

The technique of retrieval of BrO has already been discussed in Chapter 5. In order to have further confidence in the retrieved profiles, they need to be validated with the BrO profiles retrieved using different measurement techniques. The rationale of satellite validation is to ensure that geophysical quantities inferred from in-orbit radiometric measurements meet quality requirements of the intended scientific studies and applications [*Piters et al.*, 2005]. As a first step towards a validation of our SCIAMACHY BrO retrievals a comparison of our BrO profiles with the set of balloon-borne BrO measurements compiled by *Dorf et al.* [2005] is done. The balloon-borne BrO profile measurements using different techniques were performed for a wide range of geophysical conditions (high, mid and low latitudes during different seasons) and within the scope of ENVISAT/SCIAMACHY validation [*Dorf et al.*, 2005]. Since the different instruments used to retrieve balloon-borne BrO profiles have different sources of random and sytematic errors it is not possible to compare these profiles with the SCIAMACHY BrO profiles directly. Moreover, the large diurnal variation of BrO radical and to a lesser extent, presumably small spatial gradients in total stratospheric bromine prevent direct comparison of balloon-borne and satellite limb measurements even if a perfect match of both observations could be achieved [*Dorf et al.*, 2005]. Hence the balloon-borne profiles have been photochemically corrected using three dimensional chemical transport model, a trajectory model and a one dimensional photochemical model, the details of which are given in *Dorf et al.* [2005]; *Dorf* [2005].

This chapter presents a comparison of some of these balloon-borne BrO profiles, retrieved using different techniques, with our SCIAMACHY retrievals. Prior to that, the basic concepts involved in the BrO measurement technique of these methods and discussed in brief.

6.1 Other measurement techniques

6.1.1 Chemical conversion resonance flurosescence

Chemical Conversion Resonance Flurorescence (CCRF) technique is used to measure BrO *in-situ* from platforms such as balloon and aircraft. At the heart of the CCRF technique is the reaction of BrO with NO forming Br and NO_2. The instrument on board the appropriate platform, sucks the stratospheric air into the duct. NO is added to the fast flowing ambient air. BrO reacts with NO to form Br atoms on a millisecond time scale. The atoms are detected using an arrangement of resonance flurosescence which

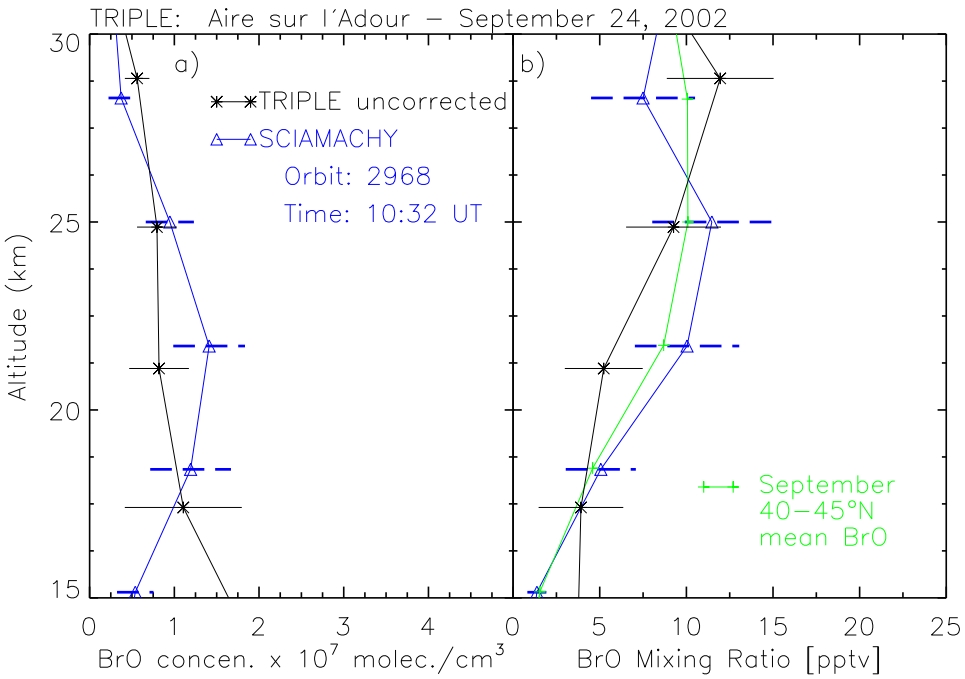

Figure 6.1: Comparison of SCIAMACHY BrO retrievals with balloon borne BrO observations from the TRIPLE instrument. (a) BrO number density profiles from the TRIPLE flight on 24 September 2002 from Aire sur l'Adure (43.7°N), together with the corresponding SCIAMACHY profile from Orbit 2968. The retrieval errors are approximately 40% between 15 - 20 km and 25 and 30 km, while it is 30% between 20 - 25 km. (b) as in panel (a) but expressed as volume mixing ratio. In addition, the corresponding monthly mean profile from SCIAMACHY for the range from 40°N to 45°N is shown.

consists of an emission lamp and a photomultiplier detector. The NO addition is periodically switched on and off. This is done to determine the resonance flurosescence signal due to Br and the background signal. Further a kinetic model which includes relevant reactions generating and consuming Br atoms and measured temperature and pressure is used to convert measured Br atoms concentration into BrO initial concentration. More details about the technique can be found elsewhere [*Brune et al.*, 1989; *Dorf et al.*, 2005].

TRIPLE instrument

One such instrument, which uses the above CCRF technique and has been used within the framework of the SCIAMACHY validation campaigns, is the TRIPLE multi-instrument payload. TRIPLE measures *in-situ* ClO/BrO using chemical conversion resonance flurosescence technique described above. It consists of a cryogenic whole air sampler of the University of Frankfurt [*Schmidt et al.*, 1987] and the Jülich Fast *in-situ*

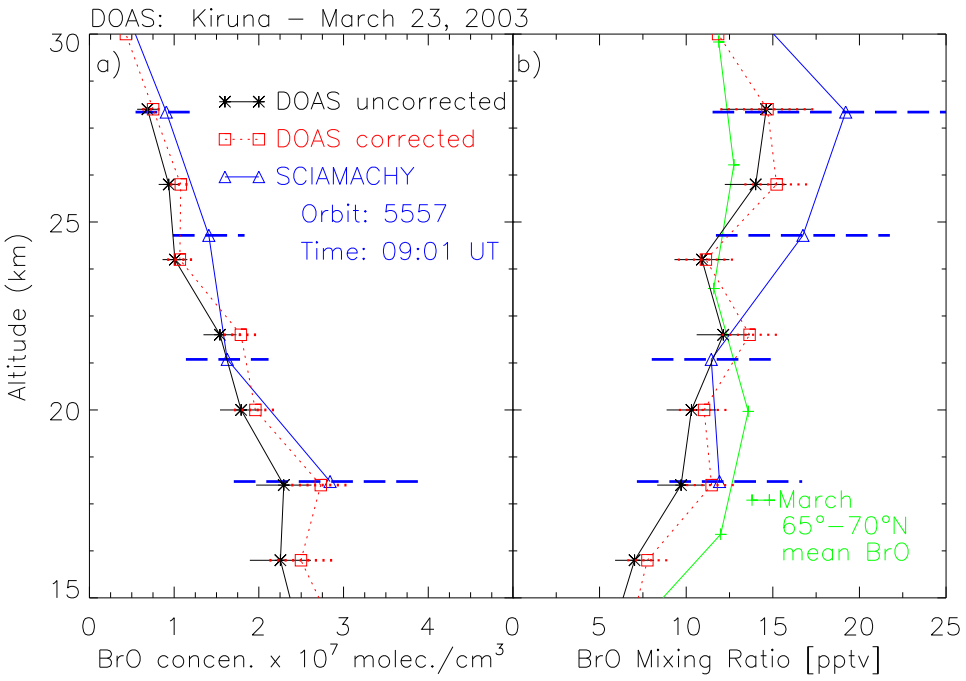

Figure 6.2: Same as fig. 6.1 but for a comparison with the DOAS balloon flight on 23 March 2003 from Kiruna (67.9°N). In addition to the measured BrO profile from the DOAS instrument also a photochemically corrected profile is shown.

Stratospheric Hygrometer (FISH).

6.1.2 Balloon-borne differential optical absorption spectroscopy

Differential Optical Absorption Spectroscopy (DOAS) is a technique which is used to retrieve atmospheric trace gases using absorption spectra of the trace gas in UV - vis. The technique of retrieval is similar to the one discussed in Chapter 5. The word ”differential” used here implies that only high frequency part of the absorption spectrum is used in the analysis. The technique is used on different platforms, for example balloon [*Platt*, 1994; *Pundt et al.*, 2002], satellite instruments [*Chance*, 1998; *Richter et al.*, 1998], aircraft [*Pfeilsticker and Platt*, 1994; *Wang et al.*, 2005], ground based stations [*Noxon*, 1975; *Richter*, 1997; *Wittrock*, 2006]. More details of the technique can be found elsewhere [*Richter*, 1997; *Wittrock*, 2006].

In the context of this work, BrO profiles, retrieved using the DOAS technique but from two different instruments, are used for the validation purpose. The two instruments are described in brief below.

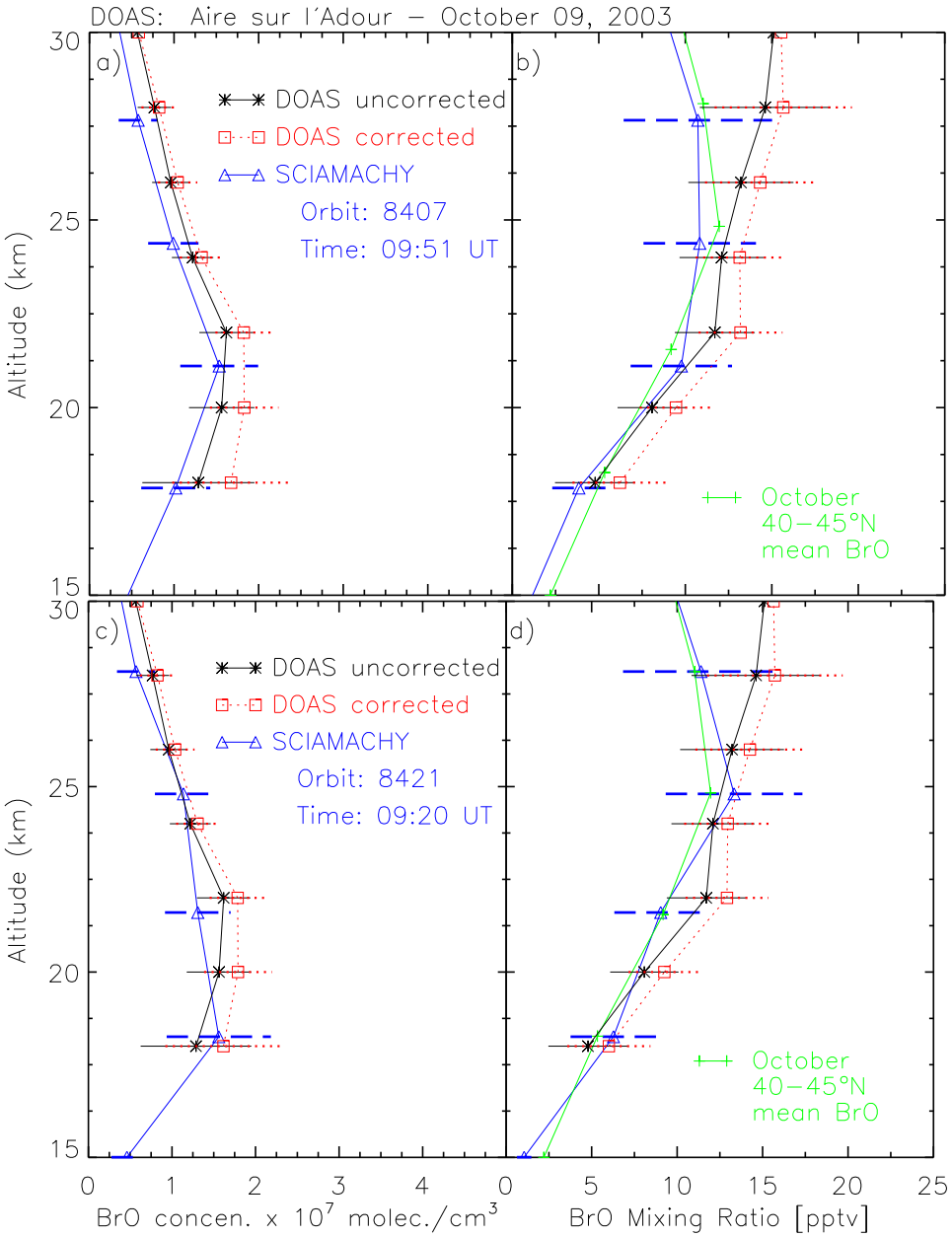

Figure 6.3: Same as fig. 6.2 but for a comparison with the DOAS balloon flight on 9 October 2003 from Aire sur l'Adure (43.7°N). Panels (a) and (b) show a backward trajectory match, while panels (c) and (d) show a forward trajectory match. See text for details on the trajectory matches.

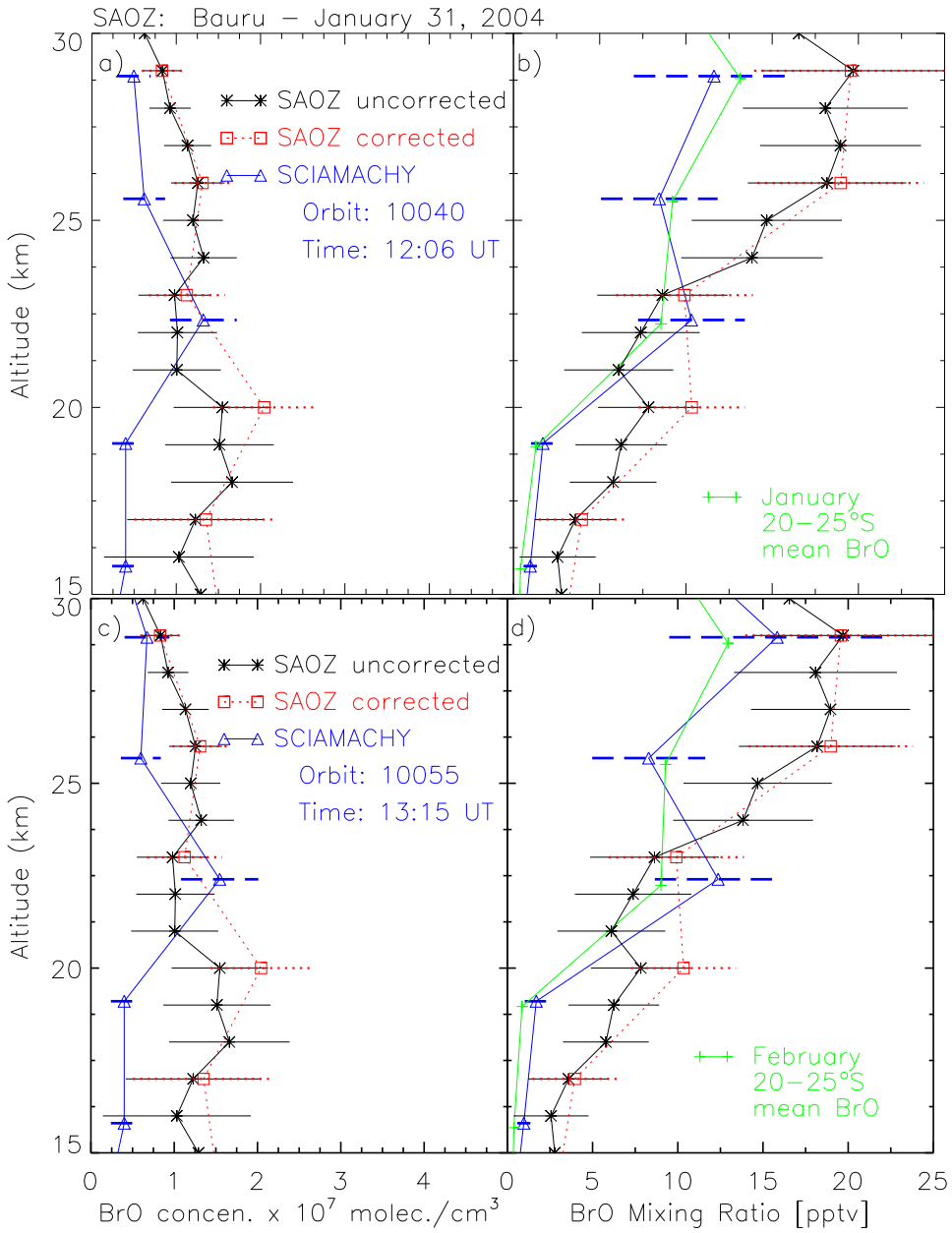

Figure 6.4: Same as fig. 6.3 but for a comparison with the SAOZ balloon flight on 31 January 2004 from Bauru (22.4°S).

LPMA/DOAS BrO measurements

The Limb Profile Monitor of the Atmosphere (LPMA)-DOAS is a balloon payload and collects the solar spectra. The instrument consists of the sun tracker [*Hawat et al.*, 1995] and three optical spectrometers which analyse direct sunlight over virtually the entire wavelength band from UV-NIR. The stratospheric BrO measurements using the solar occultation DOAS technique on balloon platform have been performed since 1996, [*Platt*, 1994; *Harder et al.*, 1998]. The solar occulatation DOAS technique involves the measurement of the slant column densities. Since 2002 there is also an on board UV-vis spectrometer which operates in the limb geometry and observes scattered sunlight. The details of the instrument setup and performance and first results have been published in *Weidner et al.* [2005].

For the BrO profiles used in this work, the BrO observations are done in the wavelength range 346 – 360 nm [*Aliwell et al.*, 2002], which includes the UV vibration absorption bands of the electronic transition of BrO [*Dorf et al.*, 2005]. The absolute cross sections are taken from *Wahner et al.* [1988]. In addition NO_2, O_3, and O_4 spectra are also used for BrO profile retrieval, the details of which can be found in [*Dorf et al.*, 2005]. The precison and accuracy of the technique is $\pm$ 4% and $\pm$12%, respectively in the inferred BrO SCDs [*Harder et al.*, 1998, 2000]

SAOZ/DOAS BrO measurements

The Systeme d'Analyse par Observation Zenithale (SAOZ) - BrO balloon sonde is a light weight UV-vis sonde specifically designed for the measurement of BrO as well as other UV- absorbing species such as OClO and CH_2O, by solar occultation from small and relatively inexpensive balloons [*Pommereau et al.*, 1999]. The solar occultation measurements can be done during the ascent of the balloon (or descent) and from float at 30 km during sunset (or sunrise). An on-board CPU, which drives the instrument is connected to meteorological sensors which measure pressure, temperature and humidity, a global positioning system to locate altitude, latitude and longitude. The measurements are done every 30 seconds. This results in a vertical sampling of 200 m during the balloon ascent.

For the BrO profiles used in this work, BrO is measured by solar occultation in the 320 – 400 nm UV spectral range during the after noon ascent of the balloon at SZA $<$ 90° and at the begining of the sunset from float altitude up to 92° – 93° SZA, when the contribution of the scattered light becomes too large for continuing the measurements [*Dorf et al.*, 2005]. The spectral analysis of BrO is done using the DOAS technique using the WINDOAS algorithm [*Roozendael and Fayt*, 2000] according to the setting mentioned in *Pundt et al.* [2002]. The onion peeling technique is used for the BrO profile retrieval. More details can be found in *Pundt et al.* [2002]; *Dorf et al.* [2005].

6.2 Validation of BrO profiles

As a first step towards a validation of our SCIAMACHY BrO retrievals we compared our BrO profiles with the set of balloon-borne BrO measurements compiled by *Dorf et al.* [2005]. Due to the diurnal variation of BrO it is necessary to include a photochemical correction of the measured BrO profiles that takes into account the differences in the time of day (and thus solar zenith angles) between the two measurements. Forward and backward trajectories are started at the location of the balloon measurements and used to find optimal matches with SCIAMACHY profiles [*Dorf et al.*, 2005]. For more details on photochemical correction the reader is directed to *Dorf et al.* [2005]; *Dorf* [2005]. For two of the four balloon profiles forward and backward matches are available, for the other two only forward matches.

The relatively large statistical error of about 30% for individual SCIAMACHY BrO profiles makes it difficult to detect possible systematic differences when comparing individual profiles. Therefore we have also included the SCIAMACHY monthly mean BrO profiles for the corresponding latitude band in the comparison.

Figure 6.1 shows the comparison between the measured BrO profile from a TRIPLE flight conducted on 24 September, 2002 at Aire sur l'Adour, France (44°N) with the SCIAMACHY BrO limb retrieval. As the TRIPLE flight was close in time to the SCIAMACHY overpass no photochemical correction was needed in this case. Figures 6.2 and 6.3 show the comparison with a DOAS flight on 23 March 2003 in Kiruna (68°N) and with a DOAS flight on 9 October 2003 at Aire sur l'Adour. Figure 6.4 shows the comparison with a SAOZ flight at Bauru, Brazil (22°S) on 31 January 2004. For further information about the measurement techniques, photochemical correction of BrO profiles, and forward and backward trajectory mapping the reader is referred to *Dorf et al.* [2005].

The mean relative differences over the altitude range from 18 to 30 km are +17% for the September 2002 TRIPLE flight at Aire sur l'Adour, +14% for the March 2003 DOAS flight, −20% and −29% for the two matches of the October 2003 DOAS flight at Aire sur l'Adour, and −32% and −42% for the two matches of the January 2004 SAOZ flight at Bauru. Below 20 km our retrievals show very low amounts of BrO while the SAOZ profile shows much higher BrO mixing ratios between 2 and 5 pptv. Although it is difficult to be fully conclusive at this stage because of the large differences between the comparisons for the different balloon flights, the agreement between SCIAMACHY and the photochemically corrected balloon-borne BrO profiles is encouraging, in particular at mid-latitudes.

6.3 Conclusion

In this chapter, other techniques (used to retrieve BrO profiles) namely chemical conversion resonance flurosescence and DOAS techniques have also been presented. As a part of validation of the retrieved SCIAMACHY BrO profiles, a comparison of the SCIAMACHY BrO retrievals with a set of balloon-borne BrO measurements has also been

presented. The comparison shows that mean differences in the altitude region from 18 to 30 km between +17% and −29% at mid and high latitudes of the Northern Hemisphere. Larger discrepancies of −32% and −42% are found in comparison to a SAOZ balloon profile in the tropics.

7 Global observations of stratospheric BrO

In this chapter, the first global results of SCIAMACHY bromine monoxide (BrO) profiles retrieved for a 10 day period in September, 2002 are presented. In order to test whether the SCIAMACHY BrO observations agree with our current understanding of the stratospheric bromine chemistry, a comparison of the retrieved BrO profiles with modeled BrO profiles, based on inorganic bromine (Br_y) in the stratosphere derived from MIPAS CFC-11 using the empirical correlation of [*Wamsley et al.*, 1998] and the calculated BrO/Br_y ratio from a photochemical model constrained by NO_2 profiles, which are also retrieved from SCIAMACHY measurements, is done. The material for this discussion is mainly taken from our publication in *Sinnhuber et al.* [2005]. Further, a climatology of BrO, constructed from the SCIAMACHY BrO profile retrievals of the years 2003 and 2004, is also presented along with the model runs which demonstrate the relation between nitrogen oxides and bromine chemistry. The material for this discussion is mainly taken from our publication in *Sheode et al.* [2006].

7.1 First global SCIAMACHY limb BrO retrievals

An overview of the SCIAMACHY instrument and its mode of measurements have already been presented in Chapter 5. SCIAMACHY was launched on board ENVISAT in March, 2002. It measures the scattered and reflected solar radiation in limb and nadir geometry in the spectral range from 240 to 2380 nm. ENVISAT is in a sun-synchronous orbit with an equator-crossing time of about 10 LT. A more detailed description of the instrument design and capabilities can be found in *Bovensmann et al.* [1999].

Also, an overview of the retrieval technique of BrO profiles has already been discussed in Chapter 5. To summarise in brief, BrO profiles are retrieved from the SCIAMACHY measurements using the University of Bremen retrieval processor version CDI-(V1.2.17-2) (www.iup.physik.uni-bremen.de/scia-arc) as described by [*Rozanov et al.*, 2005b] and the temperature-dependent BrO absorption cross-sections from [*Fleischmann et al.*, 2004]. The BrO retrieval is possible in the altitude range from about 15 to about 30 km with a precision of about 30 – 50% for a single profile and an estimated systematic error of 10 to 20% or at least 1 pptv (including the contribution due to remaining pointing uncertainty). One of the largest uncertainties for the BrO retrieval is imperfect pointing knowledge [*von Savigny et al.*, 2005a] (e.g. see Chapter 5). For the results of the first SCIAMACHY global BrO observations of September, 2002 presented in this section, the retrieval process includes a global tangent height offset of -1.5 km relative to the engineering tangent heights provided by the Level 1 data set. This offset is

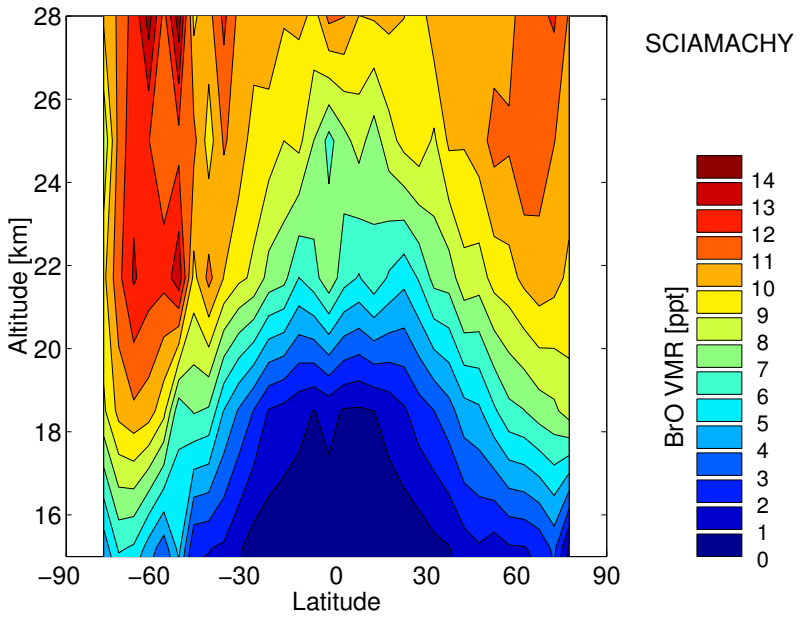

Figure 7.1: Zonal mean BrO volume mixing ratio measured by SCIAMACHY

consistent with the mean tangent height offset during September 2002, as derived from SCIAMACHY tangent height retrievals [*von Savigny et al.*, 2005a], as well as the mean tangent height offset retrieved from MIPAS measurements [*von Clarmann et al.*, 2003]. The focus here is on zonally averaged BrO. BrO is averaged over the 10 day period in 5° latitude bins, with about 40 to 50 profiles per bin from a total of 1312 profiles. This reduces the error due to measurement noise to about ±5% (one sigma).

The zonal mean BrO VMR for the investigated period from 18 to 27 September, 2002 is shown in Figure 7.1. As is seen in the figure, the VMR of BrO increases with altitude primarily due to the dissociation of organic bromine compounds into inorganic bromine. Also it is seen that as one moves towards the higher latitudes the BrO VMR increases. Larger VMRs of BrO are seen in the altitude range 20 – 28 km in the polar regions, especially in the southern hemisphere.

7.2 Comparison with photochemical model output

In order to test how well the SCIAMACHY BrO measurements agree with our current understanding of the stratospheric bromine chemistry we have compared the observed BrO with modeled BrO (Figure 7.3). The modeled BrO here was calculated by multiplying our Br_y[1] estimate of approximatly 18.16 pptv from MIPAS CFC-11 measurements with the BrO/Br_y-ratio from the 1-D photochemical model.

[1]The methods to estimate Br_y are dicussed in Chapter 10. In this case, it has been estimated using the empirical relation proposed by [*Wamsley et al.*, 1998] and the CFC-11 data from MIPAS on board

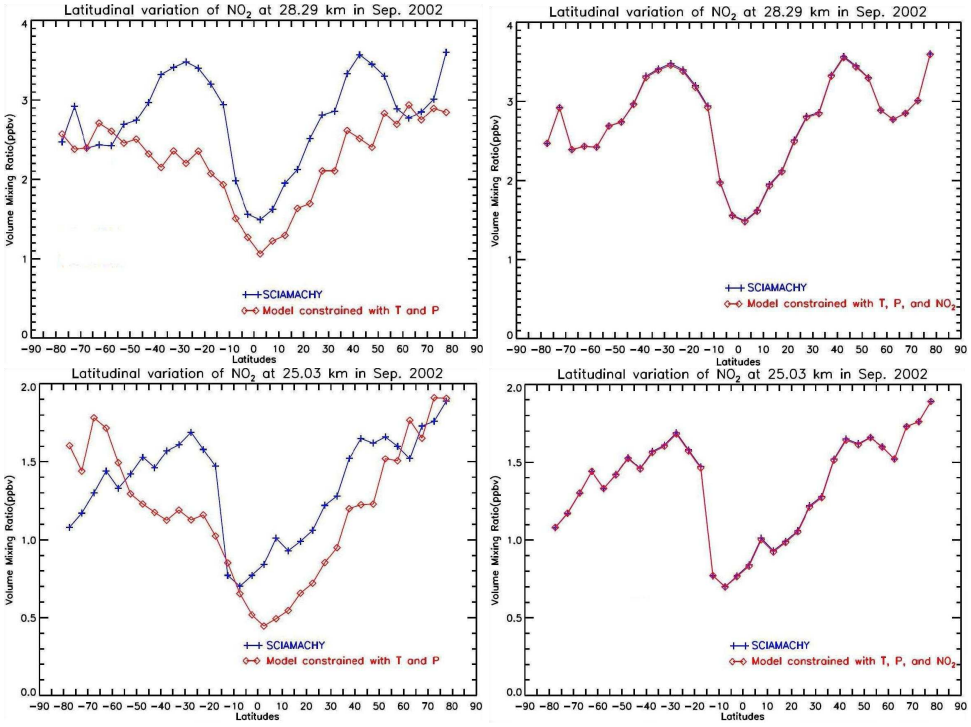

Figure 7.2: Comparison of the NO_2 retrieved from the SCIAMACHY measurments and that calculated by the photochemical model. Left column: The model is constrained with ECMWF temperatures and pressures only. Right column:The model is constrained with ECMWF temperatures, pressures, NO_2 retrieved from SCIAMACHY measurements.

7.2.1 Photochemical model

The one dimensional photochemical model used in this study is the same as described in detail in Chapter 3. To summarise, the photochemical model calculates the expected BrO/Br_y ratio based on the chemistry scheme from the SLIMCAT model [*Chipperfield*, 1999]. The model has a state-of-the-art treatment of stratospheric (bromine) chemistry. Reaction rate constants are taken from JPL-2002 recommendations [*Sander et al.*, 2003], unless otherwise noted. The model is initialized by the output of a two-dimensional (latitude-height) model [*Sinnhuber et al.*, 2003] and references therein]. Temperature and pressure profiles are taken from ECMWF analyses.

7.2.2 NO_2 in the photochemical model

During the day time BrO and $BrONO_2$ form a large fraction of total inorganic bromine in the stratosphere as discussed in Chapter 4. The NO_2 concentrations controls the

ENVISAT. See Chapter 10 for more details.

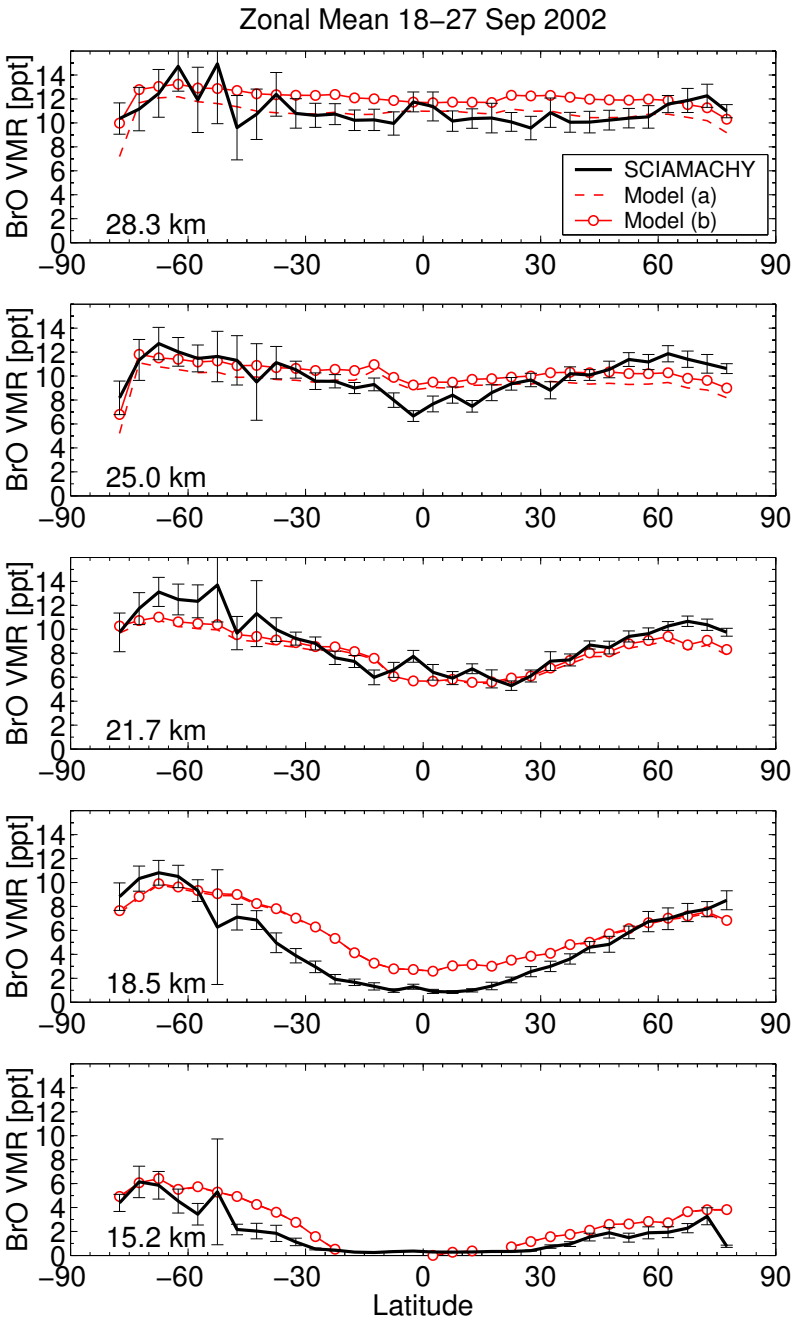

Figure 7.3: Comparison between BrO VMR from SCIAMACHY measurements and BrO from model calculations for five different altitudes. The modeled BrO was calculated from the product of our estimate of Br_y, which is derived from MIPAS CFC-11 measurements, and the BrO/Br_y ratio from our photochemical model. Model run (a) uses JPL-2002 kinetics, while model run (b) includes in addition the reaction of $BrONO_2 + O(^3P)$ [*Soller et al.*, 2001]. Errorbars are derived from the standard deviation of BrO measurements within each latitude bin (2 sigma).

bromine partitioning during the day time through formation of $BrONO_2$(For example see Chapter 4). Thus in order to simulate the bromine chemistry as closely as possible to the real situation in the atmosphere as on the days of SCIAMACHY measurements considered here, it is important to have same amount of NO_2 in the model as on the day of measurements. In order to achieve this, the model is constrained by the SCIAMACHY NO_2 profiles by scaling NO, NO_2 , NO_3, N_2O_5, and HNO_3 in the initialization until the modeled NO_2 agreed with measured NO_2 at the local time of the SCIAMACHY measurements. $ClONO_2$ or $BrONO_2$ were not scaled for the simple reason that, this would affect the chlorine and bromine partitioning in the model and consequently the chemistry simulated by the model. The left column of Figure 7.2 shows the NO_2 concentrations calculated by the 1-D model constrained with just ECMWF temperatures and pressures. Also shown are the concentrations measured by SCIAMACHY. The right column of Figure 7.2 shows the NO_2 concentrations calculated by the 1-D model constrained with ECMWF temperatures, pressures and SCIAMACHY NO_2 measurements along with the concentrations measured by SCIAMACHY. The right column of Figure 7.2 gives us the confidence in the stratospheric chemistry simulated by the model.

In the context of this work, two model runs were conducted: (a) a base model run that uses JPL-2002 chemical kinetics and (b) a model run that in addition includes the reaction of $BrONO_2 + O(^3P)$ [*Soller et al.*, 2001]. The results of the comparison of SCIAMACHY BrO and modeled BrO are shown in Figure 7.3. Inclusion of the reaction of $BrONO_2 + O(^3P)$ increases modeled BrO at higher altitudes, but has a negligible effect below about 25 km. The reason for this is that as we move high in altitude, the concentration of $O(^3P)$ increases and consequently the reaction of $BrONO_2$ with $O(^3P)$ thus increasing the BrO VMR.

In general we find a good agreement between the SCIAMACHY BrO observations and our model calculations assuming 18.16 ppt (Also see Chapter 10 for more details on total bromine) of total bromine in the stratosphere. The largest differences are seen at low latitudes in the lowermost stratosphere at 18.5 km. Here the SCIAMACHY observations show around 1 ppt while the expected BrO is at least around 3 ppt. A more comprehensive validation of the BrO and CFC-11 measurements needs to be done in this region before we can finally decide whether this discrepancy is due to uncertainties in the observations or whether this indicates shortcomings in our understanding of the bromine chemistry in this region.

7.3 Towards a climatology of stratospheric BrO

With the availability of SCIAMACHY BrO profile retrievals for the years 2003 and 2004, a global seasonal climatology of stratospheric BrO has been prepared. However, data were not available for May, June, and July 2003 due to a change in the measurement mode of SCIAMACHY during this period. This means that the climatology presented in this work is based so far on observations from 21 months.

The area weighted monthly mean profiles are calculated over five latitude bands: The Arctic (north of 60°N), Northern Hemisphere mid-latitudes (30°N – 60°N), tropics

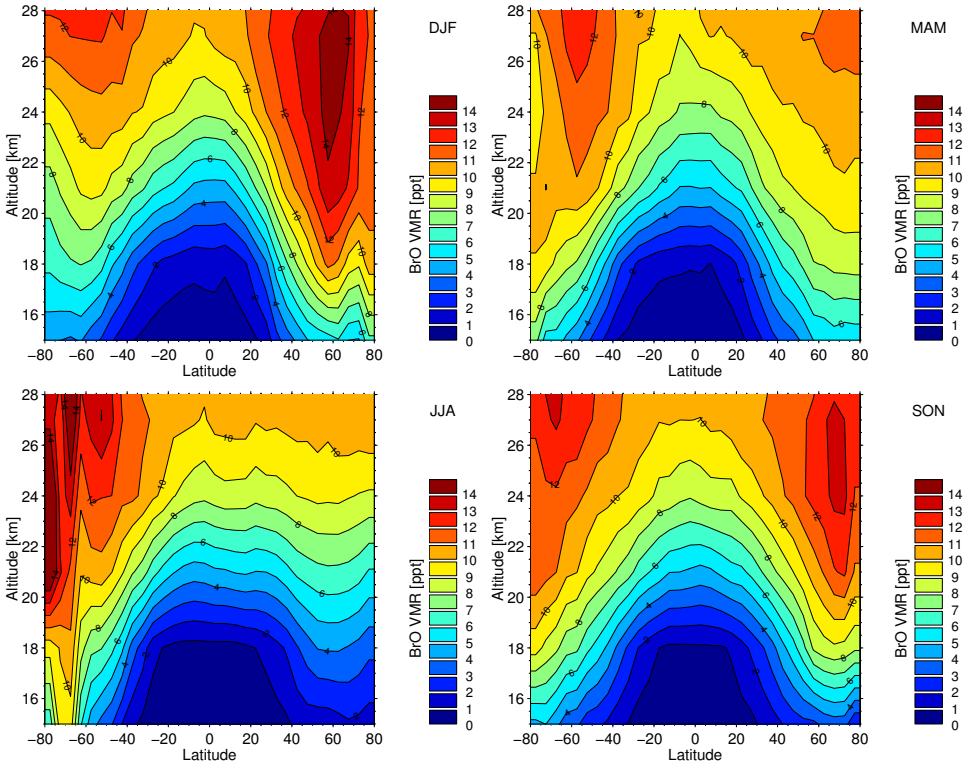

Figure 7.4: BrO climatology derived from SCIAMACHY observations during 2003 and 2004. Data have been averaged for the four seasons December/January/February (DJF), March/April/May (MAM), June/July/August (JJA) and September/October/November (SON).

(30°S – 30°N), Southern Hemisphere mid-latitudes (30°S – 60°S), and the Antarctic (south of 60°S). Prior to this, the tangent height (TH) corrections are applied to the monthly averaged profiles using the TH offsets given in Table 1 of *von Savigny et al.* [2005a]. Note that due to the inability of the instrument to measure in darkness, data are not available above 75°N in November, above 70°N in December and above 75°N in January. Similarly the data are not available above 70°S in May, above 65°S in June, and above 70°S in July. The seasonal averages were then calculated according to the availability of the monthly zonal means. Temperature and pressure profiles needed to convert the BrO number densities to volume mixing ratios were taken from ECMWF.

On an average there are approximately 130 profiles per 5° latitude bin per month. In calculating the seasonal zonal averages for two years, approximately 90,000 profiles have been used. The calculated seasonal means presented here, were interpolated to a common altitude grid for a better comparison.

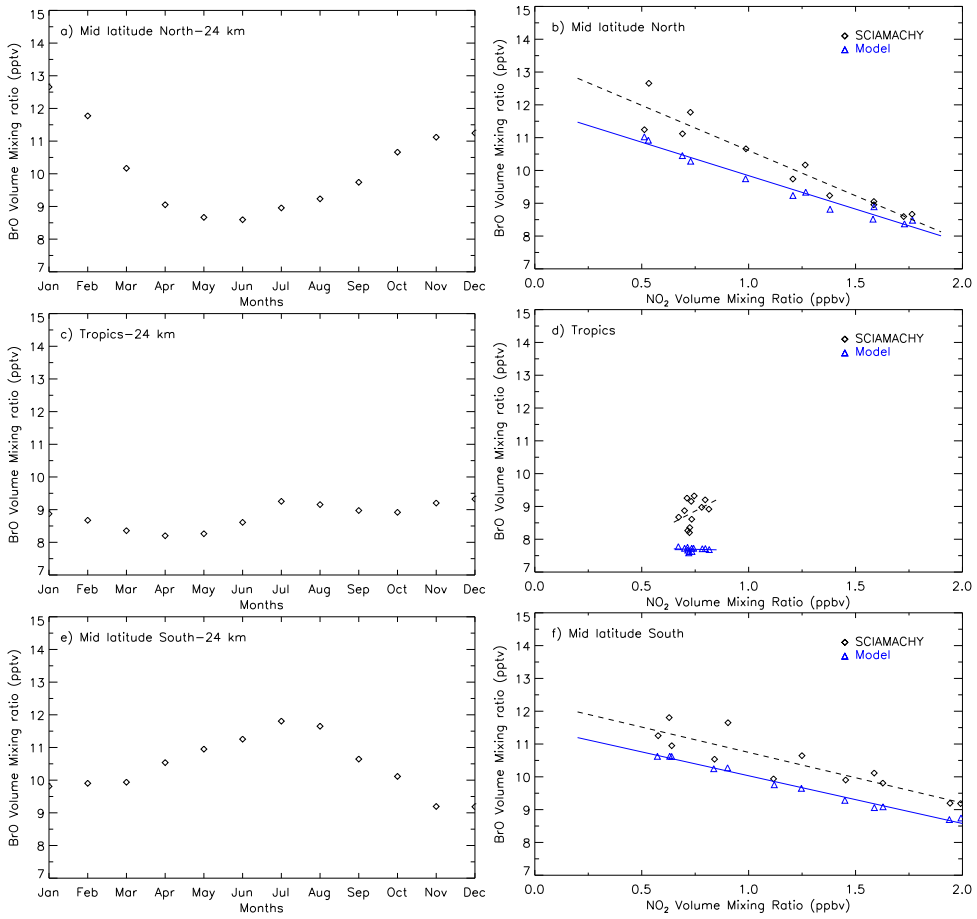

Figure 7.5: Seasonal variation of BrO and its relation to NO_2. Panels (a), (c), and (e) show the seasonal variation of BrO at 24 km for Northern Hemisphere mid-latitudes, tropics, and Southern Hemisphere mid-altitudes, respectively. Panels (b), (d) and (f) show the corresponding relation of BrO to the observed NO_2 mixing ratios. For comparison also the relation between NO_2 and BrO from the photochemical model is shown.

7.3.1 Seasonal variation of stratospheric BrO

Figure 7.4 shows the seasonal and zonal climatology of SCIAMACHY BrO between 15 and 28 km. BrO VMRs increase with altitude at all latitudes mainly due to the dissociation of the organic bromine source species [*Wamsley et al.*, 1998]. During December-January-February (DJF) in the Northern Hemisphere (NH), BrO VMRs are larger at higher latitudes and altitudes as compared to the corresponding latitudes and altitudes in the Southern Hemisphere (SH). During March-April-May (MAM) BrO VMRs appear to be increasing at higher latitudes in the SH and during June-July-August (JJA) the scenario is opposite to that during DJF. During September-October-November (SON) again the increase in BrO VMRs NH higher latitudes is observed.

7.4 Influence of NO_x on BrO

The seasonal variation of BrO will in general be a result of changes in Br_y due to transport and changes in the bromine partitioning due to chemistry. It is expected that the BrO/Br_y ratio will show a seasonal variation anti-correlated to the seasonal cycle of NO_2: A rise in NO_2 concentration will result in the rise in $BrONO_2$ and consequently in the decrease in BrO [*Fish et al.*, 1995]. It is thus interesting to test, to what extent the observed seasonal variation of BrO can be explained by the seasonal cycle of NO_2. Figures 7.5 a, c, and e show the annual variation of BrO at 24 km in northern mid-latitudes, the tropics and southern mid-latitudes, respectively. A strong annual variation of BrO at mid-latitudes of both hemispheres is evident, with a maximum in winter and a minimum in summer. The amplitude of the seasonal cycle of BrO at 24 km in the northern hemisphere is larger than in the southern hemisphere.

According to our present knowledge of bromine chemistry, NO_2 controls the concentration of BrO and $BrONO_2$ during the day time as discussed in Chapter 4. The BrO and NO_2 concentrations are expected to be inversly related to each other. This is confirmed by the simultaneous retrievals of BrO and NO_2 from SCIAMACHY presented in this study.

Figures 7.5 b, d, and f show that the annual variation of BrO is closely anti-correlated with the NO_2 concentrations, measured simultaneously by SCIAMACHY. The variation is qualitatively similar to the one addressed previously by *Richter et al.* [1999] over Bremen (53°N). A comparison with the photochemical model shows that in the Northern Hemisphere the change in BrO is larger than expected from changes in NO_2 alone. This could mean that either other processes, in particular transport, contribute to the seasonal variation of BrO or current photochemistry underestimates the sensitivity of BrO to changes in NO_2. However, since the BrO observations in the southern hemisphere do not show a higher sensitivity to changes in NO_2 when compared to the model, this would argue against a chemical explanation and suggests that transport contributes to the observed BrO changes. Both NO_2 and BrO show only little seasonal variation in the tropical lower stratosphere.

7.5 Conclusion

We have presented a first global observations of stratospheric BrO from SCIAMACHY limb measurements for September, 2002. The BrO retrievals are compared with modeled BrO profiles, based on estimated Br_y from CFC-11 retrievals by the MIPAS on ENVISAT and the calculated BrO/Br_y ratio from a photochemical model constrained by SCIAMACHY NO_2 retrievals. The BrO observations are broadly consistent with our current understanding of stratospheric bromine chemistry and a total stratospheric bromine loading of approximately 18.16 pptv.

Also, a first global climatology of stratospheric BrO, based on retrievals from two years of measurements of the SCIAMACHY instrument has also presented in this chapter. BrO shows a strong annual variation at mid-latitudes while no significant annual variation in the tropics is observed. The seasonal variation at mid-latitudes is inversely correlated with NO_2, confirming our present understanding of the gas phase bromine chemistry.

8 Comparison with ground based measurements of BrO in the tropics

The field campaigns to measure BrO in tropical regions have been short and limited as compared to those in the mid and high latitude regions [*Gabriel. et al.*, 2002; *Leser et al.*, 2003]. In order to have a long term measurements of BrO, a permanent DOAS measurement station was set up in 2002 in Nairobi (1°, 36°E) as a part of BRemian DOAS network of atmospheric measurements (BREDOM). The measurements done by the DOAS station at Nairobi are also used to retrieve NO_2 which has direct effect on BrO (for example see Chapters 4 and 7).

The BrO columns are being measured from space by instruments such as GOME since 1995 and SCIAMACHY since 2002 and have been used in many studies [*Richter et al.*, 1998; *Wagner et al.*, 2001; *Sinnhuber et al.*, 2005]. However GOME BrO measurements are usually normalised in low latitudes [*Richter et al.*, 2002; *Richter and Burrows*, 2002a; *Roozendael et al.*, 2002] due to the time dependent interference pattern exhibited by GOME diffuser plate, which correlates with BrO. Hence they do not provide independent information on low latitudes. The comparison of SCIAMACHY profile measurements in the tropics with balloon borne measurements have shown significant discrepancy (see for example, Chapter 6, Figure 6.4). Also the model calculations of BrO in the tropical region overestimate the SCIAMACHY BrO measurements in the same region. Measurements of BrO in tropics are important due to an expected absence of seasonal variation because of small variations in NO_2 values during the year and smaller impact of horizontal transport. A long term measurement data base is necessary for many studies e. g. to study trends, annual variation, test and validate our present understanding of chemistry using models, etc. They can also serve as an important validation source for instruments such as GOME and SCIAMACHY.

This chapter apart from presenting the zenith-sky measurements of stratospheric BrO and NO_2 for the year 2003, also presents a comparison of the zenith-sky measurements of stratospheric BrO for the year 2003 with slant column densities from a 1-D photochemical model coupled with a radiative transfer model [*Rozanov et al.*, 2001] in order to test our understanding of bromine chemistry. Such a comparison provides an important low-latitude extension of model-measurement comparisons reported in *Sinnhuber et al.* [2002]

8.1 BrO and NO_2 at the tropical site in Nairobi

The annual variation of vertical columns of NO_2 in the morning (AM) and in the evening (PM) is shown in Figure 8.1. The zenith-sky measurements were done be-

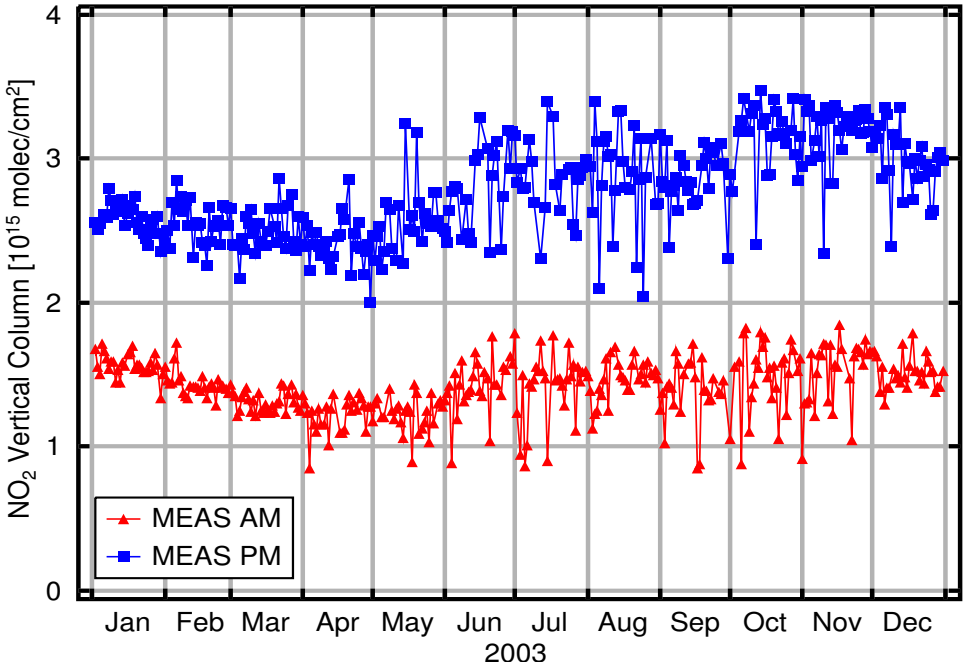

Figure 8.1: NO_2 vertical columns above Nairobi observed at solar zenith angles around 90°. Morning and afternoon values are given

tween 80° and 90°. A significant diurnal variation is observed in vertical columns of NO_2 (Figure 8.1). The main reason for the diurnal variabilty is due to known photolysis of N_2O_5. In comparison the seasonal variation of NO_2 variabilty is small.

Figure 8.2 shows annual variation of the AM 90° - 80° and PM 90° - 80° DSCDs of BrO in 2003 over Nairobi. The PM values are clearly higher than the AM values. The absolute values of BrO DSCD are 1.3 x 10^{14} molecules/cm^2 for the morning and 1.5 x 10^{14} molecules/cm^2 for the evening. The order of magnitude of the morning and evening measurements is similar to that observed at mid and high latitude sites. Further AM and PM values correlate with each other. The seasonal variation in the AM and PM values is small relative to the errors. Figure 8.3 shows the difference between AM and PM values. The differences are explained by photolysis of $BrONO_2$ and HOBr during the day time and conversion of BrO to the same reservoir species in the evening. As already discussed NO_2 controls the the seasonal variation of BrO and it is expected that BrO and NO_2 are anticorrelated (see for example Figure 7.5). The results of small annual variation of BrO over Nairobi are consistent with similarly observed small variation of NO_2.

A pronounced seasonal variation in BrO for a midlatitude site - Bremen (53°N) has been shown previously by [*Eisinger et al.*, 1997; *Richter et al.*, 1999] with winter DSCDs measuring upto 1.9 x 10^{14} molecules/cm^2 and summer DSCDs measuring upto 0.5 x 10^{14}. A similar seasonality was reported by *Schofield et al.* [2004] over Lauder (45°S) with measurements ranging between 3.0 x 10^{14} molecules/cm^2 in win-

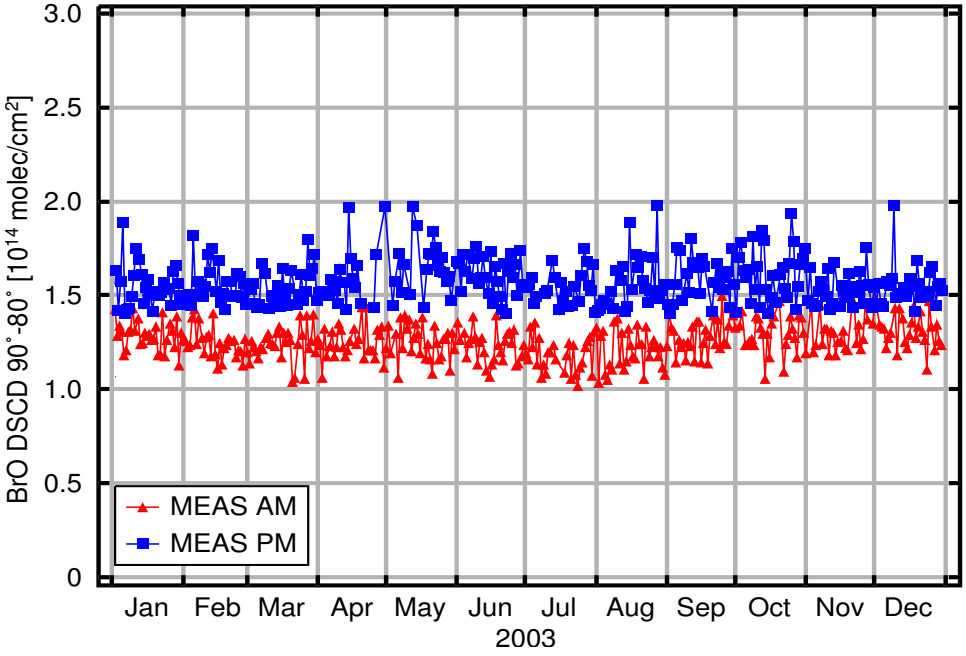

Figure 8.2: Observations of differential slant columns of BrO between solar zenith angles 90° and 80° above Nairobi, 2003.

ter to 1.5 x 10^{14} molecules/cm^2 in summer. BrO DSCDs measurements over another midlatitude site at Colorado (40°N) have also been reported by *Arpag et al.* [1994] for a period from 22 January to May 24 1993. The BrO DSCDs ranged from 0.8 - 1.8 x 10^{14} molecules/cm^2. However the measurement setup used by *Arpag et al.* [1994] is different than that used for measurements over Bremen and Nairobi. In their setup the telescope was first pointed at an 80° angle relative to the zenith towards the setting Sun and was reoriented towards east in April. In comparison to these measurements the amounts of BrO above Nairobi range from 1.3 x 10^{14} molecules/cm^2 to 1.5 x 10^{14} molecules/cm^2. Thus the seasonal variation at the tropical site is smaller as compared to the midlatitude site and is consistent with the absence of seasonality of NO_2. The relation of NO_2 with BrO and its effect on bromine chemistry in general has already been discussed.

8.2 Comparison with photochemical model output

The model used for simulation of data over Nairobi is same as discussed in Section 7.2. The model is initialized by the output of a two-dimensional (latitude-height) model [*Sinnhuber et al.*, 2003] and references therein]. Reaction rate constants are taken from JPL-2002 recommendations [*Sander et al.*, 2003]. The chemical integration time step was five minutes. The model was run on the 15^{th} of every month at 1.27°S. In all three runs were performed. The first run was done using the climatological data, the second run included the temperature and pressures from ECMWF while other initializations

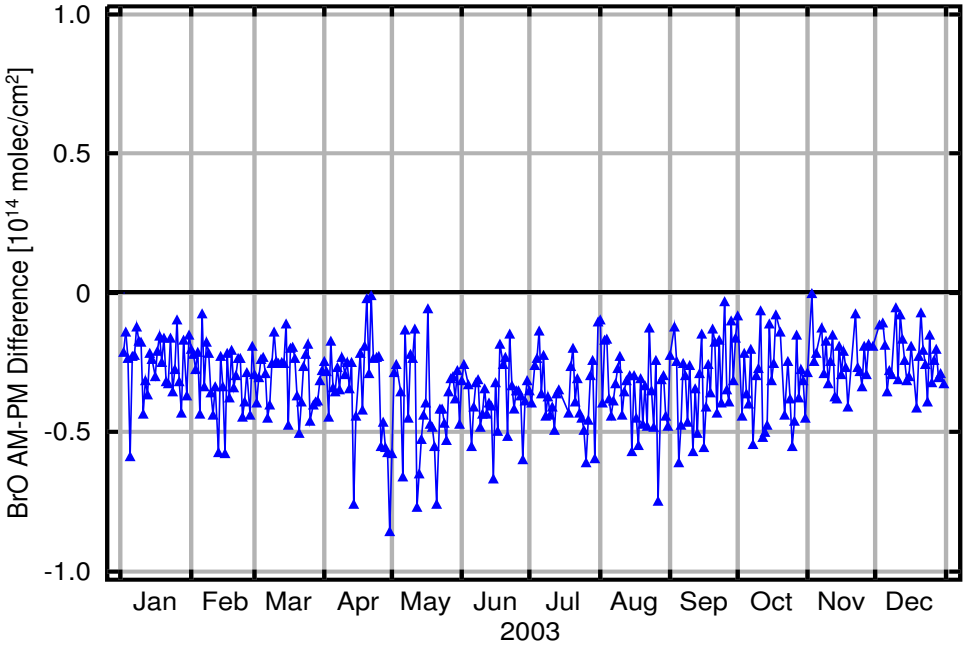

Figure 8.3: Difference between morning and evening values of BrO differential slant column densities

were similar to the first run. In the third run the reaction of $BrONO_2$ with $O(^3P)$ [*Soller et al.*, 2001] along with the ECMWF data was used. The 1-D photochmical model was coupled with radiative transfer model (RTM) [*Rozanov et al.*, 2001] in order to calculate the slant column density. The RTM uses a full spherical geometry and also considers multiple scattering, variation of BrO with SZA along slant column path. The calculations presented here were done at wavelength of 350 nm which is the center wavelength for fitting window.

Figure 8.4 shows the BrO slant columns calculated by the model for different runs. Run one and two which used the climatological data and the ECMWF data respectively show no significant difference in the BrO slant columns. However, the third run which includes the reaction proposed by *Soller et al.* [2001] shows an increase in the BrO slant column densities by approximately 20% in the morning and 10% in the evening as compared to the the first two runs for the same time period. This result is consistent with the sensitivities studies presented by *Sinnhuber et al.* [2002] for the mid latitude region. The reaction is found to be important above 20 km [*Sinnhuber et al.*, 2005]. The reason for this is obvious. As we move high in altitude, the concentration of $O(^3P)$ increases and consequently the reaction of $BrONO_2$ with $O(^3P)$. The effect is small below 20 km due to low concentration of $O(^3P)$.

A comparison of the BrO monthly mean measurements over Nairobi with all the three model runs is shown in Figure 8.5. The model captures the diurnal and seasonal variation quite well. However, it is seen that the observed BrO DSCDs are higher than

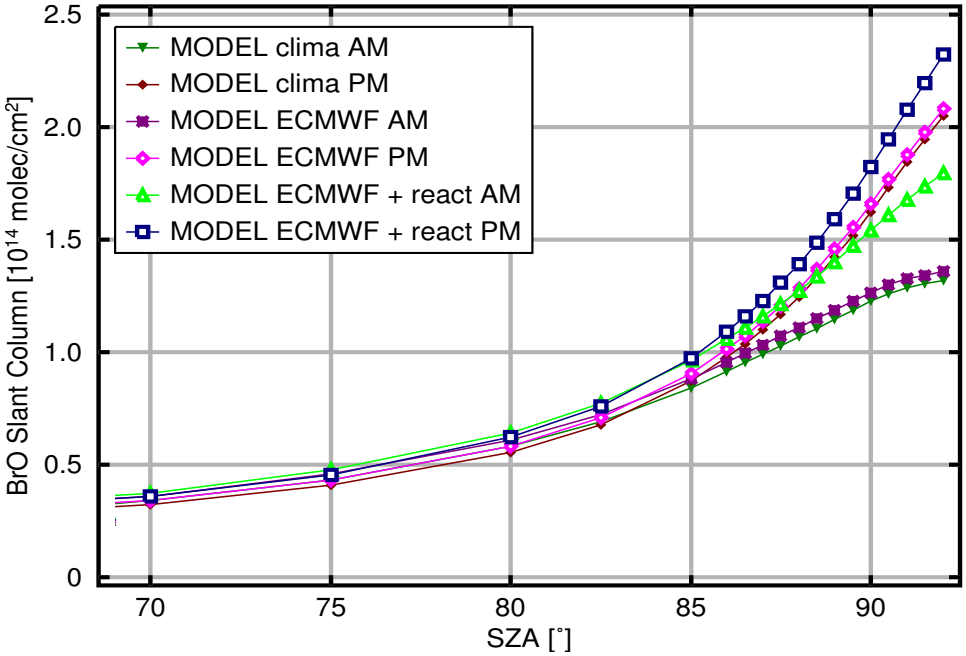

Figure 8.4: Modelled BrO slant columns for Nairobi, August 15th, 2003

the BrO DSCDs calculated by the model runs which used climatological or ECMWF data. The observed BrO DSCDs are higher by about 4.0 x 10^{13} molecules/cm^2 (25%) in the evening and 6.0 x 10^{13} molecules/cm^2 (45%) in the morning. The difference decreases to about 2.0 x 10^{13} molecules/cm^2 (15%) in the evening and 3.0 x 10^{13} molecules/cm^2 (20%) in the morning as compared to the third model run which included the reaction of $BrONO_2$ with O(^{3}P) [*Soller et al.*, 2001]. *Sinnhuber et al.* [2002] have reported differences between the modelled and observed BrO DSCDs for different latitudes ranging from 0.4 x 10^{13} molecules/cm^2 to 2.8 x 10^{13} molecules/cm^2 for AM values and from 0.6 x 10^{13} molecules/cm^2 to 3.2 x 10^{13} molecules/cm^2 for PM values. The differences of the modelled and observed BrO DSCDs reported here are comparable to those reported by *Sinnhuber et al.* [2002]. *Sinnhuber et al.* [2002] performed model runs for another tropical site at Kashidoo (5°N, 73°E) which showed no seasonal variation which is consistent with the model runs performed for different tropical site at Nairobi. The PM/AM ratio for Kashidoo was reported to be 1.4 [*Sinnhuber et al.*, 2002], while for the Nairobi station it ranges from 1.35 to 1.65. Considering the combined uncertainties of model and fit errors, measurements of about 20% the measurements and the model calculations are generally in good agreement.

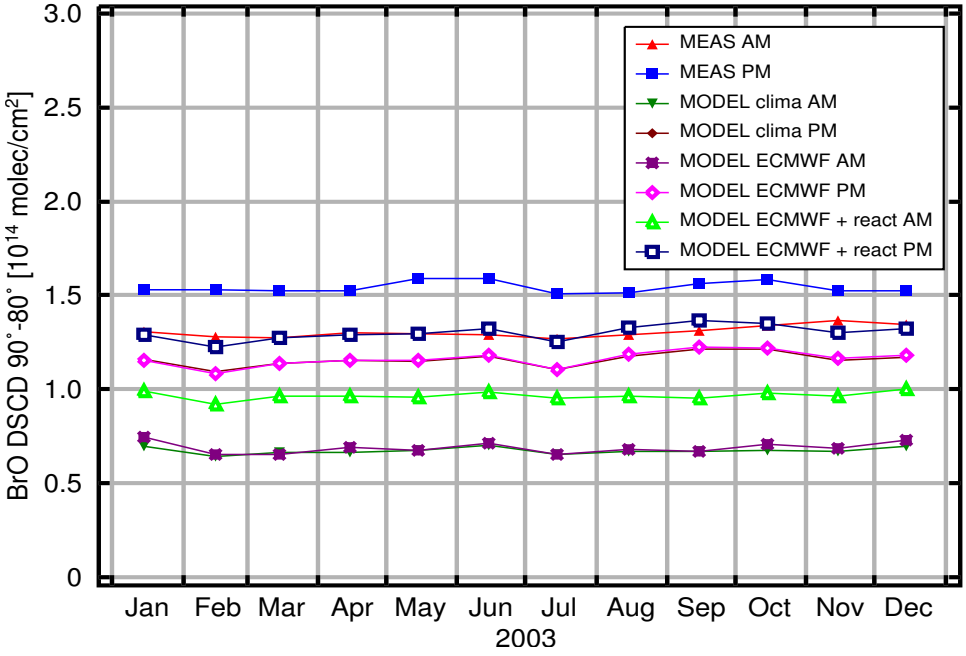

Figure 8.5: Comparison of observed and modelled BrO differential slant columns densities for the year 2003. For the observations only the monthly means are presented.

8.3 Conclusion

A first comprehensive BrO measurements at low latitudes has been presented from one year of ground based zenith-sky measurements of BrO over Nairobi (1°, 36°E). This data can be used to validate BrO retrievals from SCIAMACHY. The measured BrO shows a diurnal variation with average BrO DSCDs being 1.3 x 10^{14} molecules/cm^2 in the morning 1.5 x 10^{14} molecules/cm^2 in the evening. The PM/AM ratio is found to be 1.2 which is slightly lower than at midlatitude. That seasonal variation of BrO is very small in the tropics is further confirmed by the measured BrO DSCDs (90°-80° SZA) which show very little seasonal variation.

A comparison of the measured BrO DSCDs at Nairobi (1°, 36°E) with the values calculated from 1-D model is also presented. The model reproduces the diurnal and seasonal variation quite well but the morning values are 45% smaller and the evening values are 25% smaller than the measured DSCDs. The agreement between the model and the measured values can be improved by including the reaction of $BrONO_2$ with $O(^3P)$ [*Soller et al.*, 2001]. The measured BrO values are then just 20% higher in the morning and 15% higher in the evening as compared to the model calculations. These values are within the combined uncertainties of model and measurements. This indicates that the reaction of $BrONO_2$ with $O(^3P)$ plays an important role at low latitudes.

9 BrO in the troposphere

Ozone depletion events such as those in the stratosphere have also been observed in the tropospheric boundary layer during spring time at many sites in the Arctic and northern high and midlatitudes [*Barrie et al.*, 1988; *Oltmans et al.*, 1989; *Solberg et al.*, 1996; *Bottenheim et al.*, 1990; *Matveev et al.*, 2001; *Wagner and Platt*, 1998; *Richter et al.*, 1998], as well as the Antarctic [*Kreher et al.*, 1997]. The low ozone episodes are found to be very well correlated to the observations of high amount of bromine monoxide (BrO) at these sites linking these events to halogen chemistry similar to that in the stratosphere but dominated by bromine. BrO VMR as high as 100 ppt has been observed during the polar spring in the Planatary Boundary Layer (PBL) [*Hausmann and Platt*, 1994; *Wagner and Platt*, 1998; *McElroy et al.*, 1999]. Similarly, BrO VMR as high as 80 ppt has been detected emitted from salt pans located at at a midlatitude site at the Dead sea, Israel [*Hebestriet et al.*, 1999]. Subsequently, comparison of collocated ground based, balloon borne, satellite instrument GOME [*Pundt et al.*, 2002; *Fitzenberger et al.*, 2000; *Roozendael et al.*, 2002] measurements showed discrepancies between the integrated stratospheric profiles measured using balloons and column measurements done from ground or satellite leading to the speculation that BrO is ubquitous in the free troposphere [*Harder et al.*, 1998; *Fitzenberger et al.*, 2000; *Roozendael et al.*, 2002; *Pundt et al.*, 2002; *Schofield et al.*, 2004]. The presence of reactive halogen species within the free troposphere may have significant effects on ozone and it could effect other key chemical parameters as well [*Platt and Hönninger*, 2003]. Thus it is important to know the amount of such species in the troposphere.

This chapter calculates the amount of BrO present below 15 km in the atmosphere using the nadir-limb measurments for the years 2003 and 2004 from the SCIAMACHY instrument. This is a first attempt to see the picture globally. Further, a discussion on possible sources of bromine in the troposphere is presented.

9.1 Bromine in the free troposphere from SCIAMACHY

Prior to the SCIAMACHY data, the calculation of BrO in the troposphere has been attempted using collocated GOME column BrO and the stratospheric integrated profiles from balloon data or 3-dimensional chemical transport model output in the stratospheric region [*Richter et al.*, 1998; *Fitzenberger et al.*, 2000; *Richter et al.*, 2002] . The tropospheric concentration was calculated by simply subtracting the collocated stratospheric integrated profiles from balloon data or 3-dimensional chemical transport model output from the total column.

A similar calculation of the amount of BrO present in the troposphere, is possible with the help of instrument like SCIAMACHY. One of the important and novel features

of SCIAMACHY is the ability to observe the same air mass first in limb and thereafter in nadir-viewing geometry within about 8 minutes. This special feature of SCIAMACHY can be used to detect the amount of BrO present in the troposphere by subtracting the stratospheric column (obtained by integrating the limb BrO) from the total BrO column retrieved from the nadir measurements.

9.1.1 Retrieval of SCIAMACHY BrO vertical column

The nadir BrO columns of BrO are retrieved using the forward model SCIATRAN [*Rozanov et al.*, 1997], which includes the effects of multiple scattering, atmospheric refraction, and sphericity but no polarisation. The inversion procedure uses the DOAS technique [*Platt*, 1994], which is an application of the Beer-Lambert's law. The basic implementation of the technique is similar to that used for GOME [*Richter et al.*, 1998, 2002] and the details of the implementation can be found in *Richter et al.* [1998]. More details on the technique of the nadir retrieval of BrO can be obtained in *Afe et al.* [2004]; *Afe* [2005]

9.1.2 Unresolved issues in BrO nadir retrieval

The main error source of the nadir BrO columns is the uncertainty in the airmass factors. Satellite nadir measurements are much less sensitive to BrO in the lower troposphere than in the stratosphere [*Afe et al.*, 2004]. Any BrO contribution from the lower troposphere in particular, if the BrO is present close to the surface, will therefore be underestimated [*Richter et al.*, 2005], while BrO over bright clouds might be slightly overestimated and lead to enhanced columns over snow, ice, and also over low clouds [*Richter et al.*, 2005]. The spectral analysis and a possible bias from the irradiance spectrum used also contribute to the overall error, which is estimated to be 20% at mid and high latitudes and 30% in the tropics.

The standard wavelength region used in the algorithm which is used to retrieve BrO from the GOME measurements ranges from 344.7 – 359 nm. However since this range interferes with the SCIAMACHY polarization sensitivity, it made the results unreliable and hence the wavelength window was UV-shifted toward the to 336 – 347 nm. And though the results are now consistent with GOME data [*Richter et al.*, 2005], there are still unresolved issues of the intereference from the formaldehyde (HCHO) over the tropical forests and has not been removed.

Also as a result of high spatial resolution of SCIAMACHY[1] as compared to GOME, SCIAMACHY BrO has larger scatter and a tendency for larger values. Futher it should be noted that though the same algorithm as that used for GOME nadir BrO retrieval is used for SCIAMACHY nadir BrO retrieval and both products have shown good agreement, the algorithm used for the retrieval of SCIAMACHY nadir BrO has not been validated.

[1]The spatial resolution of SCIAMACHY is 60 x 30 km^2 as compared to 320 x 40 km^2 of GOME.

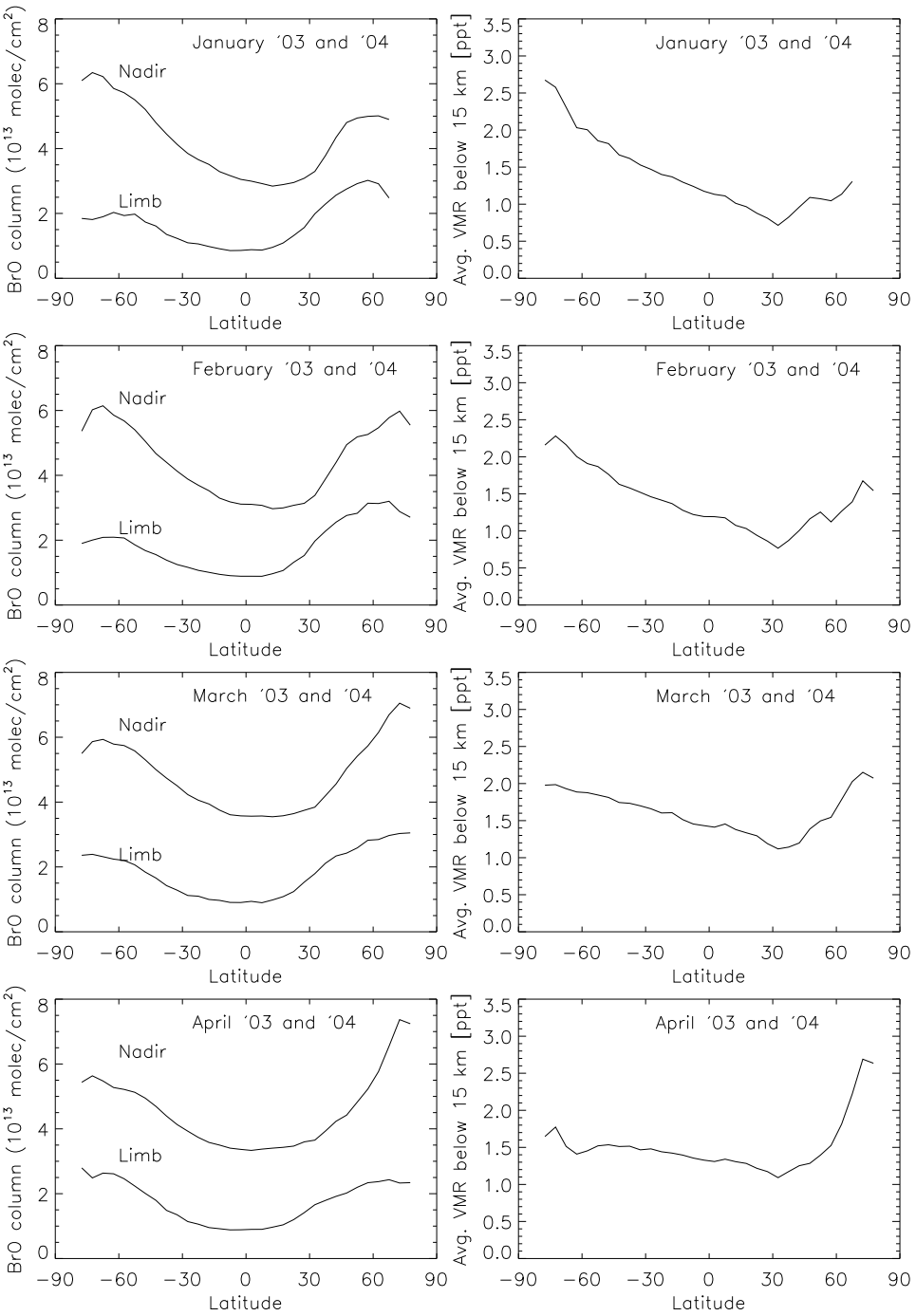

Figure 9.1: (a) Vertical BrO column above 15 km from SCIAMACHY limb measurements and total BrO column from SCIAMACHY nadir measurements, zonally averaged each month during 2003 and 2004. (b) Inferred average BrO mixing ratio below 15 km altitude

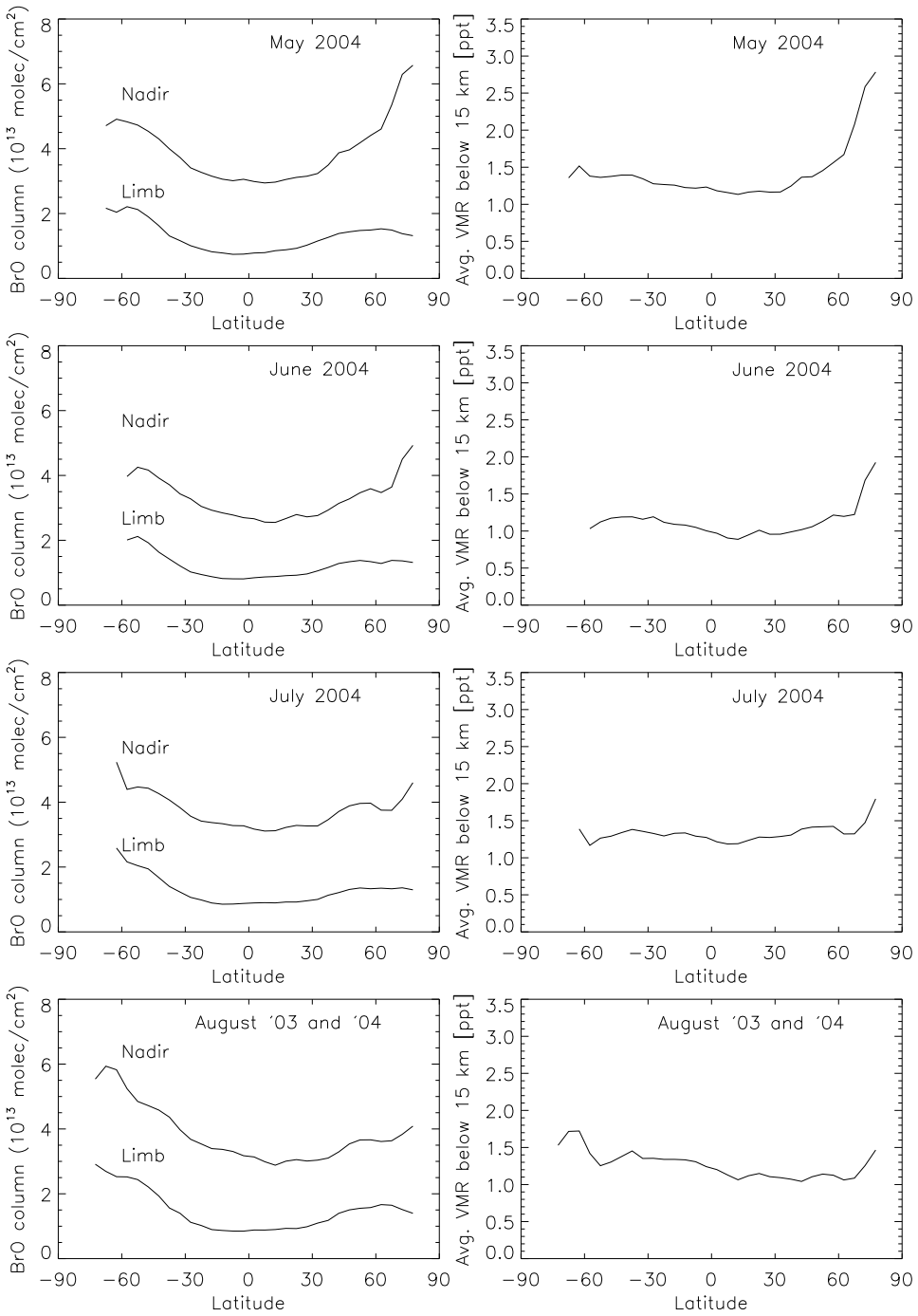

Figure 9.1: *Continued.* Note: The limb measurements are not available during May, June, and July, 2003. Hence for this period, only the data of 2004 are used.

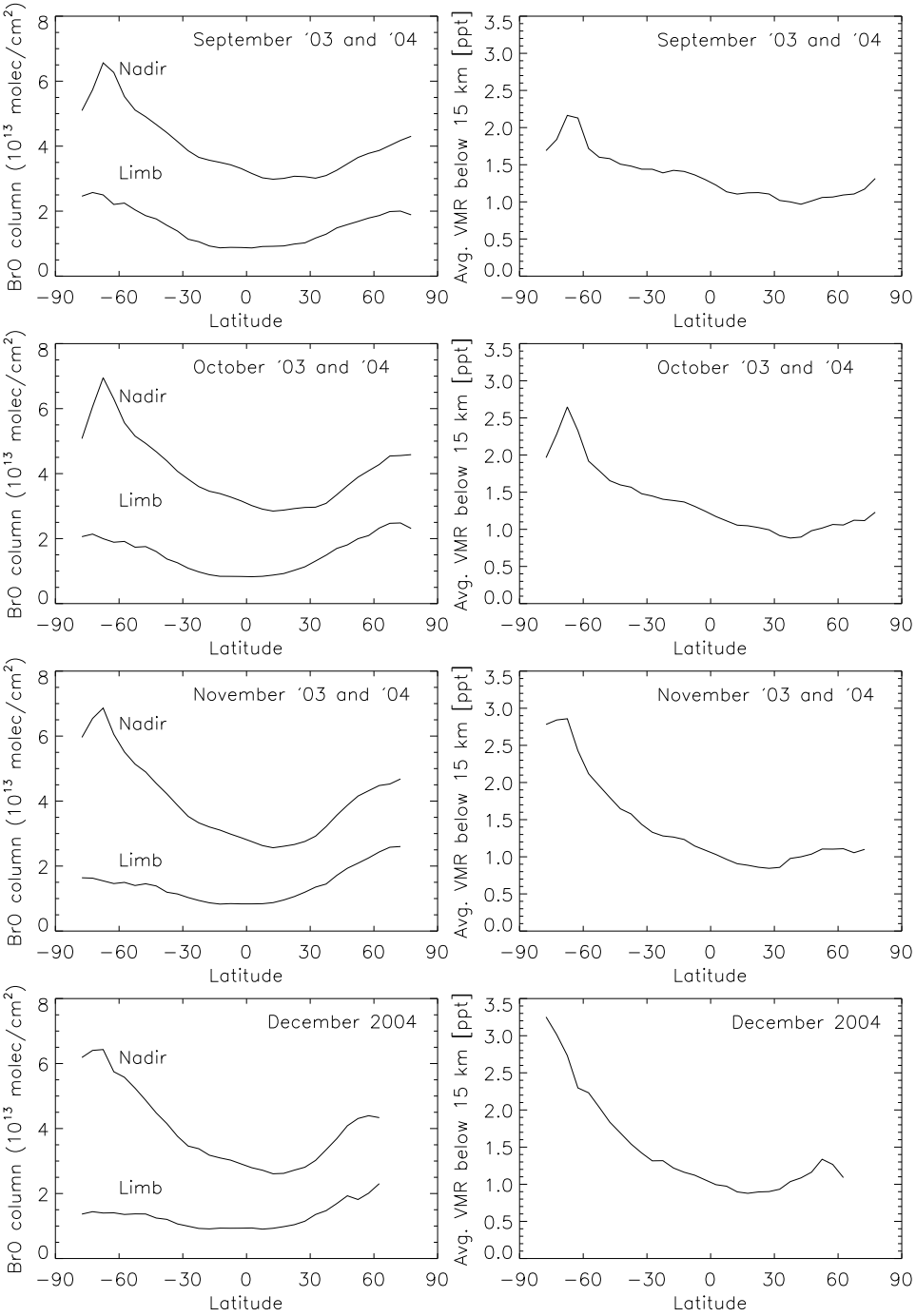

Figure 9.1: *Continued.* Note: The nadir measurements are not available during December 2003. Hence for this period, only the data of 2004 are used.

9.2 Integration of statospheric profiles

In the first step, a mean volume mixing ratio was calculated by using the VMRs at two altitude grid points. In the second step, the air density/area^2 was calculated by multiplying the pressure difference, $\triangle$p, between the same two altitude grid points by a constant factor, α, which was calculated as follows:

$$\alpha = \frac{\mathrm{A}}{\mathrm{M} \times \mathrm{g}} \tag{9.1}$$

where,
A = Avagadro's constant = 6.022 $\times$ 10^{23} mol^{-1}
M = Molecular weight of air = 28.9644 $\times$ 10^{-3} kg $\times$ mol^{-1}
g = Acceleration due to gravity = 9.80665 m/s^2

The BrO number density between these grid points was then calculated by multiplying the calculated mean BrO VMR by the air density between the same two altitude grid points. The pressure values needed to calculate the air density was taken from ECMWF. The integrated stratospheric BrO profiles were obtained by adding the calculated BrO number densities.

By subtracting the stratospheric BrO column from the total column, the number density below 15 km is obtained. The BrO VMR between surface and 15 km was obtained by dividing this calculated BrO number density by the air density between surface and 15 km, which was calculated using the same procedure as explained above.

9.3 BrO below 15 km in the atmosphere

BrO in the free troposphere is calculated by subtracting the integrated stratospheric BrO profiles from the total vertical column of BrO. The left columns of Figure 9.1 show a comparison between the total BrO vertical column density derived from the SCIAMACHY nadir measurements and the integrated BrO column above 15 km altitude derived from SCIAMACHY limb measurements for the period 2003 and 2004 using the climatology constructed in this work and the climatology of column BrO for the same period (courtesy: Dr. A. Richter). Also the amount of BrO in volume mixing ratio for the corresponding period is shown in the right columns of the same figures. It should be noted that the limb data were not available during May, June, and July 2003 and the nadir data during December 2003. Thus during this period the data of only 2004 is used. The BrO VMR starts increasing at higher latitudes in February/March and reaches to peak of approximately 3 ppt in May. The BrO VMR in the tropics is seen to a large extent constant below 15 km. The total BrO column from nadir observations with about $3-7\times10^{13}$ molecules/cm^2 is similar to previously published total BrO columns derived from GOME observations [*Richter et al.*, 1998]. The integrated BrO column above 15 km is much smaller, implying that there is a significant amount of BrO below 15 km of about $2-4\times10^{13}$ molecules/cm^2. Assuming that this BrO background is well mixed between the surface and 15 km, this corresponds to an average tropospheric BrO

VMR of about 1.4 ± 0.7 ppt (estimated total uncertainty), with values reaching 2 ppt in the high southern latitudes. Part of the residual column below 15 km altitude will come from BrO in the lowermost stratosphere between the tropopause and 15 km altitude, in particular at high latitudes where this may contribute to the enhanced average BrO VMR seen at high southern and northern latitudes. However, it seems unlikely that a large part of the residual column resides in the lower stratosphere. The tropospheric BrO background of about 1.4 ppt agrees well with previous estimates from balloon measurements of 0.6 – 2.0 ppt [*Fitzenberger et al.*, 2000] and is still consistent with the upper limit of 0.9 ppt estimated by [*Schofield et al.*, 2004].

The elevated amount of column BrO is clearly visible during the spring period of each hemisphere. The amount of BrO VMR at high latitudes in the southern hemisphere during winter/spring is seen to increasing in September, reaching close to approximately 3 ppt in December/January. A similar feature is observed during the winter/spring period of the northerm hemisphere. Observations of enhanced tropospheric BrO columns in high latitude spring have been reported before [*Richter et al.*, 1998]; [*Wagner and Platt*, 1998] and are attributed to processes on sea ice that release bromine into the atmosphere [*Kaleschke et al.*, 2004].

9.4 Sources of bromine in the troposphere

The sources of bromine in the free troposphere are still a topic of debate. It is speculated that bromine explosion events occuring in the polar region could be significant sources of bromine in the troposphere. Another possible source could be the photochemical production through destruction of organic bromine species [*Dvortsov et al.*, 1999] or the transport of inorganic bromine species from the stratosphere to the troposphere due to dynamical activity.

Sea salt aerosols generated by breaking of waves on the ocean surface have been identified as the main source of bromine over the open oceans [*Tang and McConnel*, 1996; *Sander et al.*, 2003]. But the tranfer mechanism of bromine from sea water to atmsophere still remains a field of research. An interesting observation has been that high amount of BrO has always been observed over sea during polar sunrise [*Ridley et al.*, 2003; *Zeng et al.*, 2003; *Frieß et al.*, 2004]. *Rankin et al.* [2002] have proposed that frost flowers could be one of the potential sources of BrO in the polar region. Frost flowers are ice crystals growing in the linear breaks in the sea ice cover or small openings between drift ice and fast ice. They have been found to have salinties and bromide ion concentration of about three times of bulk sea water [*Perovich and Richetr-Menge*, 1994; *Rankin et al.*, 2002; *Kaleschke et al.*, 2004]. The BrO released during these events can be transported to the free troposphere. However though these events appear to be very appealing source of bromine in the troposphere it should be noted that these events occur only during the sunrise in the polar regions whereas BrO in the free troposphere has also been detected at midlatitudes [*Fitzenberger et al.*, 2000] and the tropics [*Pundt et al.*, 2002].

Fitzenberger et al. [2000] have proposed the presence of BrO through heterogeneous

activation of HBr, HOBr and $BrONO_2$ possibly by reactions involving HCl taken up by tropospheric hydrometeores (ice crystals and water droplets). This leads to the formation of photolabile BrCl. The photodissociation of BrCl leads to the formation of Br atom which subsequently reacts with O_3 to form BrO. As already stated above another possible source could be the photochemical production through destruction of organic bromine species or the transport of inorganic bromine species from the stratosphere and the troposphere due to dynamical activity [*Dvortsov et al.*, 1999].

9.5 Conclusion

The difference in the nadir-limb measurements of SCIAMACHY BrO are used to calculate the amount of BrO below 15 km in the atmosphere. The BrO below 15 km in the atmosphere shows a seasonal variation at higher latitudes in the spring hemisphere. A BrO VMR of 1.4 ppt averaged over all latitudes and months, is found to exist throughout the year below 15 km in the atmosphere. The chapter also discusses the possible sources of BrO in the troposphere.

10 Total bromine in the stratosphere

The knowledge of the total bromine and its partitioning between the organic and inorganic species in the stratosphere is an important input for the atmospheric models to study their impact on ozone destruction [*Wennberg et al.*, 1994, 1997; *Gao et al.*, 1997]. A large fraction of the total bromine is contributed from methyl bromide (CH_3Br) and halons (e.g. see Chapter 4). While CH_3Br has both natural and anthropogenic sources, halons are entirely man-made. Our recent study has shown that anthropogenic bromine emissions are responsible for 45% of the column ozone loss at northern hemisphere midlatitudes between 1980 and 2005 [*Sinnhuber et al.*, 2006]. The very short lived species (VSLS) of organic bromine also contribute to the total bromine. These VSLS are converted to the inorganic bromine [*Dvortsov et al.*, 1999] in the upper troposphere and lower stratosphere and make a non negligible contribution to the inorganic bromine (Br_y) in the stratosphere. A small contribution to total bromine from the VSLS could make a significant impact on the stratospheric ozone depletion [*Salawitch et al.*, 2005]. Another contribution could also come from the influx of Br_y from the troposphere to the stratosphere [*Ko et al.*, 1997, also see Chapter 9]. Further, our recent study has found that the chemical efficiency (also called α factor) of bromine relative to chlorine for global total ozone depletion from our model calculations is 68 on an annual average [*Sinnhuber et al.*, 2006], which is much higher than the previously calculated value of 45 [*Daniel et al.*, 1999]. Thus the knowledge of total bromine in the atmosphere is important owing to its significant impact on the stratospheric ozone depletion.

This chapter estimates the amount of inorganic bromine (Br_y) in the stratosphere using the SCIAMACHY BrO and modeled Bro/Br_y ratio obtained from the simulations of the 1-D photochemical model constrained with SCIAMACHY NO_2. Further, the total bromine in the atmosphere is also estimated along with the estimation of the contribution of VSLS to the total bromine. Prior to this, the two methods to estimate the bromine loading in the stratosphere are discussed.

10.1 The organic method

The organic bromine present in the atmosphere can be calculated by *in-situ* measurements of the brominated species [*Wamsley et al.*, 1998; *Schauffler et al.*, 1998; *Pfeilsticker et al.*, 2000]. A budget of the known organic bromine sources for 2002 is summarised in Table 10.1. Six of these gases contribute predominantly to the organic bromine budget in the troposphere [*Wamsley et al.*, 1998]. The total organic bromine mixing ratio (CBry) considering only the dominant species [*Wamsley et al.*, 1998] can be calculated as:

$$CBr_y = [CH_3Br] + [CBrClF_2] + [CBrF_3] + 2\,[C_2Br_2F_4] + [CH_2BrCl] + 2\,[CH_2Br_2] \quad (10.1)$$

The square brackets indicate the mixing ratios and multipliers before the brackets indicate the numbers of bromine atoms per molecule. Since the method is based on the calculation of mixing ratios of organic brominated compounds in the troposphere and the stratosphere, it is called as the "organic method". The problem in determining the organic bromine using the *in-situ* measurements of brominated species is that the current techniques measure limited number of brominated species. In the absence of the measuremements they can be estimated using a simple paramaterization of the relationship that is represented by a power law with power coefficient representing the effective stratospheric loss rate. *Wamsley et al.* [1998] proposed an empirical relationship between brominated species and CFC-11 in the form of a simple power law with a power coefficient equal to ratio of loss rates of the species relative to CFC-11. It is represented as:

$$[X] = [X]_0 \left(\frac{[CFC-11]}{[CFC-11]_0} \right)^{\frac{1}{d}} \quad (10.2)$$

where,

[X] = VMR of each brominated species.

$[X]_0$ = Mixing ratio of the species at the tropopause in mid October 1994.

[1/d] = Power coefficient.

[CFC-11] = VMR of CFC-11.

$[CFC\text{-}11]_0$ = Mixing ratio at the tropopause in mid October 1994.

The correlation is very reproducible when normalised for the atmospheric growth species [*Wamsley et al.*, 1998; *WMO*, 1998]. The normalization is necessary if one wants to compare datasets from different locations and time. A more detailed description of the oragnic method can be found in *Wamsley et al.* [1998].

10.1.1 Estimate of bromine loading in the stratosphere[3]

The bromine loading in the stratosphere using the organic has been estimated in this work for the period 18 to 27 September 2002. The CFC-11 profiles have been retrieved from MIPAS measurements as described by [*Glatthor et al.*, 2005]. 100 to 120 individual profiles from the period 18 to 27 September 2002 were averaged to create each zonal mean profile representing a 5° latitude bin, except for the 5 to 10°N and 80 to 85°N latitude bins where only about 60 profiles each were available. The total precision is estimated to be 5 – 17% in the lower stratosphere, while systematic error contributions which do not cancel out by zonal averaging amount to 4 – 15%.

[3] A part of the material for this section is taken from our publication in *Sinnhuber et al.* [2005]

Table 10.1: Budget of organic bromine source gases for 2002

Source gas	Mixing ratio[1]		Ref.[2]
Included by Wamsley et al. [1998]			
Methyl bromide	CH_3Br	8.1	[2]
Halon-1211	$CBrClF_2$	4.1	[2]
Halon-1301	$CBrF_3$	2.6	[2]
Halon-2402	$C_2Br_2F_4$	0.4	[1]
Dibromomethane	CH_2Br_2	1.21 (0.9–1.5)	[3]
Bromochloromethane	CH_2BrCl	0.14	[4]
Total		18.16	
Not included by Wamsley et al. [1998]			
Halon-1202	CBr_2F_2	0.04	[1]
Bromoform	$CHBr_3$	1.63 (0.9–2.3)	[3]
Dibromochloromethane	$CHBr_2Cl$	0.16 (0.06–0.26)	[3]
Bromodichloromethane	$CHBrCl_2$	0.19 (0.14–0.26)	[3]

[1]For long-lived species global mean surface mixing ratios are given. For very short-lived gases the median and range of tropical boundary layer mixing ratios are given.

[2]References: [1]*Montzka et al.* [2003a];[2] *Montzka et al.* [2003b]; [3] *Ko et al.* [2003]; [4] *Wamsley et al.* [1998]

Table 10.2: Power Coefficients (d) for the correlations of brominated species considered by *Wamsley et al.* [1998] and this work to calculate bromine loading

Molecule		d
Methyl bromide	CH_3Br	0.67
Halon-1211	$CBrClF_2$	0.6
Halon-1301	$CBrF_3$	0.98
Halon-2402	$C_2Br_2F_4$	0.65
Dibromomethane	CH_2Br_2	0.12
Bromochloromethane	CH_2BrCl	0.16

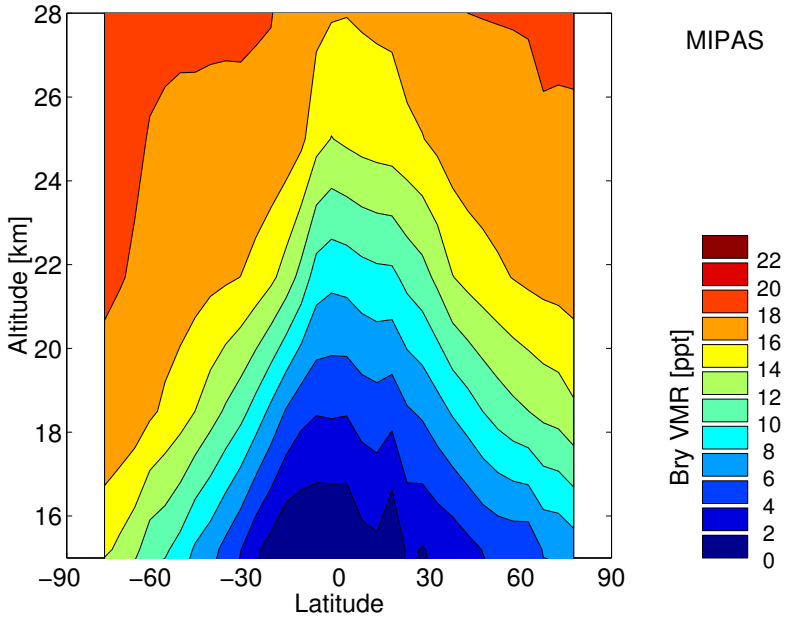

Figure 10.1: Zonal mean inorganic bromine Br_y derived from MIPAS measurements of CFC-11, using the empirical relationship of *Wamsley et al.* [1998]. Note that this estimate of Br_y does also include the contribution of CH_2Br_2 and CH_2BrCl, but not the contribution from $CHBr_3$ or any influx of Br_y from the troposphere

An estimate of Br_y is calculated from the MIPAS CFC-11 measurements using the empirical correlation of [*Wamsley et al.*, 1998] (Equation (10.2)) and the power coefficients summarised in Table 10.2. Tropospheric source gas concentrations were taken as indicated in Table 10.1. Figure 10.1 shows zonal mean Br_y VMR for the investigated period from 18 to 27 September 2002. As is seen in Figure 10.1, the VMR of Br_y increases with altitude primarily due to the dissociation of organic bromine compounds into inorganic bromine. Also it is seen that as one moves towards the higher latitudes the BrO VMR increases. We estimate total bromine loading of 18.16 ppt in the stratosphere for the period from 18 to 27 September 2002. As the total bromine loading was rather constant during the last few years prior to 2002 [*Montzka et al.*, 2003a, b], a variation of the bromine loading with age of air is not considered. Note that the estimate of Br_y includes also the contribution from the two short-lived source gases CH_2Br_2 and CH_2BrCl, but not other short lived gases such as bromoform or any influx of Br_y from the troposphere. Thus, this estimate of Br_y may be considered a lower limit for the available inorganic bromine.

10.2 The inorganic method

In this method the estimation of the Br_y is based on the measurements of BrO and the BrO/Br_y ratio obtained from a photochemical model. Br_y is obtained by dividing the measured BrO by the BrO/Br_y ratio obtained from a photochemical model simulations [*Wamsley et al.*, 1998; *Pfeilsticker et al.*, 2000]. This methos has been used in this work to estimate the Br_y.

10.2.1 Estimate of bromine loading in the stratosphere

The seasonal and zonal means of SCIAMACHY BrO presented in Chapter 7 are used along with BrO/Br_y ratio simulated by the 1-D photochemical model in order to estimate Br_y. The one dimensional photochemical model (1-D model) used here is same as that discussed in Chapter 3. To summarise in brief, the 1-D model is based on the photochemical scheme from the SLIMCAT model [*Chipperfield*, 1999]. The model contains a detailed stratospheric chemistry which includes gas phase as well as heterogeneous reactions. In all, there are 135 chemical reactions and 44 photolysis reactions of 52 species which are considered to be important for the stratospheric chemistry. The model was initialised with output from a 2-D chemistry, transport and photochemistry model, which is a composite of the SLIMCAT chemistry [*Chipperfield*, 1999; *Sinnhuber et al.*, 2003] and the THINAIR dynamics code [*Kinnersley*, 1996]. Temperature and pressure in the model were taken from ECMWF analysis. The reaction rate constants and photolysis cross sections were taken from the latest JPL-2002 recommendations [*Sander et al.*, 2003]. The reaction of $BrONO_2$ with $O(^3P)$ [*Soller et al.*, 2001] could be an important source of BrO at higher altitudes [*Sinnhuber et al.*, 2005]. This reaction has not been considered in the JPL 2002 catalogue. However, we have included this reaction in our model simulations. To estimate Br_y in the stratosphere using the inorganic method, it is important to have a realistic partitioning of bromine species in the model. Since bromine partitioning is controlled by NO_2 [*Fish et al.*, 1997; *Richter et al.*, 1999], the 1-D model is constrained by the SCIAMACHY NO_2 profiles by scaling NO, NO_2, NO_3, and HNO_3 (but not $ClONO_2$ and BrONO2!) in the initialization until the modeled NO_2 agreed with measured NO_2 at the local time of the SCIAMACHY measurements. The model is run for a period of 5 days in order to allow for spin up and all calculations are done using the output of the fifth day.

The general partitioning of inorganic bromine species in the model for the four seasons and five latitude zones is shown in Figure 10.2. In general it is observed that BrO and $BrONO_2$ form a major part of the daytime Br_y. Other reservoir species like HBr, HOBr, BrCl form a very small fraction of Br_y. The model calculations show that BrO is on an average 40 – 70% of Br_y, consistent with previous studies [*Sinnhuber et al.*, 2002; *Pundt et al.*, 2002]. *Avallone et al.* [1995] compared model calculations of the BrO/Br_y ratio in the NH lower stratosphere with in situ airborne observations. While their modeled BrO/Br_y ratio was around 50 – 60%, comparable to our results, the observations suggested a much smaller BrO/Br_y ratio of only about 40%. The reason for the discrepancy between their observed the modeled BrO/Br_y is still not clear.

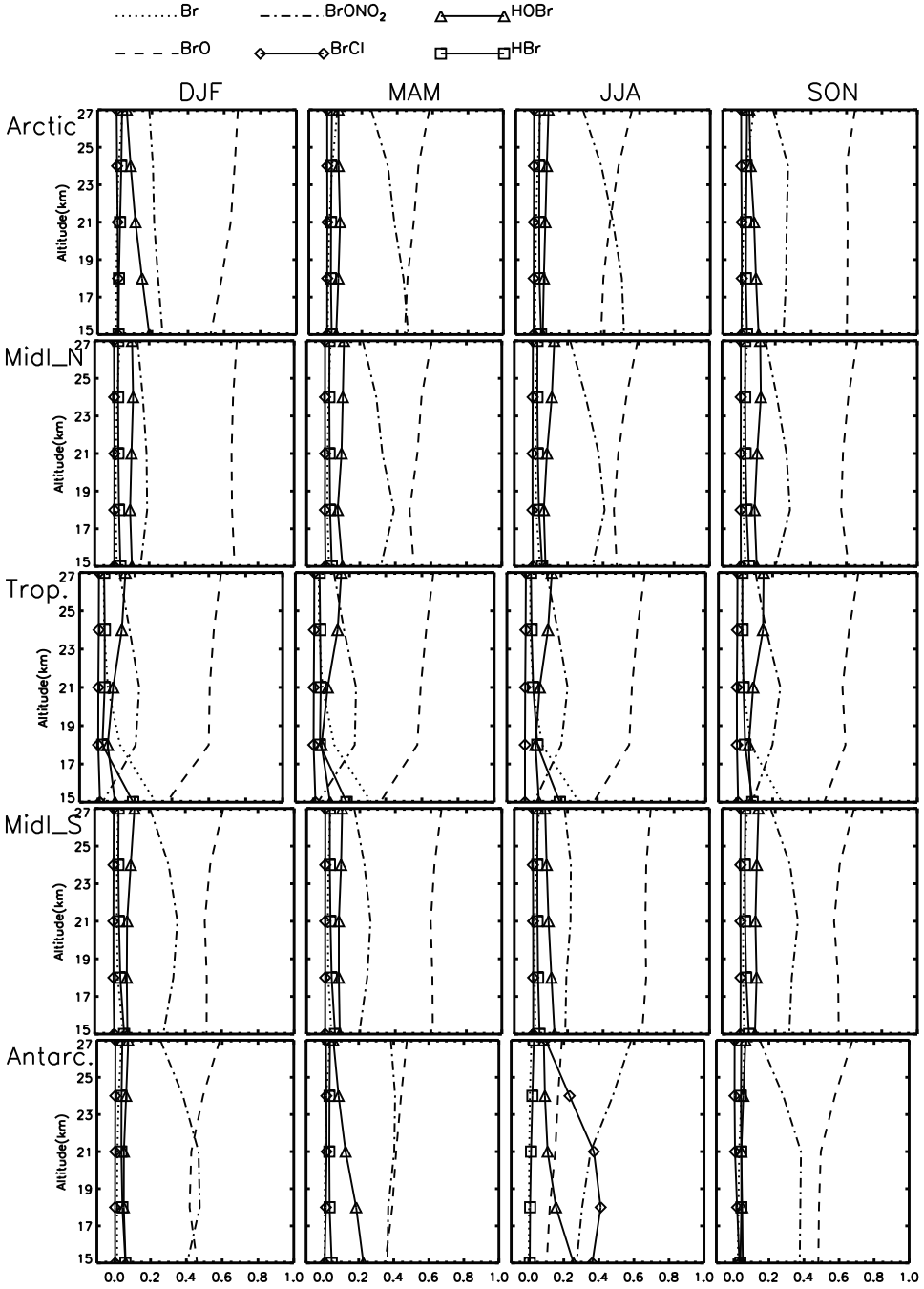

Figure 10.2: Partitioning of bromine species as calculated by the 1-D photochemical model. The model was constrained by SCIAMACHY NO_2 measurements. Calculations were performed for the four seasons December/January/February (DJF), March/April/May (MAM), June/July/August (JJA) and September/October/November (SON) and five latitude bands: Arctic (north of 60°N), Northern Hemisphere mid-latitudes (30°N–60°N), tropics (30°S–30°N), Southern Hemisphere midlatitudes (30°S–60°S), and Antarctic (south of 60°S).

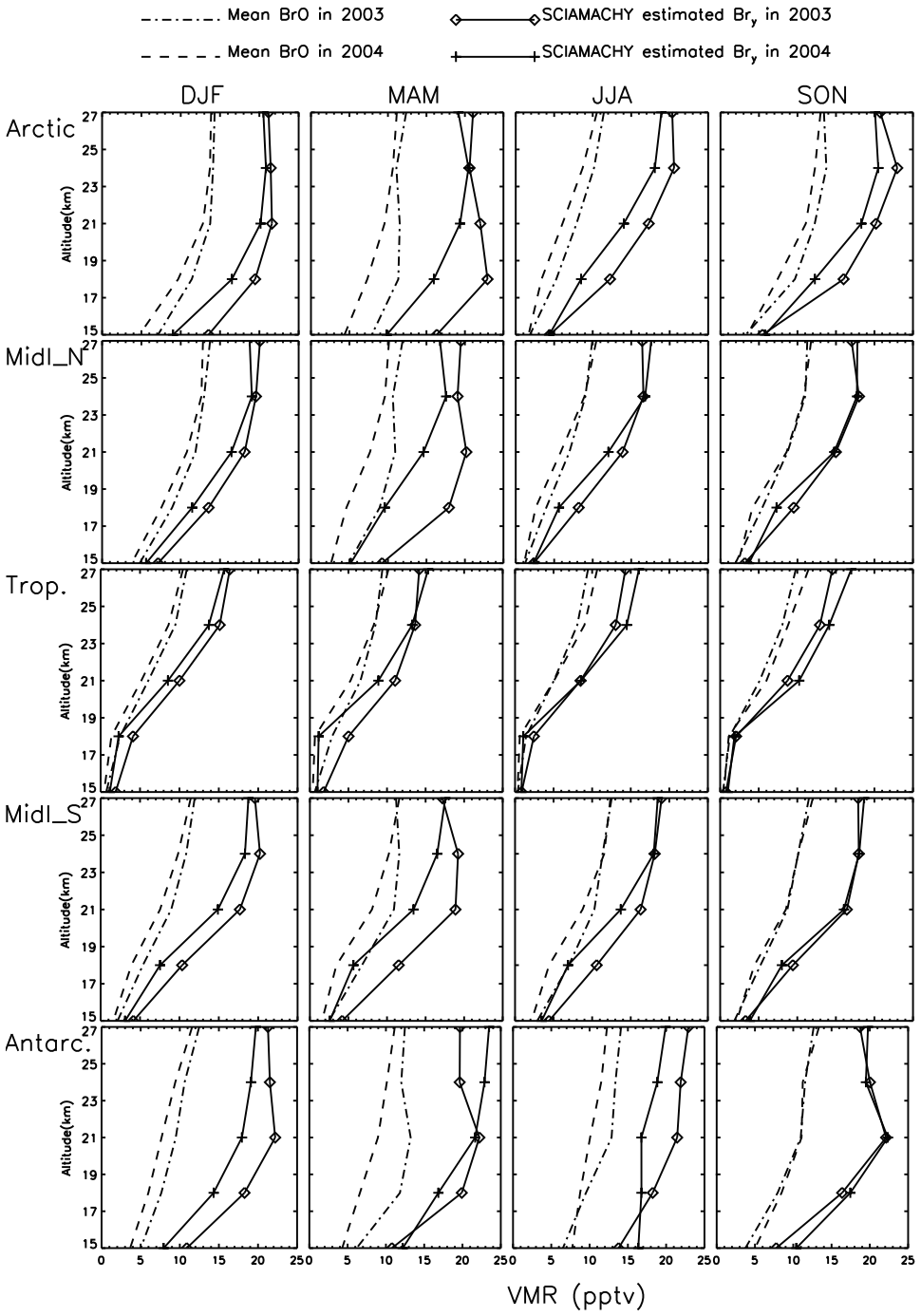

Figure 10.3: Seasonal, zonal mean BrO VMRs for the two years 2003 and 2004 along with estimated Br_y for the same period.

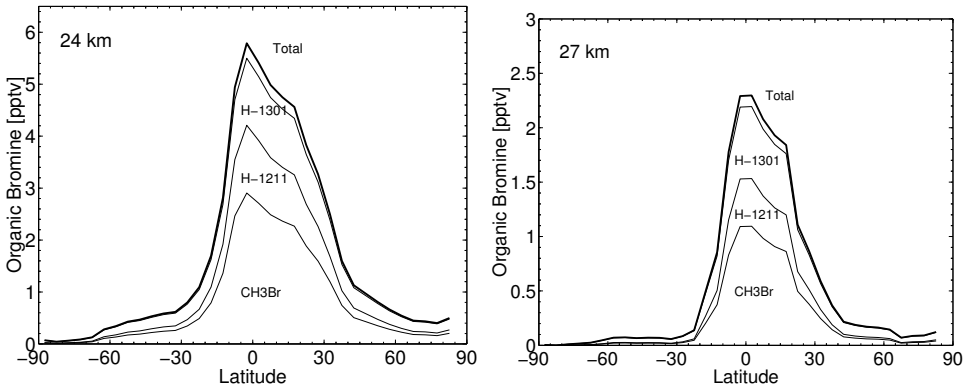

Figure 10.4: Left panel: Total organic bromine at 24 km. Right panel: Total organic bromine at 27 km.

During high-latitude winter (December-January-February in the Arctic and June-July-August in the Antarctic) BrO is around 75% and $BrONO_2$ forms only a small fraction of Br_y. This is due to the very low levels of NO_x in this region and further demonstrates the role of NO_x in bromine partitioning. In the tropics, the partitioning of bromine species is similar to the other zones in the upper stratosphere. However in the lowermost stratosphere and in the uppermost troposphere, it is found that HBr and Br form 10 – 40% of Br_y while the concentration of $BrONO_2$ is between 10 – 20% as against around 40% in the upper stratosphere. The reaction of Br with HO_2 is a source of HBr while the reaction of Br with ozone is an important sink of Br. The VMR of ozone is significantly low in the tropopause and the uppermost troposphere as compared to the stratospheric values. This results in Br and HBr forming a larger fraction of Br_y. NO_2 does not appear to play a significant role in bromine partitioning in the lowermost stratosphere in the tropics. Antarctic winter is the only region where a significant amount of BrCl is predicted by the model. Under these conditions the model predicts also enhanced levels of HOBr.

As these model calculations were constrained by NO_2 from SCIAMACHY observations, the results will depend to some extent on the accuracy of the SCIAMACHY NO_2 observations. In order to check the effect of changes in NO_2 on BrO/Br_y ratio, we conducted some sensitivity tests. An increase in NO_2 concentration results in an increase in $BrONO_2$ concentration through the reaction 4.2. Consequently this results in a decrease in BrO. The change in $BrONO_2$ and BrO is altitude dependent due to the pressure dependent nature of reaction 4.2. On an average it is found that if we increase the NO_2 concentration by 50% then BrO decreases by approximately 11% at altitudes of around 25 km. Thus the BrO/Br_y ratio would decrease by 11%. The statistical results from the comparison of all SCIAMACHY with Halogen Occultation Experiment instrument (HALOE) collocated NO_2 profiles show a systematic negative offset of less than 5% between 20 km and 38 km [*Bracher et al.*, 2004, ; A. Bracher, personal communication, 2005]. This 5% bias in NO_2 would thus lead only to a bias in the calculated BrO/Br_y ratio of about 1% which is negligible compared to other potential error sources.

Figure 10.3 shows the profiles of Br_y for the two years 2003 and 2004. The mean total stratospheric bromine loading (Br_{total}^{mean}) can be estimated by summing the calculated Br_y and the estimate for the contribution of remaining organic bromine compounds. Figure 10.4 show the amount of organic bromine at 24 and 27 km as contributed by CH_3Br and halons based on CFC-11 observations in September, 2002 from the Michelson Interferometer for Passive Atmospheric Sounding (MIPAS) also onboard ENVISAT [*Glatthor et al.*, 2005] and the empirical relationship of *Wamsley et al.* [1998]. The estimated average of organic bromine in the extra-tropics is found to be 0.77 pptv at 24 km and 0.15 pptv at 27 km [see also *Sinnhuber et al.*, 2005]. The calculated extra-tropical Br_y from SCIAMACHY BrO is on average 18.0 pptv at 24 km and 17.9 pptv at 27 km. Using the average organic bromine at 24 and 27 km for September, 2002 (as representative of the whole year to a first approximation) and the average value of estimated Br_y at the same altitudes, the mean total bromine loading in the stratosphere around 25 km (Br_{total}^{mean}) is found to be 18.5 pptv. Assuming an accuracy of about 20% for the SCIAMACHY BrO profile retrievals the uncertainty in Br_{total}^{mean} will be about $\pm$ 3.7 pptv.

This estimate of Br_{total}^{mean} is consistent (albeit with higher uncertainty) with the works of *Schauffler et al.* [1998], who calculated the total organic bromine loading at the tropical tropopause to be 17.4 $\pm$ 0.9 using the organic method which included 3 short lived species namely CH_2Br_2, CH_2BrCl, and $CHCl_2Br$ apart from CH_3Br and halons. The calculated value is also consistent with works of *Wamsley et al.* [1998] (which ranged from (16.4 $\pm$ 2 pptv) in 6 year old air investigated in 1994 to (18.2 $\pm$ 2) in 0 year old air) using organic method which included CH_3Br, halons and two short lived species namely CH_2Br_2 and CH_2BrCl and that of *Pfeilsticker et al.* [2000] who estimated for early 1999, the total organic bromine at 25 km in air of 5.6 year mean age to be 18.4 (+1.8/-1.5) pptv from organic precursor measurements which included all known major organic bromine species.

However, the estimated value of total bromine loading in this work is on the lower side (though within stated error of measurements) as compared to previous works which calculated the total bromine loading using BrO measurements and known BrO/Br_y from the model e.g. the work of *Pfeilsticker et al.* [2000] who estimated inorganic bromine loading of 21.5 $\pm$ 3 pptv for air of 5.6 year mean age for winter 1998/99, *Harder et al.* [2000] (20 $\pm$ 2.5) and of *Sinnhuber et al.* [2002] (20 $\pm$ 4 pptv). The inclusion of the reaction proposed by *Soller et al.* [2001] decreases the gap between between this work and that of *Pfeilsticker et al.* [2000], *Harder et al.* [2000], and *Sinnhuber et al.* [2002].

The major contribution to the bromine in the stratosphere is from CH_3Br, Halon-1211 and Halon-1301 [*Wamsley et al.*, 1998; *Pfeilsticker et al.*, 2000] and this sums up to 15 pptv [*Sinnhuber et al.*, 2005]. The total bromine loading of 18.5 $\pm$ 4 pptv estimated in this work indicates a contribution of 3.5$\pm$4 pptv from short lived to stratospheric bromine loading in addition to that from CH_3Br and halons in agreement with previous studies [*Pfeilsticker et al.*, 2000; *Sinnhuber et al.*, 2002; *Salawitch et al.*, 2005; *Sinnhuber et al.*, 2005].

10.3 Contribution of very short lived organic bromine species to total bromine

The halogen species with atmospheric life time of few days to months (0.5 years at the maximum) are called as Very Short Lived Species (VSLS) [*WMO*, 2002]. There is a continuing debate and research about the contribution of the VSLS to the total halogen loading in the atmosphere. The knowledge of total halogen loading is important in order to evaluate and quantify their effect on stratospheric ozone. The VSLS have been found to make significant contribution to total halogen loading apart from traditionally known long lived halogen species, CFCs and halons (e.g see [*Ko et al.*, 2003]).

A list of some of the known short lived bromine species is given in Table 10.1. Most of the bromocarbons are found to have high concentration in the marine boundary layer with high ocean productivity [*WMO*, 2002]. The supply is mainly by biogenic processes in ocean. Dibromomethane CH_2Br_2, which has a lifetime of approximately 4 months, is reasonably well mixed throughout the troposphere and is found to have mixing ratio in the range of 0.8 - 1.2 pptv at the altitude of 12 km [*Blake et al.*, 2001] whereas it is found to be in the range 0.3 - 0.7 pptv at 15 to 19 km in the tropical region [*Schauffler et al.*, 1998]. Among the short lived species, bromoform ($CHBr_3$) is probabely the most abundant species and may be an important source to stratospheric bromine [*Sturges et al.*, 2000]. Again the main source of $CHBr_3$ is in the oceans with large seasonal differences in the emission rates and near surface air concentration [*Quack and Wallace*, 2003; *Quack et al.*, 2004; *Blake et al.*, 2001]. *Blake et al.* [2001] have reported a mixing ratio in the range 0.7 - 1.9 pptv over the pacific. A minor source from industrial processes has also been predicted by *Blake et al.* [2001]. Modeling studies [*Dvortsov et al.*, 1999; *Nielsen and Douglass*, 2001; *Sinnhuber and Folkins*, 2005] have concluded that bromoform may contribute about 1 pptv to the stratospheric bromine loading. *Carpenter et al.* [1999] have reported that the other short lived bromine species like CH_2BrCl, $CHBrCl_2$, and $CHBr_2Cl$ have similar oceanic sources and similar source distribution. Mixing ratios in the range of 0.15 - 0.25 pptv have been reported by [*Schauffler et al.*, 1998] at 10 km in the tropics and 0.01 pptv at 20 km. The same study reports the mixing ratios in the range of 0.05 - 0.2 pptv at 10 km and 0.2 pptv above 15 km for $CHBr_2Cl$, 0.1 - 0.15 pptv at 10 km and below 0.03 pptv above 15 km for $CHBrCl_2$. Hence owing to the contribution of short lived bromine species to the total bromine in the ozone depletion, the quantification of the contribution of brominated short lived species has gained importance and is now an important area of research.

Previous modeling studies studying the stratospheric ozone depletion considered the source of bromine only from long lived species CH_3Br + halons which sum upto around 15 pptv. The contribution of VSLS to the total bromine cannot be neglected owing to their potential to increase Br_y and consequently the stratospheric ozone depletion. For example, [*Salawitch et al.*, 2005] have shown that a few ppt of extra bromine (at the 4 to 8 pptv level) can lead to a significant increases in stratospheric ozone depletion. Hence the quantification of the VSLS is an important issue. The direct estimation of these VSLS is difficult due to the sparsity in their measurements and hence are estimated indirectly

by subtracting the Br_y estimated from suite of organic bromine measurements from the Br_y inferred from BrO measurements. Previous studies, including this study have shown that on an average 0-6 pptv of additional bromine is contributed by very short lived bromine species [see for example, *Sinnhuber et al.*, 2002; *Schofield et al.*, 2004; *Salawitch et al.*, 2005; *Sinnhuber et al.*, 2005; *Dorf et al.*, 2005].

10.3.1 Transport of very short lived species to the stratosphere

One of the major goals in the study of halogen source gases has been to track the life cycle of a source gases so that one can evaluate how its emission may affect the inorganic halogen budget in the present day stratosphere [*WMO*, 2002]. It is important to know the percentage of halogen atom delivered to the stratosphere in order to define the relative ozone depletion potential (ODP) of the source gas. In the case of the VSLS, two pathways have been identified for the transport of the VSLS emitted at the surface to the stratosphere [*WMO*, 2002]. First is the Source Gas Injection (SGI), where the source gas is transported to the stratosphere and then releases halogen atom through chemical or physical processes. The second pathway is called as Product Gas Injection (PGI) in which the transport is of the intermidiate or final products to the stratosphere. In both cases the efficiency of the pathways depends on the properties of the source gas/degradation products e.g. removal rate by chemical/physical processses in the troposphere as compared to the transport from ground to the stratpsphere [*WMO*, 2002]

The most efficient pathway of air entering the stratosphere is in the tropics through the tropical tropopause layer (TTL) [*Sinnhuber and Folkins*, 2005]. Air parcels are lifted from the boundary layer upto upper troposphere by deep convection process with a fraction detraining deep into the TTL. A part of it is injected directly into the stratosphere [*WMO*, 2002]. Stratsopheric Tropospheric Exchange (STE) processes can also transport air parcels from TTL to the stratsophere. But in general, the mechanisms of transport across the tropopause and the various processes the VSLS undergo in the process of transport have not been understood and various hypothesis are being proposed and is an active area of reasearch.

10.4 Conclusion

This chapter presents the two methods to estimate the total bromine in the stratosphere. The total bromine loading was estimated from the BrO observations using the inorganic method. The estimated total bromine loading is 18.5 ± 4 pptv consistent with previously published results [*Schauffler et al.*, 1998; *Wamsley et al.*, 1998; *Pfeilsticker et al.*, 2000; *Harder et al.*, 2000; *Sinnhuber et al.*, 2002; *WMO*, 2002]. Our estimate is slightly on the lower side (though within the stated error estimates) as compared to the estimates of [*Pfeilsticker et al.*, 2000; *Harder et al.*, 2000]. Part of the difference to previous studies can be explained by the inclusion of the reaction of $BrONO_2$ with $O(^3P)$ [*Soller et al.*, 2001] which has not been considered in most previous studies. The estimated total bromine loading of 18.5 ± 4 pptv suggests a contribution of 3.5 ± 4 pptv from short lived organic bromine compounds in addition to methyl bromide and the halons.

11 Summary, Conclusions, and Outlook

This thesis presents the global observations and analysis of bromine monoxide (BrO), which was retrieved globally for the first time in the altitude range 15 - 30 km using the limb measurements of the SCIAMACHY instrument on board ENVISAT. In order to validate our understanding of bromine chemistry, a comparison of the retrieved data with calculations from a one dimensional photochemical model has also been done. Further using the two year retrievals of BrO, a climatology of the same has also been prepared. The amount of BrO in the troposphere is still an active area of reasearch. The amount of BrO below 15 km has been calculated from the difference between the nadir-limb retrievals of BrO.

The knowledge of the total bromine and its partitioning between the organic and inorganic species in the stratosphere is an important input for the atmospheric models to study their impact on ozone destruction [*Wennberg et al.*, 1994, 1997; *Gao et al.*, 1997]. This thesis has estimated the total bromine in the atmosphere.

11.1 Summary and conclusions of chapters

Chapter 2 briefly discusses the vertical structure and composition of the atmosphere. It also gives an overview of the importance and general distribution of the ozone in the atmosphere. The formation of the ozone hole at the poles is also discussed in this chapter.

In Chapter 3 the one dimensional photochemical model used in this work is discussed. As a real, illustration of how a model can be used to validate and understand the chemistry of the stratosphere, a first retrieved NO_3 profiles from SCIAMACHY lunar occultation measurements over the Antarctica is presented and compared with model calculations. The NO_3 profiles calculated from the full 1-D photochemical model are found to be in good agreement with retrieved NO_3 profiles between 24 and 45 km with estimated accuracy of 20 – 35%. Steady state (SS) model NO_3 agree with retrieved NO_3 in the altitude range 24–40 km. The agreement supports the use of steady state approximation model to calculate global NO_3 concentrations in the middle stratosphere (24 – 40 km) and use of full photochemical model to calculate NO_3 concentrations above 40 km. The NO_3 chemistry in the stratosphere depends strongly on temperature and inaccuracy in the stratospheric temperature of less than 5 K will contribute approximately 30% error in the observed NO_3 concentrations. The lunar occultation measurements of SCIAMACHY demonstrate that we have a reasonable understanding of the behaviour of NO_3 in the stratosphere. The ratio of NO_3 and N_2O_5 is very sensitive to temperature.

Bromine compounds are chemically more efficient at per molecule level in destroying ozone than their chlorine counterparts. Further, the bromine chemistry to a large

extent is controlled by nitrogen oxides. Chapter 4 discusses the stratospheric bromine and nitrogen chemistry and sets the pace for the main objective of this thesis. This chapter also presents the calculation of the diurnal variation of bromine and nitrogen compounds.

The stratospheric BrO data used in this study are retrieved globally from the limb measurements of the SCIAMACHY instrument on board ENVISAT. Chapter 5 gives an overview of the SCIAMACHY instrument on board the ENVISAT. The basic concepts involved in the retrieval of atmospheric constituents from satellite instrument have also been discussed in brief. The technique used to retrieve BrO from SCIAMACHY limb measurements along with sensitivity studies is also presented in this chapter. The retrieval error is approximately 40% between 15 - 20 km and 25 - 30 km and it is approximately 30% between 20 - 25 km. The largest influence on the retrieved BrO profile is of temperature. While the influence is insignificant between 20 - 28 km it cannot be ignored in the lower stratosphere and at higher altitudes. The influence of pressure and scattering events on the retrieved BrO is moderate. The effect of the mispointing on the retreival of BrO has also been tested. A mispointing of 1 km can result in error of about 10 - 20% above 21 km and increasing to about 40% in the lower layer.

In order to have further confidence in the quality of the retrieved SCIAMACHY BrO profiles, they need to be compared and validated with BrO profiles retrieved using methods. The other measurement techniques used to retreive BrO namely, chemical conversion resonance flurosescence and DOAS techniques are presented in Chapter 6. As a part of validation of the retrieved SCIAMACHY BrO profiles, a comparison of the SCIAMACHY BrO retrievals with a set of balloon-borne BrO measurements has been presented in this chapter. The comparison shows that mean differences in the altitude region from 18 to 30 km between $+17\%$ and -29% at mid and high latitudes of the Northern Hemisphere. Larger discrepancies of -32% and -42% are found in comparison to a SAOZ balloon profile in the tropics.

In Chapter 7, first global observations of stratospheric BrO from SCIAMACHY limb measurements for September, 2002 are presented. The BrO retrievals are compared with modeled BrO profiles, based on estimated inorganic bromine (Br_y) from CFC-11 retrievals by the MIPAS on ENVISAT and the calculated BrO/Br_y ratio from a photochemical model constrained by SCIAMACHY NO_2 retrievals. The BrO observations are broadly consistent with our current understanding of stratospheric bromine chemistry and a total stratospheric bromine loading of 18 ± 3 pptv. A first global climatology of stratospheric BrO, based on retrievals from two years of measurements of the SCIAMACHY instrument has been presented in this chapter. BrO shows a strong annual variation at mid-latitudes while no significant annual variation in the tropics is observed. The seasonal variation at mid-latitudes is inversely correlated with NO_2, confirming our present understanding of the gas phase bromine chemistry.

In Chapter 8, comparison of a first comprehensive BrO measurements at low latitudes with 1-D photochemical model is presented. The presented data are from a one year ground based zenith-sky measurements of BrO over Nairobi (1°, 36°E). The measured BrO shows a diurnal variation with average BrO DSCDs being 1.3 x 10^{14} molecules/cm^2 in the morning 1.5 x 10^{14} molecules/cm^2 in the evening. The PM/AM

ratio is found to be 1.2 which is slightly lower than at midlatitude. That seasonal variation of BrO is very small in the tropics is further confirmed by the measured BrO DSCDs (90°-80° SZA)which show very little seasonal variation. The model reproduces the diurnal and seasonal variation quite well but the morning values are 45% smaller and the evening values are 25% smaller than the measured DSCDs. The agreement between the model and the measured values can be improved by including the reaction of $BrONO_2$ with $O(^3P)$ [*Soller et al.*, 2001]. The measured BrO values are then just 20% higher in the morning and 15% higher in the evening as compared to the model calculations. These values are within the combined uncertainties of model and measurements. This indicates that the reaction of $BrONO_2$ with $O(^3P)$ plays an important role at low latitudes.

The amount of bromine in the free troposphere is still a topic of debate. Chapter 9 calculates the amount of background tropospheric BrO using the nadir-limb measurements of combination. It is found to be 1.4 ppt throughout the year at all latitudes, averaged over all latitudes and months. The chapter also discusses the sources of bromine.

The knowledge of the total amount of bromine present in the atmosphere is an important issue as it has direct implications on our prediction of the ozone trends. Also VSLS make a non-negligible contribution to the total bromine. A small contribution in total bromine from the VSLS could make a signficant impact on the stratospheric ozone depletion [*Salawitch et al.*, 2005]. The concern is enhanced as bromine is far more active at per molecule level in destroying ozone than chlorine [*Sinnhuber et al.*, 2006]. Chapter 10 discusses our estimate of Br_y based on the SCIAMACHY BrO observation and BrO/Br_y ratio obtained from the simulations of the 1-D photochemical model constrained with SCIAMACHY NO_2(so called inorganic method). Further, the estimate of the total bromine in the atmosphere and contribution of VSLS is discussed. The estimated total bromine loading is 18.5 ± 4 pptv consistent with previously published results [*Schauffler et al.*, 1998; *Wamsley et al.*, 1998; *Pfeilsticker et al.*, 2000; *Harder et al.*, 2000; *Sinnhuber et al.*, 2002; *WMO*, 2002]. Our estimate is slightly on the lower side (though within the stated error estimates) as compared to the estimates of [*Pfeilsticker et al.*, 2000; *Harder et al.*, 2000]. Part of the difference to previous studies can be explained by the inclusion of the reaction of $BrONO_2$ with $O(^3P)$ [*Soller et al.*, 2001] which has not been considered in most previous studies. The estimated total bromine loading of 18.5 ± 4 pptv suggests a contribution of 3.5 ± 4 pptv from short lived organic bromine compounds in addition to methyl bromide and the halons.

11.2 Overall summary and conclusions

The overall summary and conclusions are as follows:

• Global BrO profiles retrieved from SCIAMACHY limb measurements have been presented and analysed.

• The BrO retrievals have been validated with a set of photochemically corrected balloon-borne BrO profiles. The comparison shows that mean differences in the altitude region from 18 to 30 km between $+17\%$ and -29% at mid and high latitudes

of the Northern Hemisphere. Larger discrepancies of -32% and -42% are found in comparison to a SAOZ balloon profile in the tropics.

• The BrO retrievals are compared with modeled BrO profiles, based on estimated inorganic bromine (Br_y) from CFC-11 retrievals by MIPAS on ENVISAT and the calculated BrO/Br_y ratio from a photochemical model constrained by SCIAMACHY NO_2 retrievals. The BrO observations are broadly consistent with our current understanding of stratospheric bromine chemistry and a total stratospheric bromine loading of 18 ± 3 pptv.

• A climatology of BrO based on two years of data from SCIAMACHY has been constructed. BrO shows a strong annual variation at mid-latitudes while no significant annual variation in the tropics is observed. The seasonal variation at mid-latitudes is inversely correlated with NO_2, confirming our present understanding of the gas phase bromine chemistry.

• Background BrO in the troposphere has also been calculated using the nadir-limb retrievals of BrO from SCIAMACHY and is found to be 1.4 ppt throughtout the year when averaged over all latitudes and months.

• The total bromine loading in the atmosphere is estimated to be 18.5 ± 4 pptv. Our estimate is slightly on the lower side (though within the stated error estimates) as compared to the estimates of [*Pfeilsticker et al.*, 2000; *Harder et al.*, 2000]. Part of the difference to previous studies can be explained by the inclusion of the reaction of $BrONO_2$ with $O(^3P)$ [*Soller et al.*, 2001] which has not been considered in most previous studies. The estimated total bromine loading of 18.5 ± 4 pptv suggests a contribution of 3.5 ± 4 pptv from short lived organic bromine compounds in addition to methyl bromide and the halons.

11.3 Outlook

With the available SCIAMACHY BrO data, the following issues can be investigated further:

• There remains some uncertainty about the amount of BrO in the tropical region. A large discrepancy is found between SCIAMACHY BrO and the only available SAOZ balloon-borne BrO profile in the tropics. However, it is difficult to be fully conclusive at this stage about these differences solely on the basis of a single comparison. A further validation of SCIAMACHY BrO is necessary in order to conclude whether observed discrepancy is due to uncertainties in the observations or whether this indicates shortcomings in our understanding of the bromine chemistry in this region. But the agreement between SCIAMACHY and the photochemically corrected balloon-borne BrO profiles is encouraging, in particular at mid-latitudes.

• With available SCIAMACHY BrO data and photochemical model, the study of bromine chemistry in polar conditions can be done.

• The comparison of the SCIAMACHY BrO data with simulations from a 3-D chemical transport model would be an important step towards our better understanding of SCIAMACHY BrO and bromine chemistry.

Appendix

K1 : $O + O + M \rightarrow O_2 + M$
K2 : $O + O_2 + M \rightarrow O_3 + M$
K3 : $O + O_3 \rightarrow 2O_2$
K6A: $O(^1D) + N_2 \rightarrow O + N_2$
K6B: $O(^1D) + O_2 \rightarrow O + O_2$
K8 : $OH + O \rightarrow H + O_2$
K10: $HO_2 + O \rightarrow OH + O_2$
K11: $OH + O_3 \rightarrow HO_2 + O_2$
K12: $H + O_3 \rightarrow OH + O_2$
K13: $OH + HO_2 \rightarrow H_2O + O_2$
K14: $OH + OH \rightarrow H_2O + O$
K16: $NO_2 + O \rightarrow NO + O_2$
K17: $O_3 + NO \rightarrow NO_2 + O_2$
K18: $NO_2 + O_3 \rightarrow O_2 + NO_3$
K20: $HNO3 + OH \rightarrow H_2O + NO_3$
K24: $HO_2 + HO2 \rightarrow H_2O_2 + O_2$
K26: $H_2O_2 + OH \rightarrow H_2O + HO_2$
K29: $H_2O_2 + rain \rightarrow$
K30: $OH + CH4 \rightarrow CH_3 + H_2O$
K34: $CO + OH \rightarrow CO_2 + H$
K35: $NO + HO_2 \rightarrow NO_2 + OH$
K36: $HO_2 + O_3 \rightarrow OH + 2O_2$
K38: $HNO_3 + rain \rightarrow$
K40: $HO_2NO_2 + OH \rightarrow H_2O + O_2 + NO_2$
K41: $HO_2NO_2 + rain \rightarrow$
K50: $Cl + O_3 \rightarrow ClO + O_2$ C
K51: $ClO + O \rightarrow Cl + O_2$
K52: $Cl + H_2O_2 \rightarrow HCl + HO_2$
K53: $ClONO_2 + OH \rightarrow HOCl + NO_3$
K54: $ClONO_2 + Cl \rightarrow 2Cl + NO_3$
K55: $ClO + NO \rightarrow Cl + NO_2$
K57: $CH4 + Cl \rightarrow CH_3 + HCl$
K58: $H_2 + Cl \rightarrow H + HCl$
K59: $HO_2 + Cl \rightarrow O_2 + HCl$
K59b: $HO_2 + Cl \rightarrow OH + ClO$

K60: $OH + HCl \rightarrow H_2O + Cl$
K61: HCl + rain → (also used for HBr + rain)
K63: $ClONO_2 + O \rightarrow ClO + NO_3$
K65: $HO_2 + ClO \rightarrow HOCl + O_2$
K65b: $HO_2 + ClO \rightarrow HCl + O_3$
K66: $OH + HOCl \rightarrow H_2O + ClO$
K67: $O + HOCl \rightarrow OH + ClO$
K68b: $ClO + ClO \rightarrow Cl + Cl + O_2$
K68c: $ClO + ClO \rightarrow OClO + Cl$
K70: $N + NO \rightarrow N_2 + O$
K71: $N + O_2 \rightarrow NO + O$
K75a: $OH + ClO \rightarrow HO_2 + Cl$
K75b: $OH + ClO \rightarrow HCl + O_2$
K82: $CH_3CCl3 + OH \rightarrow 3Cl$
K84: $CH_3Cl + OH \rightarrow Cl$
K86: $CHF_2Cl + OH \rightarrow Cl$
K101: $CH_3O_2 + NO \rightarrow CH_3O + NO_2$
K102: $CH_3O2 + HO_2 \rightarrow CH_3OOH + O_2$
K103: $CH_3O_2 + CH_3O_2 \rightarrow 2CH_3O + O_2$
K104a: $CH_3OOH + OH \rightarrow CH_3O_2 + H_2O$
K104b: $CH_3OOH + OH \rightarrow CH_2O + OH + H_2O$
K105: $CH_3O + O_2 \rightarrow CH_2O + HO_2$
K106: $CH_2O + OH \rightarrow CHO + H_2O$
K107: $CH_2O + O \rightarrow CHO + OH$
K108: $HCO + O_2 \rightarrow CO + HO_2$
K109: $H_2 + OH \rightarrow H_2O + H$
K110: $CH_2O + Cl \rightarrow HCl + CHO$
K112: CH_2O + rain →
K113: CH_3OOH + rain →
K114: $CH_3O_2 + ClO \rightarrow Cl + CH_3O + O_2$
K116: $CH_3O_2 + NO_2 \rightarrow CH_3NO_4$ (Not included)
K120: $Br + O_3 \rightarrow BrO + O_2$
K121: $BrO + O \rightarrow Br + O_2$
K123: $BrO + NO \rightarrow Br + NO_2$
K124: $BrO + OH \rightarrow Br + HO_2$
K125a: $BrO + ClO \rightarrow Br + OClO$
K125b: $BrO + ClO \rightarrow Br + Cl + O_2$
K125c: $BrO + ClO \rightarrow BrCl + O_2$
K127: $BrO + BrO \rightarrow Br + Br + O_2$
K130: $BrO + HO_2$ -¿ $HOBr + O_2$
K130b: $BrO + HO_2$ -¿ $HBr + O_3$
K131: $HOBr + O \rightarrow BrO + OH$
K134: $Br + HCHO \rightarrow HBr + HCO$
K135: $Br + HO_2 \rightarrow HBr + O_2$

K136: $HBr + OH \rightarrow Br + H_2O$
K139: $HBr + O \rightarrow Br + OH$
K142: $CH_3Br + OH \rightarrow Br$
K145: $BrONO_2 + O \rightarrow BrO + NO_3$
K146: $BrONO_2 + Br \rightarrow 2Br + NO_3$

Heterogeneous reactions

K150: $N_2O_5 + H2O(s) \rightarrow 2\ HNO_3$
K151: $ClONO_2 + H2O(s) \rightarrow HOCl + HNO_3$
K152: $ClONO_2 + HCl(s) \rightarrow 2\ Cl + HNO_3$
K153: $N_2O_5 + HCl(s) \rightarrow Cl + NO_2 + HNO_3$
K154: $HOCl + HCl(s) \rightarrow Cl + Cl + H_2O$
K155: $HOBr + HBr(s) \rightarrow Br + Br + H_2O$
K156: $HOBr + HCl(s) \rightarrow BrCl + H_2O$
K157: $HOCl + HBr(s) \rightarrow BrCl + H_2O$
K158: $BrONO_2 + HBr(s) \rightarrow Br + Br + HNO_3$
K159: $BrONO_2 + HCl(s) \rightarrow BrCl + HNO_3$
K160: $ClONO_2 + HBr(s) \rightarrow BrCl + HNO_3$
K161: $BrONO_2 + H2O(s) \rightarrow HOBr + HNO_3$
K162: $N_2O_5 + HBr(s) \rightarrow Br + NO_2 + HNO_3$

Acknowledgements

I would like to take this opportunity to thank Prof. Dr. John P. Burrows for accepting me as a Ph.D. student and catapulting me to the frontiers of active research in the field of atmospheric science. He has been an inspiring force during this work with his enthusiastic and encouraging talks during the weekly seminars at the institute and also during his pop-ups in my office to know the latest about my progress. I would also like to thank Dr. Bjoern-Martin Sinnhuber for supervising me during this period of research. We had many interesting scientific discussions during our meetings in his or my office. I must say, he changed my attitude to look towards a problem in science. He is a perfectionist. Acknowledgements are rightfully due to Dr. Alexei Rozanov. Without his retrievals of BrO, this work stands no chance of getting completed. I also would like to thank Dr. Miriam Sinnhuber for providing the model which is an important component of this work. I would also like to express my deep sense of gratitude to Dr. C. von Savigny for providing me with the tangent height offsets needed for BrO tangent height corrections. I would like to express my gratitude to Dr. M. Dorf (University of Heidelberg) for providing me with the photochemically corrected balloon-borne BrO profiles for the validation purpose. I would like to thank Dr. L. Amekudzi for the collaborative work which resulted in my first peer reviewed research paper in an international scientific journal as a co-author. Thanks are due to Prof. Dr. Justus Notholt for providing me with funding for one and half years. I thank Marco Schwarringshausen for proof-reading some chapters of my thesis. Acknowledgements are due to Dr. J. Bleck-Neuhaus, who first accepted me as student of masters course in environmental physics conducted at IUP , before I got enrolled for the Ph.D work. I also would like to thank Mrs. Stefanie Bühler for helping and guiding me with administrative work throughout the period of stay in Germany. She has been just wonderful person. Thanks to Mashrab Kuvatov for always being ready to help me with the operating system problems.

I must especially mention Lok and Dr. Viju and thank them for helping me with programming issues during the first phase of my work. Thanks to Dr. Rekha - the chatter box, for her entertaining talks and Sandip for making my landing in Bremen a smooth affair. It was fun to discuss science with them and have parties on week ends. Thanks to Dr. Aveek Sarkar for being there for general discussions. Also thanks to other friends who hail from my city Pune, India and are studying or working in Germany. Life would have been too dry without them in Bremen. I sincerely thank my dear friends Sameer, Swati, Madhura, and Viral for being there during low times.

I am indebted to some people for life. This work is incomplete without mentioning their names. Mrs. Hemalata Honwad - an educator par excellence, was my school teacher and has always been a guiding force till today. She is the driving force for all

the constructive work I do. Thanks to Dr. Shirisha Sathe - a clinical psychologist par excellence, for being there whenever I felt the need to talk to her to recharge my batteries of enthusiasm. Thanks to my family for always being there especially my grand mother Mrs. Prabhavati Sheode, who unfortunately is no more to share the happiness of completion of this work. Last but not the least, I must thank my wife Anuja for her unconditional love and patience and for being there when I needed her the most.

Bibliography

Afe, O., *Retrieval and observations of atmospheric BrO from SCIAMACHY- nadir measurements, Ph.D. Thesis*, Univ. of Bremen, Bremen, Germany, 2005.

Afe, O. T., A. Richter, B. Sierk, F. Wittrock, and J. P. Burrows, BrO emissions from volcanoes: A survey using GOME and SCIAMACHY measurements, *Geophys. Res. Lett.*, *31*, doi:10.1029/2004GL020994, 2004.

Aliwell, S. R., et al., Analysis ofBrO in zenith sky spectra: An intercomparison excercise for analysis improvement, *J. Geophys. Res.*, *107*, 2002.

Amekudzi, L., *Stratospheric O_3, NO_2, NO_3, number density profiles from SCIAMACHY lunar occultation spectroscopic measurements: Retrieval, validation and interpretation, Ph.D. Thesis*, Univ. of Bremen, Bremen, Germany, 2005.

Amekudzi, L. K., A. Bracher, J. Meyer, A. Rozanov, H. Bovensmann, and J. P. Burrows, Lunar occultation with SCIAMACHY:First retrieval results, *Adv. in Space Res.*, *35*, doi:10.1016/j.assr.2005.03.017, 2005a.

Amekudzi, L. K., B.-M. Sinnhuber, N. V. Sheode, J. Meyer, A. Rozanov, L. Lamsal, H. Bovensmann, and J. P. Burrows, Retrieval of stratospheric NO_3 vertical profiles from SCIAMACHY lunar occultation measurement over the Antarctic, *J. Geophys. Res.*, *110(D20304)*, doi:10.1029/2004JD005748, 2005b.

Appenzeller, C., and A. K. W. amd J. Staehelin, North Atlantic Oscillation modulates total ozone winter trends, *Geophys. Res. Lett.*, *27*, 1,131–1,134, 2000.

Arpag, K. H., P. V. Johnston, H. L. Miller, R. W. Sanders, and S. Solomon, Oobservations of stratospheric Bro column over Colorado, 40deg N, *J. Geophys. Res.*, *99*, 8,175–8,181, 1994.

Avallone, L. M., D. W. Toohey, S. M. Schauffler, W. H. Pollock, L. E. Heidt, E. L. Atlas, and K. R. Chan, In-situ measurements of BrO during AASE-II, *Geophys. Res. Lett.*, *22*, 831–834, 1995.

Barrie, L. A., J. W. Bottenheim, R. C. Schnell, P. J. Crutzen, and R. A. Rasmussen, Ozone destruction and photochemical reactions at polar sunrise in the lower Arctic atmosphere, *Nature*, *334*, 138–141, 1988.

Bates, D., and M. Nicolet, The photochemistry of atmospheric water vapor, *Geophys. Res. Lett.*, *20*, 711, 1950.

Blake, N. J., et al., Large-scale latitudinal and vertical distribution of NMHCs and selected halocarbons in the troposphere over the Pacific Ocean during March-April 1999 Pacific Exploratory Mission (PEM-Tropics B), *J. Geophys. Res.*, *106*, 32,627 – 32,644, 2001.

Bobrowski, N., G. Hönninger, B. Galle, and U. Platt, Detection of bromine monoxide in a volcanic plume, *Nature*, *423*, 273–276, 2003.

Bogumil, K., et al., Reference Spectra of Atmospheric Trace Gases Measured by the SCIAMACHY PFM Satellite Spectrometer, pp. 443–447, proc. 1st Europ. Sympos. Atmos. Meas. from Space (ESAMS-99), ISSN 1022-6656, ESA-ESTEC, Noordwicjk, 1999.

Borrmann, S., S. Solomon, and L. Avallone, On the occurence of ClO in cirrus clouds and volcanic aerosols in the tropause region, *Geophys. Res. Lett.*, *106*, 2,647–2,650, 1997.

Bottenheim, J. W., et al., The Polar Sunrise Experiment 1988, *J. Geophys. Res.*, *95*, 18,555–18,568, 1990.

Bovensmann, H., J. P. Burrows, M. Buchwitz, J. Frerick, S. Noël, and V. V. Rozanov, SCIAMACHY:Mission objectives and measurement modes, *J. Atm. Sci.*, *56*(2), 127–149, 1999.

Bracher, A., M. Sinnhuber, A. Rozanov, and J. P. Burrows, Using photochemical model for the validation of NO_2 satellite measurements at different solar zenith angles, *Atmos. Chem. Phys. Discuss.*, *4*, 5,515–5,548, 2004.

Brasseur, G., J. J. Orlando, and G. S. Tyndall (Eds.), *Atmospheric Chemistry and Global Change*, National Center for Atmospheric Research, 1999.

Brune, W. H., J. G. Anderson, and K. R. Chan, In-situ observations of BrO over Antarctica:ER-2 aircraft results from 54deg S to 72deg S, *J. Geophys. Res.*, *94*, 16,639, 1989.

Buchwitz, M., and J. P. Burrows, Retrieval of CH_4, CO and CO_2 total columnn amounts from SCIAMACHY near-infrared nadir spectra:Retrieval algorithm and first results: K. P. Schafer and A. Cameron and M. R. Carleer and R. H. Picard (Editors) Proceedings of SPIE, 5235, pp. 375–388, 2004.

Buchwitz, M., V. V. Rozanov, and J. P. Burrows, A near-infrared optimized DOAS method for the fast global retrieval of atmospheric CH_4, CO, CO_2, H_2O, and N_2O total column amounts from SCIAMACHY Envisat-1 nadir radiances, *J. Geophys. Res.*, *105*, 15,231–15,245, 2000.

Burrows, J. P., et al., The Global Ozone Monitoring Experiment (GOME); Mission concept and first scientific results, *J. Atm. Sci.*, *56*, 151–175, 1999.

Canty, T., et al., Nighttime OClO in the Arctic vortex, *J. Geophys. Res.*, *110*, doi:10.1029/2004JD005035, 2005.

Carpenter, L. J., et al., Short lived alkyl iodides and bromides at Mace Head, Ireland: Links to biogenic sources of halogen oxide production, *J. Geophys. Res.*, *104*, 1,679 – 1,689, 1999.

Carroll, M. A., R. W. Sanders, S. Solomon, and A. L. Schmeltekopf, Visible and near-ultraviolet spectroscopy at McMurdo station, Antarctica, 6, Observations of BrO, *J. Geophys. Res.*, *94*, 16,633, 1989.

Carslaw, K., B. Luo, and T. Peter, An analytic expression for the composition of aqueous /textmdHNO_3-/textmdH_2/textmdSO_4 stratospheric aerosols including gas phase removal of /textmdHNO_3, *Geophys. Res. Lett.*, *22*, 1,877–1,880, 1995a.

Carslaw, K., S. L. Clegg, and P. Brimblecome, A thermodynamic model of the system hcl-/textmdHNO_3-/textmdH_2/textmdSO_4- /textmdH_2/textmdO including solubilities of /textmdHBr from $<$ 200 k to 328 k, *J. Phys. Chem.*, *99*, 11,557–11,574, 1995b.

Chance, K., Analysis of Bro measurements from Global Ozone Monitoring Experiment, *Geophys. Res. Lett.*, *25*, 3,335–3,338, 1998.

Chipperfield, M., Multiannual simulations with a three dimensional chemical transport model, *J. Geophys. Res.*, *104*, 1,781–2,805, 1999.

Crutzen, P., The influence of nitrogen oxides on the atmospheric ozone content, *Q. J. R. Meteorol. Soc.*, *96*, 320, 1970.

Daniel, J. S., S. Solomon, R. W. Portmann, and R. R. Garcia, Stratospheric ozone destruction: The importance of bromine relative to chlorine, *J. Geophys. Res.*, *104*, 23,871–23,880, 1999.

Danilin, M. J., and J. C. McConell, Stratospheric effects of bromine activation on/in sulfate aerosols, *J. Geophys. Res.*, *100(D6)*, 11,237–11,243, 1995.

Dennis, J. E., and R. B. Schnabel (Eds.), *Numerical Methods for Unconstrained Optimization and Nonlinear Equations*, Prentice Hall, 1983.

Dhomse, S., M. Weber, I. Wohltmann, M. Rex, and J. P. Burrows, On the possible causes of recent increases in NH total ozone from a statistical analysis of satellite data from 1979 to 2003, *Atmos. Chem. Phys. Discuss.*, *5*, 13,331–13,375, 2006.

Dorf, M., *Investigation of inorganic stratospheric bromine using balloon-borne DOAS measurements amd model simulations, Ph.D. Thesis*, Univ. of Heidelberg, Germany, 2005.

Dorf, M., et al., Balloon-borne stratospheric BrO measurements: Comparison with Envisat/SCIAMACHY BrO limb profiles, *Atmos. Chem. Phys. Discuss.*, *5*, 13,011–13,052, 2005.

Dvortsov, V. L., M. A. Geller, and S. M. S. S. Solomon, Rethinking reactive halogen budgets in the mid-latitude lower stratosphere, *Geophys. Res. Lett.*, *26*, 1,699–1,702, 1999.

Eisinger, M., A. Richter, A. Ladstätter-Weissenmayer, and J. P. Burrows, DOAS zenith sky observations ,1, Bro measurements over Bremen (53deg N 1993-1994), *J. Atmos. Chem.*, *26*, 93–108, 1997.

Erle, F., A. Grendel, D. Perner, U. Platt, and K. Pfeilsticker, Evidence of heterogeneous bromine chemistry on cold stratospheric sulphate aerosols, *Geophys. Res. Lett.*, *25*, 4329–4332, 1998.

Evans, W., C. T. McElroy, and I. E. Galby, The conversion ofN_2O_5 to HNO_3 at high latitudes in winter, *Geophys. Res. Lett.*, *12*, 825–828, 1985.

Farman, J. C., B. G. Gardiner, and J. D. Williams, Large losses of total ozone in Antarctica reveal seasonal ClO_x / NO_x interaction, *Nature*, *315*, 207, 1985.

Fish, D. J., R. L. Jones, and E. K. Strong, Mid-latitude observations of the diurnal variation of stratospheric Bro, *J. Geophys. Res.*, *100*, 18,863–18,871, 1995.

Fish, D. J., S. R. Aliwell, and R. L. Jones, Mid-latitude observations of the seasonal variation of bro, 2, interpretation and modelling study, *Geophys. Res. Lett.*, *24*, 1,199–1,202, 1997.

Fitzenberger, R., H. Bösch, C. Camy-Peyret, M. P. Chipperfield, H. Harder, U. Platt, B.-M. Sinnhuber, T. Wager, and K. Pfeilsticker, First profile measurements of tropospheric BrO, *Geophys. Res. Lett.*, *27*, 2,921–2,924, 2000.

Fleischmann, O. C., M. Hartmann, J. P. Burrows, and J. Orphal, New ultraviolet absorption cross-sections of BrO at atmospheric temperatures measured by time-windowing fourier transform spectroscopy, *J. Photochem. Photobio., A: Chemistry*, *168*, 117–132, 2004.

Foster, K. L., R. A. Plastridge, J. W. Bottenheim, P. B. Shepson, B. J. Finlayson-Pitts, and C. W. Spicer, The role of Br-2 and BrCl in surface ozone destruction at polar sunrise, *Science*, *291*, 471–474, 2001.

Frerick, J. E., H. Bovensmann, S. Noël, J. P. Burrows, and M. Dobber, SCIAMACHY on-ground/in-flighth calibration, performance verification and monitoring concepts, *Proc. SPIE*, *3117*, 176–187, 1997.

Frieß, U., M. P. Chipperfield, H. Harder, C. Otten, U. Platt, J. Pyle, T. Wagner, and P. Pfeilsticker, Intercomparison of measured and modelled BrO slant column amounts for the arctic winter and spring 1994/1995, *Geophys. Res. Lett.*, *26*, 1,861–1,864, 1999.

Frieß, U., J. Hollwedel, G. Konig-Langlo, T. Wagner, and U. Platt, Dynamics and chemistry of tropospheric bromine explosion events in the Antarctic coastal region, *J. Geophys. Res.*, *109(D6)*, 2004.

Gabriel., R. R., et al., Bromine content of sea-salt aerosol particles collected over the Indian Ocean during INDOEX 1999, *J. Geophys. Res.*, *107(D19)*, 8,032, doi: 10.1029/2001JD001133, 2002.

Gao, R. S., et al., Partitioning of the reactive nitrogen reservoirs in the lower stratosphere of the southern hemisphere: Observations and modelling, *J. Geophys. Res.*, *102(D3)*, 3,935–3,949, 1997.

Glatthor, N., et al., Mixing processes during the Antarctic vortex split in September and October 2002 as inferred from source gas and ozone from MIPAS/ENVISAT, *J. Atmos. Sci.*, *62*, 787–800, 2005.

Greenblatt, G. D., J. J. Orlando, J. B. Burkholder, and A. R. Ravishankara, Absorption measurements of oxygen between 330 and 1140 nm, *J. Geophys. Res.*, *95*, 18,577–18,582, 1990.

Hadjinicolaou, P., J. A. Pyle, M. P. Chipperfield, and J. A. Kettleborough, Effect of interannual meteorological variability on mid-latitude o_3, *Geophys. Res. Lett.*, *24*, 2,993–2,996, 1997.

Hanke, M. (Ed.), *A regularizing Levenberg-Marquardt scheme, with applications to inverse groundwater filtration problems*, Inverse Problems 13, 79-95, 1997.

Hanson, D., and K. Mauersberger, Laboratory studies of the nitric acid trihydrate: implications for the south polar stratsphere, *Geophys. Res. Lett.*, *15*, 855–858, 1988.

Hanson, H., and A. R. Ravishankara, Heterogeneous chemistry of bromine species in sulfuric acid under stratospheric conditions, *Geophys. Res. Lett.*, *22*, 385–388, 1995.

Hanson, H., A. R. Ravishankara, and E. R. Lovejoy, Reaction of $BrONO_2$ with H_2O on submicron sulfuric acid aerosol and the implication for the lower stratosphere, *J. Geophys. Res.*, *101*, 9,063–9,069, 1996.

Harder, H., et al., Stratospheric BrO profiles measured at different latitudes and seasons: Atmospheric observations, *Geophys. Res. Lett.*, *25*, 3,843–3,846, 1998.

Harder, H., et al., Comparison of measured and modeled BrO:Implications for the total amount of stratospheric BrO, *Geophys. Res. Lett.*, *27*, 3,695–3,698, 2000.

Hausmann, M., and U. Platt, Spectroscopic measurements of bromine oxide and ozone in the high Arctic during Polar Sunrise Experiment 1992, *J. Geophys. Res.*, *99*, 25,399–25,414, 1994.

Hawat, T., C. Camey-Peyret, P. Jeseck, and R. Torguet, Description and performance of a balloon-borne heliostat for solar absorption measurements, proc. 12th ESA Symp. on Rocket and Balloon Programmes and Related Research, 1995.

Hebestriet, K., J. Stutz, D. Rosen, V. Matveev, M. Peleg, M. Luria, and U. Platt, DOAS measurements of tropospheric bromine oxide in midlatitude, *Science*, *283*, 55–57, 1999.

Holton, J. R., P. H. Haynes, M. E. McIntyre, A. R. Douglass, R. B. Rood, and L. Pfister, Stratospheric-Tropospheric Exchange, *Rev. Geophys.*, *33*, 403, 1995.

Johnson, D. G., W. A. Traub, K. V. Chance, and K. W. Jucks, Detection of HBr and upper limit of HOBr: Bromine partitioning in the stratosphere, *Geophys. Res. Lett.*, *22*(11), 1,373–1,376, 1995.

Johnston, H., Reduction of stratospheric ozone by nitrogen oxide catalysts from supersonic transport exhaust, *Science*, *173*, 517, 1971.

Jucks, K. W., D. G. Johnson, K. V. Chance, and W. A. Traub, Nitric acid in the middle stratosphere as a function of altitude and aerosol loading, *J. Geophys. Res.*, *104(D21)*, 26,715–26,723, 1999.

Kaleschke, L., et al., Frost flowers on sea ice as a source of sea salt and their influence on tropospheric halogen chemistry, *Geophys. Res. Lett.*, *31*, doi:10.1029/2004GL020655, 2004.

Kinnersley, J. S., The meteorology of the stratosphere THIN AIR model, *Q. J. R. Meteorol. Soc.*, *122*, 219–252, 1996.

Kneizys, F., et al., The MODTRAN 2/3 report and LOWTRAN 7 model, Phillips Laboratory, Hanscom AFB, tech. Rep., contract F19628-91-C-0132 with Ontar Corp., 1996.

Ko, M. K. W., N.-D. Sze, C. J. ¯Scott, and D. K. Weisentein, On the relation between stratospheric chlorine/bromine loading and short-lived tropospheric source gases, *J. Geophys. Res.*, *102*, 25,507–25,517, 1997.

Ko, M. K. W., et al., Very short lived halogen and sulfur compound, chapter 2, World Meteorological Organisation, Geneva, report No. 47, 2003.

Kreher, K. V., P. V. Johnston, S. W. Wood, B. Nardi, and U. Platt, Ground based measurements of tropospheric and stratospheric Bro at Arrival Heights, Antarctica, *Geophys. Res. Lett.*, *24*, 3,021–3,024, 1997.

Kruizinga, B., C. Smorenburg, and H. Visser, Calibration concept of SCIAMACHY, *Proc. SPIE*, *2209*, 196–209, 1994.

Lamsal, L. K., et al., Climatology and total ozone retrievals, submitted to JGR, 2006.

Lary, D. J., *Photochemical studies with a three-dimensional model of the atmosphere, Ph.D. Thesis*, Cambridge University, 1991.

Lary, D. J., Gas phase atmospheric bromine photochemistry, *J. Geophys. Res.*, *101*, 1,505–1,516, 1996b.

Lary, D. J., and J. A. Pyle, Diffuse radiation, twilight and photochemistry, *J. Atmos. Chem.*, *13*, 373–392, 1991.

Lary, D. J., M. P. Chipperfield, R. Toumi, and T. Lenton, Heterogeneous atmospheric bromine chemistry, *J. Geophys. Res.*, *101*, 1,489–1,504, 1996a.

Leser, H., G. Hönninger, and U. Platt, MAX-DOAS measurements of BrO and NO_2 in the marine boundary layer, *Geophys. Res. Lett.*, *30(10)*, 1,537, doi:10.1029/2002GL015811, 2003.

Lichtenberg, G., et al., SCIAMACHY Level 1 data: Calibration concept and in-flight calibration, *Atmos. Chem. Phys. Discuss.*, *5*, 8,925–8,977, 2005.

Matveev, V., M. Peleg, D. Rosen, D. S. Tov-Alper, J. Stutz, K. Hebestreit, U. Platt, D. Blake, and M. Luria, Bromine oxide-ozone interaction over dead sea, *J. Geophys. Res.*, *106*, 10,375–10,378, 2001.

McElroy, M. B., R. J. Salawitch, S. C. Wofsy, and J. A. Logan, Reduction of Antarctic ozone due to synergistic interactions of chlorine and bromine, *Nature*, *321*, 759–762, 1986.

McElroy, M. B., R. J. Salawitch, S. C. Wofsy, and J. A. Logan, Evidence of bromine monoxide in the free troposphere during the Arctic polar sunrise, *Nature*, *397*, 338–340, 1999.

McLinden, C. A., S. C. Olsen, B. J. Hannegan, O. Wild, M. J. Prather, and J. Sundet, Stratospheric ozone in 3-D models: A simple chemistry and the cross tropopause flux, *J. Geophys. Res.*, *105*, 14,653–14,665, 2000.

McKinney, J. M. Pierson, and D. W. Toohey, A wintertime in situ profile of BrO between 17 and 27 km in the Arctic vortex, *Geophys. Res. Lett.*, *24*, 853–856, 1997.

Meier, R. R., D. E. Anderson, and M. Nicolet, Radiation field in the troposphere and stratosphere from 240-1000 nm. I General analysis, *Planet. Space Sci.*, *30*, 923–933, 1982.

Millard, G. A., A. M. Lee, and J. A. Pyle, A model study of the connection between polar and midlatitude ozone loss in the Northern Hemisphere lower stratosphere, *J. Geophys. Res.*, *108*, doi:10.1029/2001JD000899, 2003.

Molina, L. T., and M. J. Molina, Production of Cl_2O_2 from self-reaction of the ClO radical, *J. Phys. Chem.*, *91*, 433–436, 1987.

Molina, M. J., and F. S. Rowland, Stratospheric sink for chlorofluromethane:chlorine atom catalysed destruction of ozone, *Nature*, *249*, 810–812, 1974.

Montzka, S. A., J. H. Butler, B. D. Hall, D. J. Mondeel, and J. W. Elkeens, A decline in tropospheric organic bromine, *Geophys. Res. Lett.*, *30*(7), 1826, doi: 10.1029/2003GL017745, 2003b.

Montzka, S. A., et al., Controlled substances and other source gases, chapter 1, World Meteorological Organisation, Geneva, report No. 47, 2003a.

Murphy, D. M., and D. W. Fahey, An estimate of the flux of stratospheric reactive nitrogen and ozone into the troposphere, *J. Geophys. Res.*, *99*, 5,325–5,332, 1994.

Murray, F. W., On the computation of saturation vapour pressure, *J. Appl. Met.*, *6*, 203–204, 1967.

Nicolet, M., R. R. Meier, and D. E. Anderson, Radiation field in the troposphere and stratosphere from 240-1000 nm. I Numerical analysis, *Planet. Space Sci.*, *30*, 935–983, 1982.

Nielsen, J. E., and A. R. Douglass, A simulation of bromoform's contribution to stratospheric bromine, *J. Geophys. Res.*, *106*, 8,089–8,100, 2001.

Noël, S., H. Bovensmann, M. Wuttke, J. P. Burrows, M. Gottwald, E. Krieg, and R. Mager, SCIAMACHY nominal operations and special features, 4th International Symposium on Environmental Testing for Space Programmes (12-14 June 01 Luik). Eur. Space Agency Publ. SP-467, 1-8, 2000.

Noël, S., M. Buchwitz, and J. P. Burrows, First retrieval of global water vapour column amounts from SCIAMACHY measurements, *Atmos. Chem. Phys.*, pp. 111–125, 2004.

Nolt, I. G., Stratospheric hbr concentration profile obtained from far-infrared emission spectroscopy, *Geophys. Res. Lett.*, *24*, 281–284, 1997.

Norton, R. B., and J. F. Noxon, Dependence of stratospheric NO_3 upon latitude and season, *J. Geophys. Res.*, *91*, 5,323–5,330, 1986.

Noxon, J. F., Nitrogen oxide in the stratosphere and the troposphere measured by ground-based absorption spectroscopy, *Science*, *5*, 547–549, 1975.

Oltmans, S. J., et al., Seasonal surface ozone and filterable bromine relationship in the high Arctic, *Atmos. Environ.*, *23*, 2,431–2,441, 1989.

Otten, C., F. Ferlemann, U. Platt, T. Wagner, and K. Pfeilsticker, Ground based DOAS UV/visible measurements at Kiruna (Sweden) during SESAME winters 1993/94 and 1994/95, *J. Atmos. Chem.*, *30*, 141–162, 1998.

Perovich, D., and J. A. Richetr-Menge, Surface characteristics of lead ice, *J. Geophys. Res., 99(C8)*, 16,341–16,350, 1994.

Perron, G., MIPAS Level 1b Changes and Status, presentation given at the ESA textmdACVE-2 workshop, http://envisat.esa.int./workshop/acve2/, 2004.

Pfeilsticker, K., and U. Platt, Airborne measurements during the Actic Stratospheric Measurements: Observation of O_3 and NO_2, *Geophys. Res. Lett., 21*, 1,375–1,378, 1994.

Pfeilsticker, K., et al., Lower stratospheric organic and inorganic bromine budget for the arctic winter 1998/99, *Geophys. Res. Lett., 27*, 3,305–3,308, 2000.

Piters, A., K. Bramstedt, J. C. Lambert, and B. Kirchhoff, Overview of SCIAMACHY validation: 2002-2004, *Atmos. Chem. Phys. Discuss., 5*, 7,769–7,828, 2005.

Platt, U., Differential Optical Absorption Spectroscopy DOAS, in Air Monitoring by Spectroscopic Techniques, pp. 27–84, John Wiley and Sons, Inc., 1994.

Platt, U., and G. Hönninger, The role of halogen species in the troposphere, *Chemosphere*, *52*, 325 – 338, 2003.

Pommereau, J. P., et al., Small balloon for stratospheric ozone research and satellite validation, pp. 609–614, proc. 14th ESA Symp. on European Rocket and Balloon Programmes, ESA SP, Noordwicjk, Netherlands, 1999.

Pundt, I., J. P. Pommereau, M. P. Chipperfield, M. V. Roozendael, and F. Goutail, Climatology of stratospheric bro vertical distribution by balloon-borne UV-visible spectrometry, *J. Geophys. Res., 107,* 4,806, doi:10.1029/2002JD002230, 2002.

Quack, B., and D. W. R. Wallace, Air sea flux of bromoform: Controls, rates, and implication, *Global Biogeochem. Cycles*, *17*, 1,023, doi:10.1029/2002GB001890, 2003.

Quack, B., et al., Oceanic bromoform source for the tropical atmosphere, *Geophys. Res. Lett., 31*, doi:10.1029/2004GL02597, 2004.

Ramaroson, R., *Modelisation locale, a une et trois dimensions des processus photochimiques de l'atmosphere moyenne, Ph.D. Thesis*, Universite Paris VI, 1989.

Rankin, A. M., E. W. Wolff, and S. Martin, Frost flowers: Implications for tropospheric chemistry and ice core interpretation, *J. Geophys. Res., 107(D23)*, 4683, 2002.

Renard, J.-B., et al., Measurements and simulations of stratospheric NO_3 at mid and high latitudes in the northern hemisphere, *J. Geophys. Res*, *106(D23)*, 32,387–32,399, 2001.

Richter, A., *Absorptionspektroskopische Messungen stratosphaerischer Spurengase, ubber Bremen, 53°N, Ph.D. Thesis*, Univ. of Bremen, Bremen, Germany, 1997.

Richter, A., and J. P. Burrows, Retrieval of Tropospheric NO_2 from GOME measurements, *Adv. Space Res., 29*, 1,673–1683, 2002a.

Richter, A., F. Wittrock, M. Esinger, and J. P. Burrows, GOME observations of tropospheric BrO in Northern Hemispheric spring and summer 1997, *Geophys. Res. Lett., 25*, 2,683–2,686, 1998.

Richter, A., M. Esinger, A. Ladstätter-Weissenmayer, and J. P. Burrows, DOAS zenith sky observations, 2, seasonal variation of BrO over Bremen (53deg N 1994-1995), *J. Atmos. Chem., 32*, 83–99, 1999.

Richter, A., F. Wittrock, A. Ladstätter-Weissenmayer, and J. P. Burrows, GOME measurements of stratospheric and tropospheric BrO, *Adv. Space Res., 29*, 1,667–1672, 2002.

Richter, A., O. T. Afe, S. Fietkau, H. Oetjen, F. Wittrock, and J. P. Burrows, Tropospheric Halogens- Effects on Ozone, THALOZ Final Report, 2005.

Ridley, B. A., et al., Ozone depletion events observed in the high latitude surface during TOPSE aircraft program, *J. Geophys. Res., 108*, 8,356, 2003.

Rodgers, C. D. (Ed.), *Inverse Methods for Atmospheric Sounding : Theory and Practice*, World Scientific, Singapore, New Jersey, London, Hongkong, 2000.

Roozendael, M. V., and C. Fayt, WinDOAS 2.1. Sofware user manual, Belgian Institute for Space Aeronomie (BIRA/IASB), 2000.

Roozendael, M. V., et al., Intercomparison of BrO measurements from ERS-2 GOME ,ground-based and balloon platforms, *Adv. Space Res., 29*, 2002.

Rozanov, A., *Modeling of radiative transfer through a spherical planetary atmosphere: Application to the atmospheric trace gases retrieval from occultation- and limb measurements in UV- Vis- NIR, Ph.D. Thesis*, Univ. of Bremen, Bremen, Germany, 2001.

Rozanov, A., http://www.iup.physik.uni-bremen.de/sciatran, 2004.

Rozanov, A., V. Rozanov, and J. P. Burrows, A numerical radiative transfer model for a spherical planetary atmosphere: Combined differential–integral approach involving the picard iterative approximation, *J. Quant. Spectrosc. Radiat. Transfer, 69*, 513–534, 2001.

Rozanov, A., H. Bovensmann, A. Bracher, S. Hrechanyy, V. Rozanov, M. Sinnhuber, F. Stroh, and J. P. Burrows, NO_2 and BrO vertical profile retrieval from SCIAMACHY limb measurements: Sensitivity studies, *Adv. Space. Res., 36*, 846–854, 2005a.

Rozanov, A., H. Bovensmann, A. Bracher, S. Hrechanyy, V. Rozanov, M. Sinnhuber, F. Stroh, and J. P. Burrows, NO_2 and BrO vertical profile retrieval from SCIAMACHY limb measurements: Sensitivity studies, *Adv. Space. Res., 36*, 846–854, 2005b.

Rozanov, A., V. Rozanov, M. Buchwitz, A. Kokhanovsky, and J. P. Burrows, SCIATRAN 2.0 - A new radiative transfer model for geophysical applications in the 175-2400 nm spectral region, *Adv. Space. Res.*, *36*, 1,1015–1,019, 2005c.

Rozanov, V. V., , D. Diebel, R. J. Spurr, and J. P. Burrows, GOMETRAN:A radiative transfer model for the satellite project GOME- The plane parallel version, *J. Geophys. Res.*, *102*, 16,683–16,695, 1997.

Salawitch, R. J., D. K. Weisentein, L. J. Kovalenko, C. E. Siores, P. O. Wennberg, K. Chance, M. K. O. Ko, and C. A. Mclinden, Sensitivity of ozone to bromine in the lower stratosphere, *Geophys. Res. Lett.*, *32*, doi:10.1029/2004GL021504, 2005.

Sander, S. P., et al., Chemical kinetics and photochemical data for use in atmospheric studies, Jet Propulsion Laboratory, 2003.

Sanders, R. W., S. Solomon, G. H. Mount, M. W. bates, and A. L. Schmeltekopf, Visible spectroscopy at McMurdo station, Antarctica, 3, observation of NO_3, *J. Geophys. Res.*, *92*, 8,339–8,342, 1987.

Schauffler, S. M., E. L. Atlas, F. Flocke, R. A. Lueb, V. Stroud, and W. Travnicek, Measurements of bromine containing organic compounds at the tropical tropopause, *Geophys. Res. Lett.*, *25*, 317–320, 1998.

Schmidt, U., et al., Intercomparison of balloonborne cryogenic whole air samplers during MAP/GLOBUS campaign, *Planet. Space Sci.*, *35*, 647–656, 1987.

Schofield, R., K. Kreher, B. J. Connor, P. V. Johnston, A. Thomas, D. Shooter, M. P. Chipperfield, C. D. Rodgers, and G. H. Mount, Retrieved tropospheric and stratospheric BrO columns over Lauder, New Zealand, *J. Geophys. Res.*, *109*, doi: 10.1029/2003JD004463, 2004.

Sheode, N., B.-M. Sinnhuber, A. Rozanov, and J. P. Burrows, Towards a climatology of stratospheric bro from SCIAMACHY limb observations, submitted to Atmos. Chem. Phys. Discuss., 2006.

Singh, H. B., L. J. Salas, and R. E. Stiles, Methyl halides in and around the Eastern Pacific (40°N)-32°S, *J. Geophys. Res.*, *88*, 3,684–3,690, 1983.

Sinnhuber, B.-M., and I. Folkins, Estimating the contribution of bromoform to stratospheric bromine and its relation to dehydration in the tropical tropopause layer, *5*, 12,939 – 12,956, atmos. Chem. Phys. Discuss., 2005.

Sinnhuber, B. M., N. V. Sheode, M. Sinnhuber, M. Chipperfield, and W. Feng, The contribution of antropogenic bromine emissions to past stratospheric ozone trends: A modelling study, submitted to Atmos. Chem. Phys. Discuss., 2006.

Sinnhuber, B.-M., et al., Large loss of total ozone during the Arctic winter of 1999/2000, *Geophys. Res. Lett.*, *27*, 3,473–3,476, 2000.

Sinnhuber, B.-M., et al., Comparison of measurements and model calculations of stratospheric bromine monoxide, *J. Geophys. Res.*, *107*, 4,398, doi:10.1029/2001JD000940, 2002.

Sinnhuber, B.-M., et al., Global observations of stratospheric bromine monoxide from SCIAMACHY, *Geophys. Res. Lett.*, *32*, doi:10.1029/2005GL023839, 2005.

Sinnhuber, M., J. P. Burrows, M. P. Chipperfield, C. H. Jackman, M. B. Kallenrode, K. Künzi, and M. Quack, A model study of the impact of magnetic field structure on atmospheric composition during solar proton event, *Geophys. Res. Lett.*, doi:10.1029/2003GL017265, 2003.

Smith, D. L., AATSR instrument performance verification and optimisation in: Proceedings of the ENVISAT calibration review (Special publication SP 520), http://envisat.esa.int./calval/proceedings/, 2002.

Solberg, S., et al., Boundary layer ozone depletion as seen in the Norwegian Arctic spring, *J. Atmos. Chem.*, *23*, 301–322, 1996.

Soller, R., J. M. Nicovich, and P. H. Wine, Temperature-dependent rate coefficients for the reactions of Br($^2P_{3/2}$), Cl($^2P_{3/2}$), O(^3P_j) with $BrONO_2$, *J. Phys. Chem.*, *105*, 1,416–1,422, 2001.

Solomon, S., R. W. Sanders, M. A. Carroll, and A. L. Schmeltekopf, Visible and near-ultraviolet spectroscopy at McMurdo station, Antarctica, 5, Observations of the diurnal variation of BrO and OClO, *J. Geophys. Res.*, *94*, 11,393–11,403, 1989.

Solomon, S., J. P. Smith, R. W. Sanders, L. Pelirski, H. L. Miller, G. H. Mount, J. G. Keys, and A. L. Schmeltekopf, Visible spectroscopy at McMurdo station, Antarctica, 8, observation of nighttime NO_2 and NO_3 from April to October 1991, *J. Geophys. Res.*, *98*, 993–1000, 1991.

Solomon, S., et al., Ozone variability at mid-latitudes:Coupling of aerosols and temperature variability to anthropogenic chlorine, *Geophys. Res. Lett.*, *25*, 1,871–1,874, 1998.

Stolarski, R. M., and R. Cicerone, Stratospheric chlorine: a possible sink for ozone, *Can. J. Chem.*, *52*, 1610, 1974.

Sturges, W. T., D. E. Oram, L. J. Carpenter, S. A. Penkett, and A. Engel, Bromoform as a source of stratospheric bromine, *Geophys. Res. Lett.*, *27*, 2081–2084, 2000.

Tang, T., and J. C. McConnel, Autocatalytic release of bromine from Arctic smowpack during polar sunrise, *Geophys. Res. Lett.*, *23(18)*, 2633–2636, 1996.

Toohey, D. W., J. G. Anderson, W. H. Brune, and K. R. Chan, In-situ measurements of BrO in the arctic stratosphere, *Geophys. Res. Lett.*, *17*, 513, 1990.

von Clarmann, et al., Retrieval of temperature and tangent altitude pointing from limb emission spectra recorded from space by the Michelson Interferometer for Passive Atmospheric Sounding (MIPAS), *J. Geophys. Res.*, *108*, 4736, doi:10.1029/2003JD003602, 2003.

von Savigny, C., K.-U. Eichmann, H. Bovensmann, and J. P. Burrows, Report on the 1st international workshop on limb scattering, *SPARC Newsletter*, *22*, 2004.

von Savigny, C., J. W. Kaiser, H. Bovensmann, J. P. Burrows, I. S. McDermid, and T. Leblanc, Spatial and temporal characterization of SCIAMACHY limb pointing errors during the first three years of the mission, *Atmos. Chem. Phys. Discuss.*, *5*, 3,701–3,722, 2005a.

von Savigny, C., I. C. McDade, E. Griffioen, C. S. Haley, C. E. Siores, and E. J. Llewellyn, Sensitivity Studies and First Validation of Stratospheric Ozone Profile Retrieval from ODIN/OSIRIS Observation of Limb Scattered Solar Radiation, *Can. J. Phys.*, in press, 2005b.

von Savigny, C., et al., The ozone hole break up in September 2002 as seen by SCAIMACHY on ENVISAT, *J. Atm. Sci.*, in press, 2005c.

Wagner, T., and U. Platt, Satellite mapping of enhanced BrO concentrations in the troposphere, *Nature*, *395*, 486–490, 1998.

Wagner, T., C. Leue, M. Wenig, K. Pfeilsticker, and U. Platt, Spatial and temporal distribution of enhanced BrO concentrations by the GOME instrument aboard ERS-2, *J. Geophys. Res.*, *106*, 24,225–24,235, 2001.

Wahner, A., A. Ravishankara, S. Sander, and R. Friedl, Absorption cross section of BrO between 312 and 385 nm at 298 and 223 k, *Chem. Phys. Lett.*, *152*, 507–512, 1988.

Wamsley, P. R., et al., Distribution of halon-1211 in the upper troposphere and lower stratosphere and the 1994 total bromine budget, *J. Geophys. Res.*, *103*, 1,513–1,526, 1998.

Wang, P., et al., Measurements of tropospheric NO_2 with and airborne multiaxis DOAS instrument, *Atmos. Chem. Phys.*, *5*, 337–343, 2005.

Wangberg, I. T., T. Etzkorn, I. Barnes, U. Platt, and K. Becker, Absolute determination of the temperature behaviour of the $NO_3 + NO_2 + m = N_2O_5 + M$ equilibrium, *J. Phys. Chem.*, *A(101)*, 9,694–9,698, 1997.

Wayne, R. P. (Ed.), *Chemistry of Atmospheres*, Oxford University Press, 2002.

Weidner, F., et al., Balloon borne limb profiling of UV/vis skylight radiances, o_3, no_2, and bro:technical setup and validation of method, *5*, 1409–1422, atmos. Chem. Phys., 2005.

Wennberg, P., et al., Removal of stratospheric o_3 by radicals: In situ measurements of OH, HO_2, NO, NO_2, ClO, and BrO, *Science*, *266*, 398–404, 1994.

Wennberg, P., et al., The atmospheric column abundance of extmdIO:extmdImplication for stratospheric ozone, *J. Geophys. Res.*, *102(D7)*, 8,887–8,898, 1997.

Wittrock, F., *The retrieval of oxygenated volatile organic compounds by remote sensing techniques, Ph.D. Thesis*, Univ. of Bremen, Bremen, Germany, 2006.

WMO, Scientific assesment of ozone depletion: 1998. WMO, global ozone research and monitoring project: Report no. 44, 1998.

WMO, Scientific assesment of ozone depletion: 2002. WMO, global ozone research and monitoring project: Report no. 47, 2002.

Wofsy, S. C., M. B. McElroy, and Y. L. Yung, The chemistry of atmospheric bromine, *Geophys. Res. Lett.*, *2*, 215–218, 1975.

Yung, Y. L., J. P. Pinto, R. T. Watson, and S. P. Sander, Atmospheric bromine and ozone perturbations in the lower stratosphere, *J. Atm. Sci.*, *37*, 339–353, 1980.

Zeng, T., Y. H. Wang, K. Chance, E. V. Browell, B. A. Ridley, and E. L. Atlas, Widespread persistent near-surface ozone depletion at northern high latitudes in spring, *Geophys. Res. Lett.*, *30(24)*, 2298, 2003.

Zerefos, C. S., K. Tourpali, B. R. Bojkov, D. S. Balis, B. Rognerund, and I. S. A. Isaksen, Solar activity-total column ozone relationship, *J. Geophys. Res.*, *102*, 1,561–1,569, 1997.